Spring 4-23-2015

A Finite Element Method Based Microwave Heat Transfer Modeling of Frozen Multi-Component Foods

Krishnamoorthy Pitchai
University of Nebraska at Lincoln, pkrishnamoorthy@huskers.unl.edu

A FINITE ELEMENT METHOD BASED MICROWAVE HEAT TRANSFER MODELING OF FROZEN MULTI-COMPONENT FOODS

by

Krishnamoorthy Pitchai

A DISSERTATION

Presented to the Faculty of

The Graduate College at the University of Nebraska

In Partial Fulfillment of Requirements

For the Degree of Doctor of Philosophy

Major: Food Science and Technology

Under the Supervision of Professor Jeyamkondan Subbiah

Lincoln, Nebraska

April, 2015

A FINITE ELEMENT METHOD BASED MIROWAVE HEAT TRANSFER MODELING OF FROZEN MULTI-COMPONENT FOODS

Krishnamoorthy Pitchai, Ph.D.

University of Nebraska, 2015

Adviser: Jeyamkondan Subbiah

Microwave heating is fast and convenient, but is highly non-uniform. Non-uniform heating in microwave cooking affects not only food quality but also food safety. Most food industries develop microwavable food products based on "cook-and-look" approach. This approach is time-consuming, labor intensive and expensive and may not result in optimal food product design that assures food safety and quality. Design of microwavable food can be realized through a simulation model which describes the physical mechanisms of microwave heating in mathematical expressions. The objective of this study was to develop a microwave heat transfer model to predict spatial and temporal profiles of various heterogeneous foods such as multi-component meal (chicken nuggets and mashed potato), multi-component and multi-layered meal (lasagna), and multi-layered food with active packages (pizza) during microwave heating. A microwave heat transfer model was developed by solving electromagnetic and heat transfer equations using finite element method in commercially available COMSOL Multiphysics v4.4 software. The microwave heat transfer model included detailed geometry of the cavity, phase change, and rotation of the food on the turntable.

The predicted spatial surface temperature patterns and temporal profiles were validated against the experimental temperature profiles obtained using a thermal imaging

camera and fiber-optic sensors. The predicted spatial surface temperature profile of different multi-component foods was in good agreement with the corresponding experimental profiles in terms of hot and cold spot patterns. The root mean square error values of temporal profiles ranged from 5.8 °C to 26.2 °C in chicken nuggets as compared 4.3 °C to 4.7 °C in mashed potatoes. In frozen lasagna, root mean square error values at six locations ranged from 6.6 °C to 20.0 °C for 6 min of heating. A microwave heat transfer model was developed to include susceptor assisted microwave heating of a frozen pizza. The root mean square error values of transient temperature profiles of five locations ranged from 5.0 °C to 12.6 °C. A methodology was developed to incorporate electromagnetic frequency spectrum in the coupled electromagnetic and heat transfer model. Implementing the electromagnetic frequency spectrum in the simulation improved the accuracy of temperature field pattern and transient temperature profile as compared to mono-chromatic frequency of 2.45 GHz. The bulk moisture diffusion coefficient of cooked pasta was calculated as a function of temperature at a constant water activity using desorption isotherms.

ACKNOWLEDGEMENTS

I would like to take this opportunity to thank and acknowledge those who have been part of my journey in achieving my Doctoral degree. First and foremost I would like to express my utmost gratitude to my graduate committee chair and advisor Dr. Jeyamkondan Subbiah for believing in me and bestowing me an excellent opportunity to work with him as a graduate research assistant. Dr. Subbiah's constant motivation and relentless guidance to my research inspired me to do well beyond my belief. Throughout the years, Dr. Subbiah's mentorship has helped me to improve my perspective on conducting research and become more confident in science and research. His passion for science and research philosophy propelled and inspired me to understand more about science and learned a lot from him, on how to think big, and about life in general. In his capacity as my graduate committee chair and mentor, Dr. Subbiah has made enormous impact on both my professional and personal fronts. Thank you for everything.

I would like to convey my sincere gratitude to my graduate committee members, Dr. David Jones, Dr. Curtis Weller, Dr. Mehrdad Negahban, and Dr. Harshavardhan Thippareddi, for their support, time and effort in helping me with my research. Their technical guidance, ideas, and insights helped me in many ways to improve my research every day. I am very grateful to Dr. Sohan Birla and Dr. Ric Gonzalez from ConAgra Foods for being part of my research in every possible way, providing technical assistance, and giving opportunities to use facilities and equipments for data collection. I thank Dr. Ashu Guru for his technical assistance to run the models in Holland Computing Center here at the University. I am indebted to Dr. K. Alagusundaram, my undergraduate teacher for inspiring and instilling a belief in me to pursue higher studies.

My sincere appreciation goes to my colleague and friend Jiajia Chen for his enormous support and cooperation in helping me with model setup and data collection. It was my great pleasure to work with him. As with any big endeavor, many people have invested their time, effort and care to make it possible for me to complete my Doctoral degree at UNL. I am thankful to all my friends, lab mates, volunteers and fellow graduate students for their support, help and rendering warmth friendly atmosphere throughout my research. I take this opportunity to thank the faculty and staff members of Department of Food Science and Technology and Department of Biological Systems Engineering for their support and help professionally and personally.

Finally, I express my deepest gratitude and dedicate my doctoral dissertation to my father, Pitchai Krishnasamy, and my mother Vijayalakshmi Pitchai, and younger brother Ragavan Pitchai for giving me their confidence, unwavering support, and encouragement to complete my Doctoral degree and making me what I am today.

TABLE OF CONTENTS

LIST OF FIGURES

LIST OF TABLES

CHAPTER I

INTRODUCTION

Microwave heating is used extensively in domestic heating applications as an alternative to conventional heating methods to increase heating rate and to reduce process time (Ohlsson, 1983). However microwave heating of frozen foods is highly non-uniform. Thawed regions of the food absorb more microwave energy as compared to frozen region leading to runaway heating at some locations, while some portion of the food may be still under frozen state. Not-ready-to-eat (NRTE) foods contain raw ingredients or partially cooked ingredients, and therefore may contain pathogens. Food safety of microwave cooked NRTE foods might be compromised when the temperature of the food did not reach to the target microbial inactivation temperature throughout the food. The non-uniform heating in a microwave cooked food not only affects food safety but also influences food quality (Ma et al., 1995). Food product development for microwaveable foods is much more complex than conventional foods, because different ingredients in the food interact with microwave energy at different rate based on their dielectric and thermophysical properties. These material properties are the critical factors that dictate microwave energy absorption and heat dissipation. It is a challenge for food product developer to optimize various components in a multi-component frozen food so that they all heat uniformly. Due to complex interactions of different food components with microwave energy, food product developers currently rely on "cook-and-look" approach.

Experimental assessments alone cannot easily identify the reasons behind non-uniform heating in a microwave oven. The food product developers may be able to

design and optimize the microwave cooking of frozen microwavable foods for achieving uniform heating, if they gain better insights into microwave physical phenomenon and visualize virtually how the different ingredients heat during cooking process. Microwave heating is a physical phenomenon that involves mechanisms of electromagnetism, heat and mass transfer. The microwave heating mechanisms can be described in a physics based simulation model. Given the complexity of microwave interaction with food and packages, a microwave heat transfer model is a highly desirable tool to simulate the heating behavior of food in a microwave oven. The model can offer insights into microwave interactions with food components and can save a tremendous amount of time in food product development (Celuch and Kopyt, 2009).

1.1. Research gap

There are many simulation models for the domestic microwave heating developed over the years (Dinčov et al., 2004; Geedipalli et al., 2007; Wäppling-Raaholt et al., 2002; Zhang and Datta, 2003; Zhang and Datta, 2000). The developed models are not used in the food industry for food product development, because models are not robust and comprehensive and did not consider one or more of the following features: (i) temperature-dependent dielectric and thermal properties (ii) phase change from frozen to thawing, (iii) rotation of the turntable, (iv) detailed geometry of the cavity, (v) mass transfer, (vi) temperature-dependent mass transport properties. (vii) susceptor assisted microwave heating, and (viii) incorporating electromagnetic frequency spectrum. The simulation models are solved iteratively using numerical methods such as finite-difference time-domain (Tilford et al., 2007; Pitchai et al., 2012) and finite element method (Akarapu et al., 2004; Zhang and Datta, 2002).

Dielectric and thermal properties are important material properties that influence how different ingredients/food components heat in the microwave oven. Many studies measured and incorporated the dielectric and thermal properties in microwave heat transfer model. However most of those studies considered material properties only from the thawed temperature (Ma et al., 1995; Ryynänen and Ohlsson, 1996) or used constant material properties (Rattanadecho et al., 2002; Romano et al., 2005; Geedipalli et al., 2012) in the simulation models. Most reported studies in the literature consider cooking of refrigerated meals and do not consider the phase change of thawing of frozen foods (Geedipalli et al., 2007; Ma et al., 1995; Ryynänen and Ohlsson, 1996; Ryynänen et al., 2004). Most of the microwavable meals in North America are available in the market as frozen meals. Therefore, it is important to consider the phase change characteristics of microwavable foods in the model. This requires accurate measurement of temperature-dependent dielectric and thermal properties from frozen-cook conditions to predict the accurate temperature distribution during microwave cooking frozen meals.

Most of the modern day domestic microwave ovens have a turntable to rotate the food during cooking. By rotating the food inside the cavity during cooking, the heating uniformity is improved in the food. Thus, it is important to simulate the rotation of the food on the turntable. The COMSOL Multiphysics software does not have the capability to simulate microwave heating of rotating food. The electromagnetic module of COMSOL Multiphysics is not compatible with the software's inherent moving mesh algorithm for the rotation of object in the computation domain. To overcome the issue of not being able to rotate the food on the turntable during electromagnetic simulation in

COMSOL Multiphysics, a new approach needs to be developed. In this study, a custom algorithm was developed in MATLAB to enable discrete rotation of food in the turntable.

Solving microwave heat transfer models in 3D space and time requires a great amount of computational resources. In most studies, researchers have made several simplifications in their model development approach. For example, many researchers have assumed the microwave cavity and waveguide as a simple geometry without considering some of the special features of microwave design, such as crevices and dimples (Geedipalli et al., 2007; Ma et al., 1995; Wäppling-Raaholt et al., 2006; Yakovlev, 2001) primarily to minimize the number of mesh elements which reduces the computational requirements. The modern day microwave ovens are carefully designed to include many special geometric features such as metal bumps, crevices, and a turntable in order to improve heating uniformity. Each of these features inside the cavity can have a dramatic effect on electric field distribution. Electric field distribution is an important factor as it is the input heat source term in the heat transfer equations. Therefore, all the special features of microwave design are needed to be included in the model.

Most of the developed microwave heat transfer models do not consider all the physics involved in microwave heating process. Most of the models assumed that the food products are a single phase (solids without any pore space) and there is no movement of liquid or gas in the food product (Virtanen et al., 1997; Tilford et al., 2007; Pitchai et al., 2012). In reality, a domestic microwave heating is a rapid process, where evaporation of water molecules and movement of moisture is tremendous within short heating time. In case of microwave heating of frozen foods, a multiphase porous media model combining the electromagnetic heat source with heat and mass transfer, and

including phase change of thawing and evaporation, is needed to accurately describe the microwave heating process.

A very few comprehensive multiphase porous media models have been developed to study various heating processes such as conventional cooking (Dhall et al., 2012), frying (Halder et al., 2007a, 2007b, 2011) and microwave puffing (Rakesh and Datta, 2011). These models coupled different types of heating sources with heat and mass transfer for different food processes. However most of these models only considered 2-D problems. A multiphase porous media model for microwave heating of a frozen homogeneous mashed potato is developed by Chen et al. (2014). However, a 3-D multiphase porous media microwave heating model for a frozen heterogeneous food has not been reported. A multiphase porous media model for microwave heating needs accurate mass transport properties to accurately predict the temperature and moisture distribution inside the food.

Most of the mass transport properties (moisture diffusion coefficient, intrinsic permeability) are not available in the literature and/or not measured as a temperature dependent. Therefore, it is important to measure the temperature-dependent mass transport properties and provide as input to the multiphase porous media model to predict the accurate moisture and temperature profile.

Susceptors, an active package material, are used in microwavable food packages to facilitate preferential heating. Susceptors absorb electromagnetic energy rapidly during microwave heating and then convert the absorbed energy into heat to the food (Risman, 2009). The food products that are cooked in domestic ovens become soggy and are not be able to achieve the browning. Microwave food packages that are made of

susceptors can be handy to overcome the lack of browning and crispiness in foods. In spite of more than 40 years of susceptor application in microwave food packages, the interaction of susceptor and food with microwaves during heating has not been extensively studied. Modeling of susceptor and food interaction with microwaves helps in understanding the role of microwave food packages and to design better packages for improving heating uniformity. The microwave heat transfer model including the microwave interactions with food and susceptor package is needed to understand the heating performance of a food when heated with the presence of susceptor.

Domestic microwave oven magnetrons do not operate at a monochromatic frequency of 2.45 GHz; they rather produce microwaves in the allowable frequency range of 2.45±0.05 GHz. As the magnetron operating frequency changes, the number of electromagnetic (EM) modes generated inside the cavity is also affected. Most microwave heat transfer models simplify that the magnetron produces a monochromatic electromagnetic frequency of 2.45 GHz to reduce the computational complexity (Curcio et al., 2008; Dinčov et al., 2004; Liu et al., 2012). In almost all studies, researchers have not included the magnetron frequency spectrum in the microwave heat transfer model of domestic microwave heating of food. Therefore, a new methodology needs to be developed to incorporate the magnetron frequency spectrum in the microwave heat transfer model.

1.2. Objectives

This dissertation explores the use of Finite Element Method based COMSOL Multiphysics software to develop comprehensive microwave heat transfer model for various categorize of frozen foods. The overall goal of this research was to develop and

validate a comprehensive microwave heat transfer model to predict temperature distribution of microwave heated frozen multi-component foods. The specific objectives of this research were to:

i. develop and validate a microwave heat transfer model for a ***rotating frozen*** multi-component meal (mashed potato and chicken nuggets) in a domestic oven,

ii. develop and validate electromagnetic, heat and ***mass transfer*** model of microwave heating of a ***frozen heterogeneous*** meal (lasagna) rotating on a turntable,

iii. develop and validate a microwave heat transfer model for ***susceptor assisted microwave heating*** of a frozen pizza,

iv. develop a methodology to incorporate ***electromagnetic frequency spectrum*** in the microwave heat transfer model and investigate the effect of variance of frequency distribution on prediction accuracy, and

v. determine the ***temperature-dependent bulk moisture diffusion coefficient*** of cooked pasta using desorption isotherms.

1.3. Dissertation format

This dissertation is a compilation of five chapters. Each chapter is written as a research paper that has either published, or is in the process of being published. Therefore, stand-alone consists of an abstract, introduction, materials and methods, results and discussion and conclusions. Following these five chapters a summary and suggestions for future research are provided.

Objective I, covered in Chapter 2, deals with the development and validation of a microwave heat transfer model for a rotating frozen multi-component meal (mashed potato and chicken nuggets) subjected to 90 s of heating in a 1200 W rated power domestic oven. The model included detailed cavity geometry, phase change, and rotation of the food. The predicted and experimental temperature profiles were provided as inputs to a microbial inactivation kinetics model for *Salmonella* Heidelberg to assess food safety risks in chicken nuggets. Objective II, covered in Chapter 3, deals with the development and validation of a computer simulation model to predict spatial and temporal temperature profiles in frozen lasagna during microwave cooking. A multiphase porous media model combining the electromagnetic heat source with heat and mass transfer, and including phase change of melting and evaporation was developed. The model simulated for six minutes of microwave cooking of a 450 g frozen lasagna tray kept at the center of the turntable in a 1200 W domestic microwave oven. Objective III, covered in Chapter 4, deals with the development and validation of a microwave heat transfer model of susceptor assisted microwave heating of a frozen pizza. Transition boundary condition was applied in radio frequency module to discretize thin susceptor film in the computational domain. The boundary heat source was applied in the heat transfer module to calculate temperature in the susceptor film.

Objective IV, covered in Chapter 5, deals with the development of a methodology to incorporate electromagnetic frequency spectrum in the microwave heat transfer model. This study assumed that the magnetron produces a frequency spectrum defined by a Gaussian distribution of frequencies with a central frequency of 2.45 GHz and investigates the effect of Gaussian distribution variance of $(0.05\ \text{GHz})^2$, $(0.025\ \text{GHz})^2$,

$(0.017\ GHz)^2$ on prediction accuracy when compared to using monochromatic frequency of 2.45 GHz. Simulated temperature profiles of the models using the monochromatic frequency of 2.45 GHz and Gaussian frequency spectrum with three different variances were compared with experimental temperature profiles obtained using a thermal imaging camera at the end of cooking and five fiber-optic thermocouples during cooking. Objective V, covered in Chapter 6, deals with the measurement of desorption isotherm of cooked pasta from 20 °C to 60 °C using an automatic vapor sorption analyzer and fit the experimental isotherm for different sorption models to evaluate the parameters and goodness of fit for accurate prediction of isotherm behaviours of cooked pasta. The parameters and goodness of fit of four sorption models (Oswin, Halsey, Smith, and Guggenheim-Anderson-de Boer) were evaluated with the experimental isotherm data. Desorption bulk moisture diffusion coefficient was calculated as a function of temperature at constant water activity. Finally, in Chapter 7, summary and conclusions and recommendations for future research are provided.

1.4. References

Akarapu, R., Li, B.Q., Huo, Y., Tang, J., & Liu, F. (2004). Integrated modeling of microwave food processing and comparison with experimental Measurements. Journal of Microwave Power and Electromagnetic Energy, 39(3/4), 153-165.

Birla, S.L., Pitchai, K., & Subbiah, J. (2011). A critical comparison of COMSOL and QUICKWAVE software for modeling of microwave heating in domestic oven. Proceedings of 45th International Microwave Power Institute Annual Meeting, June 8-10, New Orleans, LA.

Celuch, M., & Kopyt, P. (2009). Modeling microwave heating in foods. In M.W. Lorence, P. S. Pesheck (Eds.), Development of packaging and products for use in microwave ovens. (First edn., pp. 305-346). CRC Press LLC, Boca Raton, FL.

Chen, J., Pitchai, K., Birla, S., Negahban, M., Jones, D., & Subbiah, J. (2014). Heat and mass transport during microwave heating of mashed potato in domestic oven-model development, validation, and sensitivity analysis. Journal of Food Science, 79(10), 1991-2004.

Curcio, S., Aversa, M., Calabrņ, V., & Iorio, G. (2008). Simulation of food drying: FEM analysis and experimental validation. Journal of Food Engineering, 87(4), 541-553.

Dhall, A., Halder, A., & Datta, AK. (2012). Multiphase and multicomponent transport with phase change during meat cooking. Journal of Food Engineering, 113(2), 299-309.

Dinčov, D.D., Parrott, K.A., & Pericleous, K.A. (2004). A new computational approach to microwave heating of two-phase porous materials. International Journal of Numerical Methods for Heat and Fluid Flow, 14(6), 783-802.

Geedipalli, S.S.R., V. Rakesh, & A.K. Datta. (2007). Modeling the heating uniformity contributed by a rotating turntable in microwave ovens. Journal of Food Engineering, 82(3), 359-368.

Halder, A., Dhall, A., & Datta, AK. (2007a). An improved, easily implementable, porous media based model for deep-fat frying: part i: model development and input parameters. Food and Bioproducts Processing, 85(3), 209-219.

Halder, A., Dhall, A., & Datta, AK. (2007b). An improved, easily implementable, porous media based model for deep-fat frying: Part II: results, validation and sensitivity analysis. Food and Bioproducts Processing, 85(3), 220-230.

Halder, A., Dhall, A., & Datta, AK. (2011). Modeling transport in porous media with phase change: applications to food processing. Journal of Heat Transfer, 133(3), 31010.

Liu, S., Fukuoka, M., & Sakai N. (2013). A finite element model for simulating temperature distributions in rotating food during microwave heating. Journal of Food Engineering, 115(1), 49-62.

Ma, L., Paul, D. L., Pothecary, N. M., Railton, C. J., Bows, J., Barratt, L., Mullin, J., & Simons, D. (1995). Experimental validation of a combined electromagnetic and thermal FDTD model of a microwave heating process. IEEE Transactions on Microwave Theory and Techniques, 43(11), 2565-2572.

Ohlsson, T. (1983). Fundamentals of microwave cooking. Microwave world, 2(4), 4-9.

Pitchai, K., Birla, S., Subbiah, J., Jones, D., & Thippareddi, H. (2012). Coupled electromagnetic and heat transfer model for microwave heating in domestic ovens. Journal of Food Engineering, 112(1-2), 100-111.

Rakesh, V., & Datta, AK. (2011). Microwave puffing: Determination of optimal conditions using a coupled multiphase porous media–Large deformation model. Journal of Food Engineering, 107(2), 152-163.

Rattanadecho, P., Aoki, K., & Akahori, M. (2002). Experimental validation of a combined electromagnetic and thermal model for a microwave heating of multi-layered materials using a rectangular wave guide. Transactions-American Society of Mechanical Engineers Journal of Heat Transfer, 124(5), 992-996.

Risman, P. O. & Celuch, M. (2000). Electromagnetic modeling for microwave heating applications. In 13th International Conference on Microwaves, Radar and Wireless Communications.

Risman P.O. (2009). Modelling the effects of active packaging of microwaved foods. In M. W. Lorence, P. S. Pesheck (Eds.), Development of packaging and products for use in microwave ovens. (First edn., pp. 349-371). CRC Press LLC, Boca Raton, FL.

Romano, V. R., Marra, F., & Tammaro, U. (2005). Modelling of microwave heating of foodstuff: study on the influence of sample dimensions with a FEM approach. Journal of Food Engineering, 71(3), 233-241.

Ryynänen, S., & Ohlsson, T. (1996). Microwave heating uniformity of ready meals as affected by placement, composition, and geometry. Journal of Food Science, 61(3), 620-624.

Ryynänen, S., Risman, P., & Ohlsson, T. (2004). Hamburger composition and microwave heating uniformity. Journal of Food Science, 69(7), 187-196.

Tilford, T., Baginski, E., Kelder, J., Parrott, K., & Pericleous, K. (2007). Microwave modeling and validation in food thawing applications. The Journal of Microwave Power and Electromagnetic Energy, 41(4), 30-45.

Virtanen, A., Goedeken, D., & Tong, C. (1997). Microwave assisted thawing of model frozen foods using feed-back temperature control and surface cooling. Journal of Food Science, 62(1), 150-154.

Wäppling-Raaholt, B., Scheerlinck, N., Gait, S., Banga, J. R., Alonso, A., Balsa-Canto, E., Van, I., Ohlsson, T., & Nicolai, B. M. (2002). A combined electromagnetic and heat transfer model for heating of foods in microwave combination ovens. Journal of Microwave Power and Electromagnetic Energy, 37(2), 97-111.

Wäppling-Raaholt, B., Risman, P., & Ohlsson, T. (2006). Microwave heating of ready meals–FDTD simulation tools for improving the heating uniformity. Advances in Microwave and Radio Frequency Processing, 243-255.

Yakovlev V.V. (2001). Efficient electromagnetic models for systems and processes of microwave heating. In International Seminar on Heating by Internal Sources, Padova, Italia, Sept 11- 14.

Zhang, H., & Datta, AK. (2003). Microwave power absorption in single-and multiple-item foods. Food and Bioproducts Processing, 81(3), 257-265.

Zhang, H., & Datta, AK. (2000). Coupled electromagnetic and thermal modeling of microwave oven heating of foods. Journal of Microwave Power and Electromagnetic Energy, 35(2), 71-85.

CHAPTER II

A MICROWAVE HEAT TRANSFER MODEL FOR A ROTATING MULTI-COMPONENT MEAL IN A DOMESTIC OVEN: DEVELOPMENT AND VALIDATION

K. Pitchai [a, b], J. Chen [b], S. Birla [b], R. Gonzalez [c], D. Jones [b], J. Subbiah [a, b, *]

[a] *Department of Food Science and Technology, University of Nebraska-Lincoln, NE – 68583*

[b] *Department of Biological Systems Engineering, University of Nebraska-Lincoln, NE – 68583*

[c] *ConAgra Foods, Inc., Omaha, NE - 68102*

* Corresponding author: Jeyamkondan Subbiah, Kenneth E. Morrison Distinguished Professor of Food Engineering, Departments of Food Science & Technology and Biological Systems Engineering, 212 L.W.Chase Hall, East Campus, University of Nebraska-Lincoln, Lincoln, NE-68583-0726, Ph. No: 402-472-4944, Fax No: 402-472-6338, Email: jeyam.subbiah@unl.edu.

Citation: Pitchai, K., Chen, J., Birla, S., Gonzalez, R., Jones, D., Subbiah, J. 2014. A microwave heat transfer model for a rotating multi-component meal in a domestic oven: Development and validation. Journal of Food Engineering. 128: 60-71.

2.1. Abstract

A finite element model coupling electromagnetic and heat transfer equations was developed to understand complex microwave interactions in food. The model simulated

rotation of a frozen multi-component meal consisting of nine chicken nuggets and mashed potatoes. Temperature-dependent dielectric and thermophysical properties of chicken nuggets and mashed potatoes were measured as a function of temperature from -10 °C to 110 °C. The model included detailed cavity geometry, phase change, and rotation of the food. Effect of rotation angle on temperature predictions was studied and a 45° rotation angle was found to be sufficient. Simulated temperature profiles were compared with experimental temperature profiles obtained using a thermal imaging camera and fiber-optic sensors. Predicted spatial surface temperature profile was in good agreement with the corresponding experimental profiles in terms of hot and cold spot patterns. The root mean square error values ranged from 5.8 °C to 26.2 °C in chicken nuggets as compared 4.3 °C to 4.7 °C in mashed potatoes. The predicted and experimental temperature profiles were provided as inputs to a microbial inactivation kinetics model for *Salmonella* Heidelberg to assess food safety risks in chicken nuggets. For 90 s of cooking in a 1200 W microwave oven, at least 7-log reductions of *Salmonella* Heidelberg was not achieved completely at all locations in the chicken nuggets due to non-uniform heating. The validated model can be used to optimize the layout and food system/package modification to achieve more uniform heating.

Keywords: Domestic microwave oven, computer simulation model, multi-component meal, rotation, Validation, Microbial inactivation model.

2.2. Introduction

Because of rapid and convenient heating offered by the domestic microwave oven, it has become a favorite appliance to heat/cook frozen meals (Venkatesh and

Raghavan, 2004). Frozen microwaveable meals may be available as not-ready-to-eat (NRTE), meaning that the product has to be thoroughly cooked by the consumer before consumption to ensure food safety. NRTE meals are available in a variety of product layouts such as single-component, multi-component and multi-compartment meals. Rapid microwave heating may enhance the overall food quality (Guan et al., 2002; Knoerzer et al., 2008). However, the microwave heating process could produce a non-uniform temperature distribution within the food, possibly resulting in over-cooked and under-cooked regions. NRTE foods may contain some raw ingredients or partially cooked meat and poultry products. When the cooked temperature does not reach the desired target temperature for inactivating microorganisms, they can survive in the cold regions and thus cause foodborne illness. This is evident from the several foodborne illness outbreaks associated with microwaveable frozen foods (CDC, 2008; Leitch, 2008; USDA-FSIS, 2007; USDA-FSIS, 2010).

There are many factors affecting microwave heating uniformity including: dielectric properties (dielectric constant and dielectric loss factor), thermal properties (specific heat capacity and thermal conductivity) and physical properties (size, shape, density, and location in the package) of foods (Zhang and Datta, 2000). These factors affect the degree of food components interaction with microwave energy and are important to consider for optimizing food design to achieve uniform heating. Microwave food product development is very time-consuming and expensive. However, use of the computer simulation tool can accelerate the product development cycle and reduce the cost of production. While endeavoring to optimize food and package design to achieve uniform heating, a mere ‘cook-and-measure’ experimental approach alone may not be

optimal in order to understand the complex interactions of food components and the package with microwave energy and therefore simulation can be highly useful.

Over the last two decades, computer simulation is becoming a promising tool to understand complex microwave heating with the availability of powerful computational techniques and the development of efficient numerical methods. A computer-based simulation of microwave heating of foods can assist in optimizing design of food systems and packages to improve food quality and safety. Computer-based simulations that couple electromagnetic and thermal equations to calculate the temperature field of microwave-heated foods have been reported (Dinčov et al., 2004; Geedipalli et al., 2007; Pitchai et al., 2012; Wäppling-Raaholt et al., 2002; Zhang and Datta, 2003; Zhang and Datta, 2000). These models are solved iteratively using various numerical methods such as finite-difference time-domain (Pitchai et al., 2012; Tilford et al., 2007; Kopyt and Celuch-Marcysiak, 2003) and finite element methods (Akarapu et al., 2004; Campanone and Zaritzky, 2005; Curcio et al., 2008; Hamoud-Agha et al., 2013; Zhang and Datta, 2000).

Most of the simulation models in the literature do not consider one or more of the following: (i) phase change from frozen to thawing, (ii) rotation of the turntable, (iii) detailed geometry of the cavity, and (iv) integration of the microwave model with the microbial inactivation model to assess food safety.

Most reported studies in the literature consider cooking of refrigerated meals and do not consider the phase change of thawing of frozen foods (Geedipalli et al.,2007; Ma et al., 1995; Ryynanen and Ohlsson,1996; Ryynanen et al., 2004). Because NRTE meals

contain raw and/or partially cooked ingredients, they need to be stored below 41°F (5 °C) to prevent microorganism from growing during storage. In North America, most of the NRTE meals are available in the market as frozen meals. Therefore, it is important to consider the phase change characteristics of NRTE foods in the model. One of the challenges of modeling phase change is that the dielectric properties dramatically change between frozen and thawed states and this can cause numerical convergence issues during simulation.

Currently, almost all microwave ovens have turntables. Thus, it is important to simulate the rotation of the food on the turntable. Geedipalli et al. (2007) developed a microwave heat transfer model to rotate raw potato slab kept at the center of the turntable. They demonstrated that the rotation of the turntable can improve heating uniformity by 40%. The limitations of their model include: the phase change effect was not considered as the potato was heated from room temperature; temperature-dependent dielectric properties were not considered; and a simplified geometry of the oven cavity was used. Chatterjee et al. (2007) developed a rotational mathematical model for microwave heating of containerized liquid. In their study, electromagnetic power density inside the containerized liquid was calculated using Lambert's law, which represents electromagnetic energy as planar waves. Maxwell's equations must be solved to understand hot and cold spots (multi-modes) inside the cavity.

Researchers have developed a computer simulation model using FDTD method based software QuickWave™ to calculate the electromagnetic and heat transfer field distribution in horizontally moving packages that were placed in a microwave assisted thermal sterilization system (Chen et al., 2008; Resurrecicion et al., 2013). In most cases,

FDTD based solvers are limited in simulation applications because of their inability to handle irregular geometries and boundary conditions. Whereas, FEM based solvers have been used extensively in simulating microwave heating that includes the complex geometries and boundary conditions (Liu et al., 2013). In this study, we used a FEM based numerical solver COMSOL v4.2a Multiphysics to simulate the microwave heating of a multi-component meal. However, the software is limited, in that it cannot be used to solve three-dimensional Maxwell's equations for rotating food. Therefore, we developed a three-dimensional computer simulation model to calculate the electromagnetic and heat transfer field distributions in a rotating frozen multi-component meal using a custom routine written in MATLAB.

A solution of coupled electromagnetic and heat transfer models in 3D space and time requires a great deal of computational resources. Thus far, researchers have made several simplifications in their model development approach. For example, in order to reduce the number of mesh elements required to solve the equations, many researchers have assumed the microwave cavity and waveguide as a simple geometry without considering some of the special features of microwave design, such as crevices and dimples (Geedipalli et al., 2007; Ma et al., 1995; Wäppling-Raaholt et al., 2006; Yakovlev, 2001). The modern day microwave ovens are carefully designed to include many special geometric features such as metal bumps, crevices, and a turntable in order to improve heating uniformity. Each of these features available inside the cavity can have a dramatic effect on electric field distribution. Electric field distribution is an important factor as it is the input heat source term in the heat transfer equations. Pitchai et al. (2012) have included all these features of microwave design into the model and

demonstrated the importance of including these features in modeling accuracy. Despite including all features of the microwave oven design, their work considered a homogeneous model food and did not include the rotation of food on the turntable.

As some foodborne illness outbreaks were associated with microwavable NRTE foods in the past, thermal process calculation can be useful to determine microbial inactivation during microwave heating. There have not been many published studies that attempted to integrate a microbial inactivation kinetics model and a microwave heat transfer model. As a new initiative, Hamoud-Agha et al. (2013) integrated a microwave heat transfer model with a microbial inactivation kinetics model to calculate survival of *Escherichia coli* K12 CIP 54.117 in a calcium alginate gel medium subjected to heating in a simple custom-built microwave cavity, which is not representative of a real domestic microwave oven system.

The main objective of this study was to develop a comprehensive and integrated model for a multi-component meal to predict temperature and microbial reduction during microwave heating in a domestic microwave oven. Specific objectives of this study were to:

i. develop a coupled electromagnetic and heat transfer model of a multi-component meal in a rotating turntable heated in a domestic microwave oven,
ii. validate the heat transfer model with experimental tests in terms of heating patterns and temperatures, and
iii. integrate the microwave heat transfer model with microbial inactivation kinetics model to assess food safety risk.

2.3. Model development

2.3.1. Governing equations

The electromagnetic energy distribution inside an oven cavity is governed by Maxwell's wave form equation (COMSOL, 2013).

$$\nabla\times\mu_r^{-1}\left(\nabla\times\vec{\mathbf{E}}\right) - k_0^{\,2}\left(\epsilon_r - \frac{j\sigma}{\omega\epsilon_0}\right)\vec{\mathbf{E}} = 0 \qquad (2.1)$$

An electromagnetic wave loses its energy while travelling through a lossy dielectric medium such as food. Part of the electromagnetic power is converted into thermal energy within the food. Conversion of electromagnetic energy into thermal energy is proportional to the dielectric loss factor (ε'') and square of electric field strength (Datta and Anantheswaran, 2001):

$$P_v = \pi f \varepsilon_0\, \varepsilon'' |\vec{\mathbf{E}}|^2 \qquad (2.2)$$

The dissipated power term (P_v, W/m^3) is a heat source term in transient heat transfer.

$$\rho C_p \frac{\partial T}{\partial t} = k\nabla^2 T + P_v \qquad (2.3)$$

2.3.2. Initial and Boundary conditions

Before microwave cooking, the initial temperature of the chicken nuggets and mashed potatoes was maintained at -5 °C. The surface of the multi-component meal exchanges heat with surrounding air by convection expressed as:

$$-k \frac{\partial T}{\partial n} = h\,(T - T_a) \qquad (2.4)$$

Heat exchange between air and the multi-component meal was approximated by assuming a heat transfer coefficient value of 10 $W/m^2/°C$, which is a typical value used

for natural convective heat transfer in air (Tong and Lund, 1993). To make sure this assumption was valid, the fan was turned off inside the cavity to ensure that natural convection was taking place at the air-food interface. The metallic waveguide and cavity walls are considered as perfect electric conductors, where the following boundary condition applies:

$$E_{tangential} = 0 \qquad (2.5)$$

2.3.3. Geometric model

The geometric model was developed based on a 1200 W rated power (1100 W available power measured using IEC 60705 method) microwave oven (Model no: NN – SD767W; Panasonic Corporation, Shanghai, China). The complete geometric model included oven cavity, magnetron, turntable, waveguide, crevices and metal bumps as shown in Figure 2. 1. The microwave feed port was located at the center of the right side wall of the cavity. An electromagnetic wave travels with certain patterns (modes) in the waveguide governed by the frequency and waveguide dimensions. The microwave energy field distribution prediction with the coaxial feeding is better than that with the TE_{10} mode excitation (Pitchai et al., 2012). In this study, we included the magnetron as a coaxial power source feeding microwave energy into the waveguide.

The multi-component meal consisted of nine chicken nuggets and a block of mashed potatoes placed in a PETE (Polyethylene terephthalate) tray. Chicken nuggets and mashed potatoes are popular food components among young kids and available in most of the commercially available meals. The chicken nuggets were trim cut to a uniform size as original chicken nuggets were uneven in size and shape.

2.3.4. Model assumptions

In order to simulate heat transfer in the multi-component meal during microwave heating, the following assumptions were considered.

1. The multi-component meal tray is surrounded by a cavity which has a dielectric medium of air. Air has a dielectric loss factor of zero and therefore the heat transfer was not spatially solved in the air medium. However, we considered a convective natural heat flux boundary at the food-air interface and air temperature was assumed to be constant at 20 °C.
2. Similar to air, the heat transfer analysis was not considered in the PETE tray due to the negligible dielectric loss factor ($\varepsilon'' = 0.0037$). However, the PETE tray domain was considered in the solution of electromagnetic equations since the presence of the tray does influence the electric field distribution ($\varepsilon' = 2.95$).
3. A partial-coupling method was used to solve electromagnetic and heat transfer equations, meaning that electromagnetic equations were solved for a defined time (Δt, s) to calculate the power density that feeds into the heat transfer analysis as a source term. The size of Δt corresponds to the rotation angle ($d\theta$) of the turntable. Heat transfer equations were solved at a non-linear time step based on solver convergence. Based on the temperature at the end of Δt, the dielectric constant and loss factor values were updated in the model to calculate the new electric field for the next time step.
4. The initial temperature of both chicken nuggets and mashed potatoes was considered as homogeneous and isotropic.
5. The mass and momentum transfer of moisture were not considered.

6. Simulation was performed by considering a single 2.45 GHz magnetron frequency. The summarized information of initial conditions and material properties of computational domains is given in Table 2. 1.

2.3.5. MATLAB-COMSOL interface for simulating rotation

The COMSOL Multiphysics® v4.3a software did not have the capability to simulate microwave heating of rotating food. The electromagnetic module of COMSOL Multiphysics® 4.3a was not compatible with the software's inherent moving mesh which enables the rotation of object in the computation domain. To overcome the issue of not being able to rotate the food on the turntable during electromagnetic simulation in COMSOL Multiphysics®, we developed an approach to use the MATLAB (MathWorks® Inc., Natick, MA) based algorithm to rotate the three dimensional food sample within the computational domain. MATLAB was interfaced with COMSOL Multiphysics® software (COMSOL Inc., Boston, MA) to simulate microwave heating of rotating food on the turntable. It was assumed that the PETE tray with food moves at a discrete angle instantaneously after being heated for a time step (Δt, s). One complete rotation of the tray on the turntable was measured to take 10 s. At the end of each time step (Δt , s), the temperature field in the food domain was saved along with their coordinates. Next, COMSOL Multiphysics® software called the MATLAB routine to rotate the food to the next discrete angle (dθ) (Eqs. 2.6 and 2.7) and initialized the temperatures from the previous time step.

$$X' = X\cos(d\theta) - Y\sin(d\theta) \qquad (2.6)$$

$$Y' = X\sin(d\theta) + Y\cos(d\theta) \qquad (2.7)$$

Where X and Y are the coordinates of the current angular location of the rotating food, X' and Y' refer to the coordinates of subsequent location of the rotated food, and $d\theta$ is the rotation angle.

Using the new temperature field, electric field distribution followed by temperature field was determined in COMSOL for the next time step (Figure 2. 2). This loop is continued, until the full heating time is reached.

2.3.6. Simulation strategy

Solving coupled non-linear electromagnetic wave and heat transfer equations requires an iterative computational technique to perform the simulation. A Generalized Minimal Residual (GMRES) method based iterative solver was used to solve electromagnetic and heat transfer equations. Time-averaged electric field strength was calculated by solving Maxwell's electromagnetic wave equation for a defined time step in the entire space domain and was used in Eq. 2.2 to calculate dissipated power density. In heat transfer analysis, dissipated power density is updated in Eq. 2.3 to calculate temperature field. In the current time step, thermal properties of the food are updated with respect to changes in the temperature field. As explained in the previous section, electromagnetic properties are updated based on the new temperature field in solving electric fields and dissipated power density at each rotational step. This cyclic process continues until a desired heating time is reached. The simulations were performed on a Dell Precision T7500 workstation with an operating memory of 72 GB RAM running on two quad-core Intel Xeon X5570 2.93 GHz frequency processor.

2.3.7. Meshing scheme

Meshing is an important step in obtaining reasonable results from numerical simulation. Various meshing schemes for different domains were implemented to ensure the simulation results were independent of the meshing. Air, glass turntable and PETE tray domains were assigned with free tetrahedral elements, food components (chicken nuggets and mashed potatoes) were assigned with quadrilateral elements (Figure 2. 3). Two meshes with different refinement levels were enforced for free tetrahedral elements (i.e., normal: air domain, size: 8 mm; finer: glass turntable and PETE tray domains, size: 2 mm). Quadrilateral mesh was provided to food component domains because they did not have any complex shape characteristics. Liu et al. (2013) stated that the best finite element mesh size in dielectric material for faster computational time and good accuracy temperature prediction at 2450 MHz was found to have the relationship with the free space wavelength (λ = 12.22 cm), and dielectric constant of food as described in Eq. 8.

$$h_{es} = \frac{\lambda}{6\sqrt{\varepsilon'}} \qquad (2.8)$$

According to the Eq. 8, best mesh size in chicken nuggets and mashed potatoes can be as 2.8 mm, and 3.33 mm, respectively. Therefore, the element size of chicken nuggets and mashed potatoes was maintained at 2 mm. In all the domains, minimum element quality was ensured to be > 0.02, which is recommended for faster convergence in the COMSOL Multiphysics® (COMSOL, 2013). The multi-component meal consisted of about 55,600 quadrilateral elements out of the 270,000 total elements. This meshing scheme provided relatively faster solution convergence compared to meshing of all domains containing free tetrahedral elements.

2.3.8. Effect of rotation angle

The rotation of the food on the turntable is a continuous process. In the numerical simulation, the continuous process of microwave heating is not achieved using COMSOL Multiphysics® software. Thus, the continuous process of rotating food on the turntable was approximated by moving the food tray by a discrete angle in which location of the food on the turntable changes over time. As a result, the food tray was at a different orientation at each rotational step within a one complete rotation. Finding the appropriate rotation angle of the food tray is a critical factor in optimizing simulation time as well as accurate temperature prediction. The smaller the discrete angle used for rotating the food, the longer the simulation time and vice versa. There exists a standing wave pattern inside the cavity due to interference of microwaves. Larger discrete angles may miss some of the hot or cold spots of the standing wave pattern and therefore the dissipated power density calculation may not be accurate. Therefore, finding the optimized rotation angle is a critical factor to minimize the simulation time and to predict better temperature distribution. In this work, we studied the effect of rotational angle on temperature prediction by rotating the food tray at three different discrete angles: 30°, 45° and 60°.

2.3.9. Model accuracy measurement

Model accuracy measurement was calculated by comparing the deviation between the simulated and experimental temperatures in different points over time t. The simulated temperature profile obtained for 2.45 GHz was compared with the averaged experimental temperature profile and root mean square error (RMSE) was calculated as:

$$RMSE = \sqrt{\frac{1}{n} \sum_{i=1}^{n} (T_p - T_0)^2} \quad (2.9)$$

2.3.10. Microbial inactivation kinetics model

Inactivation kinetics of microorganisms in batch systems is expressed by D and z values under the isothermal conditions. Thermal inactivation of microorganisms during microwave heating of non-isothermal conditions can be expressed using thermal death time (Bigelow, 1921).

$$F = \int_0^t 10^{\frac{(T_t - T_{Ref})}{z}} dt \quad (2.10)$$

In this approach, the thermal death time (F) is determined by integrating exposure time at various temperatures, T_t, to time at a reference temperature, T_{Ref}.

Twenty-three cases of *Salmonella* Heidelberg outbreak were reported in early 2003 in British Columbia, Canada. That outbreak was associated with consumption of frozen chicken nuggets or strips (Leitch, 2008). To determine microbial inactivation level, we used a reported D-value of 0.15 at 62 °C min and z value of 4.73 °C of *Salmonella* Heidelberg calculated for chicken nuggets (Bucher et al., 2008). There were no cases of outbreak from mashed potatoes reported in the literature; hence, microbial inactivation was not studied for mashed potatoes.

2.4. Experimental methodology

2.4.1. Sample preparation

Chicken nuggets were purchased from a local grocery store (Brand name: Great Value™ Fully Cooked; Wal-Mart Stores, Inc., Bentonville, AR) and trim cut into uniform sizes (31.8×25.4×16.0 mm). Mashed potato flakes (IDAHOAN real premium mashed potatoes, Idahoan Foods, Idaho Falls, ID) were mixed with water (53.5%), margarine (4.1%), and whole milk (18.6%). The milk and water were heated to 60 °C on a hot plate and margarine was added. The solution was stirred for 2-3 min to make the mixture more homogenous. The hot solution was then poured over the dry potato flakes, which were contained in a bowl. The solution and potato flakes were mixed using a mechanical stirrer for 5 min to thoroughly blend the mashed potatoes. A 154 g portion of the prepared mashed potatoes was placed on one side of the tray and shaped into a 38.1×101.6×16.0 mm block. The prepared trays were tightly covered with shrink-wrap and stored at -5 °C in a freezer until used.

2.4.2. Dielectric properties

The dielectric properties of the chicken nuggets and mashed potatoes were measured using a vector network analyzer (VNA) (PNA-5230A, Agilent Technologies, Englewood, CO) attached to an open-ended coaxial high-temperature probe. The high-temperature probe was calibrated using the references by air/50 Ω short/deionized water protocol before each measurement session as previously described (Blackham and Pollard, 2002). The VNA was configured to take 201 measurements uniformly spaced between 10 and 3000 MHz frequency. A 30 g sample was placed inside the stainless-steel jacketed test cell (20 mm inner diameter, 92 mm height). A firm contact between

the high-temperature probe and the sample during measurement was ensured by a spring loaded stainless-steel piston on the bottom of the test cell. Dielectric properties were measured from -10 °C to 100 °C at every 10 °C interval. The sample temperature in the test cell was maintained by circulating silicone oil through a programmable oil bath in the test cell jacket. Three replicates were carried out and average values of the dielectric properties were used in the simulation. The dielectric properties of the PETE tray were measured using a split-post dielectric resonator fixture (SPDR, operating resonant frequency: 2500 MHz, QWED Sp. z o.o, Warsaw, Poland) connected with a vector network analyzer (PNA-5230A, Agilent Technologies, Englewood, CO). A measurement procedure was followed to measure dielectric properties of the PETE tray as previously described by Jacob et al., 2006.

2.4.3. Thermophysical properties

The specific heat capacity of the chicken nuggets and mashed potatoes was measured by the differential scanning calorimetry method in accordance with the ASTM standard E1269-01. Measurements were carried out using a Pyris 1 Differential Scanning Calorimeter (DSC) equipped with an Intracooler 1P refrigeration unit (Perkin-Elmer, Inc., Norwalk, CT, USA). Nitrogen gas was used to flush the sample holder and the DSC unit was calibrated using indium. Three individual (10 mg) samples were scanned from -10 °C to 110 °C at a heating rate of 5 °C/min in stainless steel pans (Perkin-Elmer Corp., Norwalk, CT, USA) using an empty pan as the reference.

The thermal conductivity of the chicken nuggets and mashed potatoes was measured, as a function of temperature, using a KD2 Pro thermal properties analyzer (Decagon Devices, Inc., Pullman, WA, USA). Before each experiment, the calibration of

the TR-1 probe was verified using an acetal plastic standard recommended by the manufacturer. Samples were filled in a 30 cm diameter copper tube and immersed in a hot water bath maintained at a desired temperature. The calibrated TR-1 probe was used to measure thermal conductivity at every 10 °C from -10 °C to 100 °C. To measure the thermal conductivity of frozen samples, the TR-1 probe was inserted into samples maintained at -10, -5, and 0 °C in a temperature controlled freezer.

2.4.4. Experimental validation

The frozen multi-component meal tray was taken out of the freezer and subjected to 90 s of microwave heating. The transient temperature at seven locations was recorded using fiber-optic sensors (8-channel signal conditioner, FISO Technologies Inc., Quebec, Canada). Five sensors were inserted into chicken nuggets and two sensors into the mashed potatoes sample (as shown in Figure 2. 4) to record transient temperature profiles during heating. To validate, all of the sensors were at the same locations within the samples in each replication, a 2 mm drill bit was inserted from the top surface of the sample to the desired depth to make a hole. Through the holes, fiber-optic sensors were then inserted and sealed with a septum tape. This ensured that the sensors were properly inserted at predefined locations in all replications. Immediately upon completing microwave heating, a thermal image of the top surface of the meal was captured using an infrared camera (SC640, 640× 480 pixels accuracy ±2°C, FLIR systems, Boston, MA). Stand-alone software, FLIR ThermaCAM™ Researcher v2.9, was used to acquire thermal images of the heated meal.

2.5. Results and Discussion

2.5.1. Dielectric and thermal properties

The temperature-dependent dielectric constants of chicken nuggets and mashed potatoes measured at domestic microwave frequency of 2.45 GHz are shown in Figure 2. 5. For both the food components, in the frozen temperature range, the dielectric constant increased exponentially from the lowest values at frozen state (-10 °C) to the highest values at the thawed state and then the values were not changing significantly as the temperature increased from 10 to 110 °C. The temperature-dependent dielectric loss factors of chicken nuggets and mashed potatoes measured at the domestic oven microwave frequency of 2.45 GHz are shown in Figure 2. 6. From -10 to 0 °C, the dielectric loss factors of both food components exponentially increased. Above 0 °C, the dielectric loss factors of both food components decreased slightly and then linearly increased.

The specific heat capacities of chicken nuggets and mashed potatoes as a function of temperature from -10 °C to 110 °C are shown in Figure 2. 7. From -10 to 0 °C, the specific heat capacities of chicken nuggets and mashed potatoes increased from 2.7 to 8.9 and 4.7 to 30.0 kJ. kg^{-1}. $°C^{-1}$, respectively. The first peak of specific heat capacity represents the phase change from frozen to thawed state. By determining the area under the peak from the onset temperature of -5 °C to the end temperature of 5 °C, the latent heat of fusion was determined as 183.91 kJ. kg^{-1} for mashed potatoes. Whereas, using the area under the peak with the onset temperature of -5 °C and the end temperature of 20 °C, latent heat of fusion of chicken nuggets was calculated as 187.85 kJ. kg^{-1}. From 20 to 100 °C, the specific heat capacity increased linearly from the value of 4.6 to 13. 2 kJ·

$Kg^{-1}\cdot°C^{-1}$ in mashed potatoes, whereas specific heat capacity did not change in chicken nuggets. At around 100 °C, the second phase change effect, latent heat of evaporation was shown in both chicken nuggets and mashed potatoes. The latent heat of fusion and vaporization will delay the temperature rise during phase change. Both the latent heat of fusion and vaporization of mashed potatoes are higher than those of chicken nuggets, which can be attributed to the higher moisture content of mashed potatoes. The thermal conductivities of chicken nuggets and mashed potatoes as a function of temperature from -10 to 100 °C are shown in Figure 2. 8. The thermal conductivities of both chicken nuggets and mashed potatoes were decreased exponentially from the temperature of -10 to 0°C, and then stayed constant at around 0. 48 $W\cdot m^{-1}\cdot °C^{-1}$.

2.5.2. Effect of rotation angle on temperature prediction

Typically, the computational time increases, as more discrete angles for rotating the food tray are used. Using a larger discrete angle may miss the food from experiencing the actual standing wave patterns inside the cavity, and therefore dissipated power density calculation may not be accurate. Thus, it was important to find the optimal discrete angle to minimize the computational time and predict better temperature history. As shown in Figure 2. 10, the simulated transient temperature profile at a 60° discrete angle for both chicken nuggets and mashed potatoes diverges from the 30° and 45° temperature profiles. Simulated temperature profile at large discrete angle shows divergence because it did not capture the actual electromagnetic field variation. The comparison of temperature after 60 s of microwave heating demonstrated that the difference between 30° and 45° discrete angles was less than 1 °C and 4 °C in chicken nuggets and mashed potatoes, respectively, whereas the difference between 45° and 60°

discrete angles was more than 32 °C and 10 °C, respectively (Figure 2. 9). For 60 s of microwave heating, rotating at a 45° angle step took about 7 h of computational time, whereas a 30° angle took about 10 h computational time. Considering the reduction in computational time at a 45° discrete angle and difference in temperature prediction between 30° and 45° discrete angles, a 45° angle discrete angle was chosen for the validation study. In this study, each simulation consumed about 10 GB memory out of 72 GB available memory.

2.5.3. Spatial temperature profile

The simulated spatial temperature profile of a multi-component meal was compared with three replicates of experimental temperature profiles obtained using a thermal imaging camera (Figure 2. 10). Three replicates of experimental temperature profiles consistently showed the locations of hot and cold patterns in the multi-component meal. In particular, a major portion of mashed potatoes did not reach higher temperature and remained around 30 °C even after 90 s of microwave heating, whereas the temperature exceeded 72 °C in chicken nuggets except in the center and right-of-center nuggets. Similarly, the simulated spatial temperature profile shows a major portion of mashed potatoes did not reach higher temperature except on the edges. Similar to the experimental profile, the center and right-of-center chicken nuggets did not receive higher temperatures and remained around 30 °C in the simulated temperature profile. The major portion of mashed potatoes did not receive higher temperatures because of the higher latent heats of fusion and evaporation calculated from the specific heat capacity profile. The chicken nuggets did heat to above 75 °C temperature because of lower latent heats of fusion and evaporation. The maximum temperature of the simulated temperature

profile continued to increase above 100 °C particularly in chicken nuggets, whereas the maximum temperature in the experimental profiles remained at around 75 °C. As mass and momentum transfer (evaporative moisture loss) was not considered in the model physics, it is expected that some locations in the simulation would reach a temperature above 100 °C. Non-uniform heating persisted even after rotating the multi-component meal during heating. A simple placement of a multi-component meal would not guarantee uniform heating in a domestic microwave oven even after imparting rotation of the turntable. However, a simulation model could help in optimizing the product layout, thickness and modifying the properties of the food system (ingredients) to achieve more uniform heating. Overall, simulated spatial temperature profiles thermal patterns were in agreement with the experimental thermal images.

2.5.4. Transient-temperature profile

Transient temperature profiles at seven points were compared with the simulated temperature profiles. Figure 2. 11 compares three replicates of experimental and simulated transient temperature profiles at seven locations. Except at locations C3, M1 and M2, all other locations simulated transient temperature profiles fall within a standard deviation of the three replicates of the experimental profiles. Interestingly, the locations of the C1 and C5 experimental transient temperature profile show the trend of a sigmoidal curve because of latent heat of thawing and evaporation of chicken nuggets. Some of the discrepancy in the experimental transient temperature profile might be attributed to thermal lag of the fiber-optic sensors. The simulated transient temperature profiles showed a phase-change effect in their trend (change in slope around the thawing region) similar to experimental profiles. This indicates that the microwave physics and

solution techniques implemented in the model were correct. Simulated transient temperature profiles showed ripple effects in their trend at all locations. The ripple effect in the transient temperature profile might be attributed to the alternating hot and cold spots at each discrete angle. Similar ripple effects in the simulated transient temperature profile of rotating potatoes were seen in the figures reported by Geedipalli et al., (2007). Even though they used a 15° discrete angle, the magnitude of the ripple was higher compared to the one in the study. Thus, even the smaller discrete angle does not help much in removing the ripple effect; however, it increases computational time significantly.

The root mean square error (RMSE) was calculated using averaged experimental time-temperature profiles in comparison with simulated time-temperature profiles for each location using Eq. 2.9. The RMSE values and end temperature difference calculated for seven locations were given Table 2. 2. The RMSE values ranged from 5.8 °C to 26.2 °C in chicken nuggets whereas, RMSE values in mashed potatoes were 4.3 °C and 4.7 °C in locations M1 and M2, respectively. Some of the errors in model predictions can be attributed to the difficulty in maintaining the consistency of probe locations and the resulting consistency in spatially specific measurement during heating. This, in fact, is the biggest challenge in real-time temperature measurement during microwave cooking using fiber-optic probes, because a small movement or change of location of the probes in the sample might result in substantial changes in the measured temperature. The steam pocket developed during heating could also push the probe and cause errors in experimental measurement. In addition, discrepancies in experimental and simulated temperature can be attributed by assumption of single frequency of the magnetron. The

magnetron generates a bandwidth of 50 MHz around the 2.45 GHz central frequency, and the actual frequency and bandwidth could change in coupling with various foods. The end point temperature is an important value in terms of food safety, because of microbial inactivation rate is much faster at higher temperature than at lower temperatures. Table 2. 2 shows the end point temperature difference at seven locations. The model over-predicts at five out of seven locations. The temperature over prediction is attributed by neglecting moisture loss in the model. This effect can be clearly visualized from location C1 where the simulated temperature kept rising above 100 °C whereas the experimental temperature stabilizes around 95 °C.

2.5.5. Integrated microbial inactivation model

Poultry products must be subjected to an adequate cooking or processing step to achieve at least 7-log reductions of *Salmonella* (USDA-FSIS, 2012). The RMSE values of time-temperature profile calculated in chicken nuggets ranged from 5.8 °C to 26.2 °C. To interpret the validation from a microbial inactivation point of view, simulated and experimental transient temperature profiles were provided as inputs to Eq. 2.10 to calculate time to achieve ≥ 7-log reduction of *Salmonella* Heidelberg. The mid-point temperature rule was used to calculate lethality rate between two consecutive time-temperature points. Figure 2. 12 compares time needed to achieve ≥ 7 log reduction of *Salmonella* Heidelberg in chicken nuggets. It can be inferred that time calculated to achieve ≥ 7 -log reductions from the simulation profile falls within experimental error variation while at location C5 over-predicted the time. Though the simulation over-predicts the temperature compared to the experimental profile, lethality rate from the experimental transient temperature profile is faster because of the profile trend (sigmoidal

curve). On an average, simulation results showed that the time required for achieving ≥ 7-log reduction of *Salmonella* Heidelberg was 59 s, while the experiment indicated it took 54 s. Thus, the simulation prediction in terms of microbial reduction level was well in agreement with the experiment conditions.

Due to the non-uniform heating persisted in the multi-component meal after microwave heating, it is important to validate the temperature in microbial point of view as a function of space coordinates. Hamound-Agha et al. (2013) stated that microbial inactivation was not efficient in microwave heating due to the inherent non-uniform heating and therefore accurate location of cold point within the product is highly necessary for determining thermal inactivation of microorganism undergoing microwave treatment. Figure 2. 10 clearly shows that center chicken nuggets (C3) was not reaching baseline temperature of 72 °C to reduce the population of *Salmonella* Heidelberg by 7-log. Figure 2. 12 does not include C3, because the simulation temperature reached only 35 °C and therefore the time needed to achieve 7-log reduction of *Salmonella* Heidelberg is infinity. In the experiments, two out of three replications reached temperatures above 72 °C, while the third replication reached a temperature reached 63.5 °C. Therefore if microorganisms are present in the center chicken nugget, that microorganism may survive after 90 s of heating of this multi-component meal and cause foodborne illness. Thus, microbial safety of food products undergoing microwave treatment cannot be assured by measuring the point temperature profiles only in few locations. Model simulations can help identify the location of cold spots and the model can estimate temperature at several locations within the food product.

2.6. Conclusions

A partially coupled electromagnetic and heat transfer model was developed to simulate rotation of a multi-component meal consisted of chicken nuggets and mashed potatoes on the turntable, considering a single frequency of 2.45 GHz. A custom-built MATLAB routine was developed to rotate the food tray on the turntable. The effect of rotation angle on temperature predictions was studied and 45° rotation angle was found to be optimal. Simulated spatial temperature profile was found to be in good agreement with experimental spatial temperature profile. The root mean square error values ranged from 5.8 °C to 26.2 °C in chicken nuggets as compared 4.3 °C to 4.7 °C in mashed potatoes. The predicted and experimental temperature profiles were provided as inputs to a microbial inactivation kinetics model for *Salmonella* Heidelberg to assess food safety of chicken nuggets cooked by microwave heating. The model can be used to identify cold spot locations and can be used by food product developers for optimizing food composition and package design to achieve more uniform heating.

Acknowledgements

The authors gratefully acknowledge the financial support provided by the USDA CSREES – NIFSI Grant (Project Number: 2008-51110-04340). The authors would like to thank ConAgra Foods, Inc., Omaha, for providing the equipment and facility to measure the dielectric properties of food components.

Nomenclature

$\|\vec{\mathbf{E}}\|$	the time-harmonic electric field strength (V/m)
μ_r	relative permeability
ϵ_r	relative permittivity
k_o	wave number
σ	electrical conductivity (S/m)
ω	angular frequency (rad/s)
ε_0	free space permittivity (8.854×10-12 F/m)
P_v	dissipated power per unit volume (W/m3)
f	frequency (Hz)
ε''	relative dielectric loss factor
ρ	density (kg/m^3)
C_p	specific heat capacity at constant pressure (kJ/kg °C)
k	thermal conductivity (W/m °C)
T	temperature (°C) at simulation time t
n	normal to the direction
h	surface convective heat transfer coefficient (W/ m^2 °C)
T_a	ambient temperature (°C)
Δt	simulation time step (s)
h_{es}	best element mesh size in dielectric material, mm
λ	free space wavelength, cm

RMSE	root mean square error (°C)
T_p	simulated point temperature (°C)
T_o	averaged experimental point temperature (°C)
F	thermal death time (min)
T_t	Transient point temperature (°C) at particular time t
T_{Ref}	Reference temperature (°C) at which microorganism inactivated
dt	time interval between two consecutive temperature points (s)
z	Temperature required to reduce microbial population by 1 log (°C)

2.7. References

Akarapu, R., Li, B.Q., Huo, Y., Tang, J., & Liu, F. (2004). Integrated modeling of microwave food processing and comparison with experimental Measurements. Journal of Microwave Power and Electromagnetic Energy, 39(3/4), 153-165.

Bigelow, W. (1921). The logarithmic nature of thermal death time curves. The Journal of Infectious Diseases, 29(5), 528-536.

Blackham, D.V., & Pollard, R.D. (2002). An improved technique for permittivity measurements using a coaxial probe. IEEE Transactions on Instrumentation and Measurement, 46(5), 1093-1099.

Bucher, O., D'Aoust, J., & Holley, R.A. (2008). Thermal resistance of *Salmonella* serovars isolated from raw, frozen chicken nuggets/strips, nugget meat and pelleted broiler feed. International journal of food microbiology, 124(2), 195-198.

Campanone, L.A., & Zaritzky, N.E. (2005). Mathematical analysis of microwave heating process. Journal of Food Engineering, 69(3), 359-368.

CDC. (2008). Morbidity and Mortality Weekly Report. , 57(47), 1273-1296.

Chatterjee, S., Basak, T., & Das, S.K. (2007). Microwave driven convection in a rotating cylindrical cavity: A numerical study. Journal of Food Engineering, 79(4), 1269-1279.

Chen, H., Tang, J., & Liu, F. (2008). Simulation model for moving food packages in microwave heating processes using conformal FDTD method. Journal of Food Engineering, 88(3), 294-305.

COMSOL. (2013). COMSOL Multiphsics v4.3a manual.

Curcio, S., Aversa, M., Calabrņ, V., & Iorio G. (2008). Simulation of food drying: FEM analysis and experimental validation. Journal of Food Engineering, 87(4), 541-553.

Dinčov, D.D., Parrott, K.A., & Pericleous, K.A. (2004). A new computational approach to microwave heating of two-phase porous materials. International Journal of Numerical Methods for Heat and Fluid Flow, 14(6), 783-802.

Geedipalli, S.S.R., Rakesh, V., & Datta, A.K. (2007). Modeling the heating uniformity contributed by a rotating turntable in microwave ovens. Journal of Food Engineering, 82(3), 359-368.

Guan, D., Plotka, V.C., Clark, S., & Tang, J. (2002). Sensory evaluation of microwave treated macaroni and cheese. Journal of Food Processing and Preservation, 26(5), 307-322.

Hamoud-Agha, M.M., Curet, S., Simonin, H., & Boillereaux, L. (2013). Microwave inactivation of Escherichia coli K12 CIP 54.117 in a gel medium: experimental and numerical study. Journal of Food Engineering, 116(2), 315-323.

International Electrotechnical Commission (IEC). (1999). Household microwave ovens - methods for measuring performance. IEC publication 60705.

Jacob, M., Krupka, J., Derzakowski, K., & Mazierska, J. (2006). Measurements of thin polymer films employing split post dielectric resonator technique. In Microwaves, Radar & Wireless Communications, MIKON 2006, 229-231, May 22-26.

Knoerzer, K., Regier, M., & Schubert, H., 2008. A computational model for calculating temperature distributions in microwave food applications. Innovative Food Science and Emerging Technologies, 9(3), 374-384.

Kopyt, P., & Celuch-Marcysiak, M. (2003). FDTD modelling and experimental verification of electromagnetic power dissipated in domestic microwave ovens. Journal of Telecommunications and Information Technology, 1, 59–65.

Leitch, S. (2008). Microwave Instructions for Prepared but Not-Ready-To-Eat Foods - It's Just Not Worth The Risk. Food Regulations in the United States, 1-17.

Liu, S., Fukuoka, M., & Sakai, N. (2013). A finite element model for simulating temperature distributions in rotating food during microwave heating. Journal of Food Engineering. 115(1), 49-62.

Ma, L., Paul, D.L., Pothecary, N.M., Railton, C.J., Bows, J., Barratt, L., Mullin, J., & Simons, D. (1995). Experimental validation of a combined electromagnetic and thermal FDTD model of a microwave heating process. IEEE Transactions on Microwave Theory and Techniques, 43 (11), 2565-2572.

Pitchai, K., Birla, S., Subbiah, J., Jones, D., & Thippareddi, H. (2012). Coupled electromagnetic and heat transfer model for microwave heating in domestic ovens. Journal of Food Engineering. 112(1-2), 100-111.

Resurreccion, Jr F., Tang, J., Pedrow, P., Cavalieri, R., Liu, F., & Tang, Z. (2013). Development of a computer simulation model for processing food in a microwave assisted thermal sterilization (MATS) system. Journal of Food Engineering, 118, 406-416.

Ryynänen, S., & Ohlsson, T. (1996). Microwave heating uniformity of ready meals as affected by placement, composition, and geometry. Journal of Food Science, 61(3), 620-624.

Ryynänen, S., Risman, P., & Ohlsson, T. (2004). Hamburger composition and microwave heating uniformity. Journal of Food Science, 69(7), 187-196.

Tilford, T., Baginski, E., Kelder, J., Parrott, K., & Pericleous, K. (2007). Microwave modeling and validation in food thawing applications. The Journal of Microwave Power and Electromagnetic Energy, 41(4), 30-45.

Tong, C.H., & Lund, D.B. (1993). Microwave heating of baked dough products with simultaneous heat and moisture transfer. Journal of Food Engineering, 19(4), 319-339.

USDA-FSIS. (2012). FSIS Salmonella compliance guidelines for small and very small meat and poultry establishments that produce ready-to-eat (RTE) products, 1-22.

USDA-FSIS. (2010). Iowa Firm Recalls Frozen Chicken Products Due to Possible Salmonella
Contamination. Recall Release: FSIS-RC-036-2010.
http://www.fsis.usda.gov/News_&_Events/Recall_036_2010_Release/index.asp

USDA-FSIS. (2007). Ohio Firm Recalls Frozen Meat Pizzas Due to Possible E. Coli O157:H7
Contamination. Recall Release: FSIS-RC-049-2007.
http://www.fsis.usda.gov/News_&_Events/Recall_049_2007_Release/index.asp

Venkatesh, M., & Raghavan, G. (2004). An overview of microwave processing and dielectric properties of agri-food materials. Biosystems Engineering, 88(1), 1-18.

Wäppling-Raaholt, B., Scheerlinck, N., Gait, S., Banga, J.R., Alonso, A., Balsa-Canto, E., Van, I. (2002). A combined electromagnetic and heat transfer model for heating

of foods in microwave combination ovens. Journal of Microwave Power and Electromagnetic Energy, 37(2), 97-111.

Wäppling-Raaholt, B., Risman, P., Ohlsson, T. (2006). Microwave heating of ready meals–FDTD simulation tools for improving the heating uniformity. Advances in Microwave and Radio Frequency Processing, 243-255.

Yakovlev, V.V. (2001). Efficient electromagnetic models for systems and processes of microwave heating. In International Seminar on Heating by Internal Sources, Padova, Italia, Sept 11-14.

Zhang, H., & Datta, A.K. (2003). Microwave power absorption in single-and multiple-item foods. Food and Bioproducts Processing, 81(3), 257-265.

Zhang, H., & Datta, A.K. (2000). Coupled electromagnetic and thermal modeling of microwave oven heating of foods. Journal of Microwave Power and Electromagnetic Energy, 35(2), 71-85.

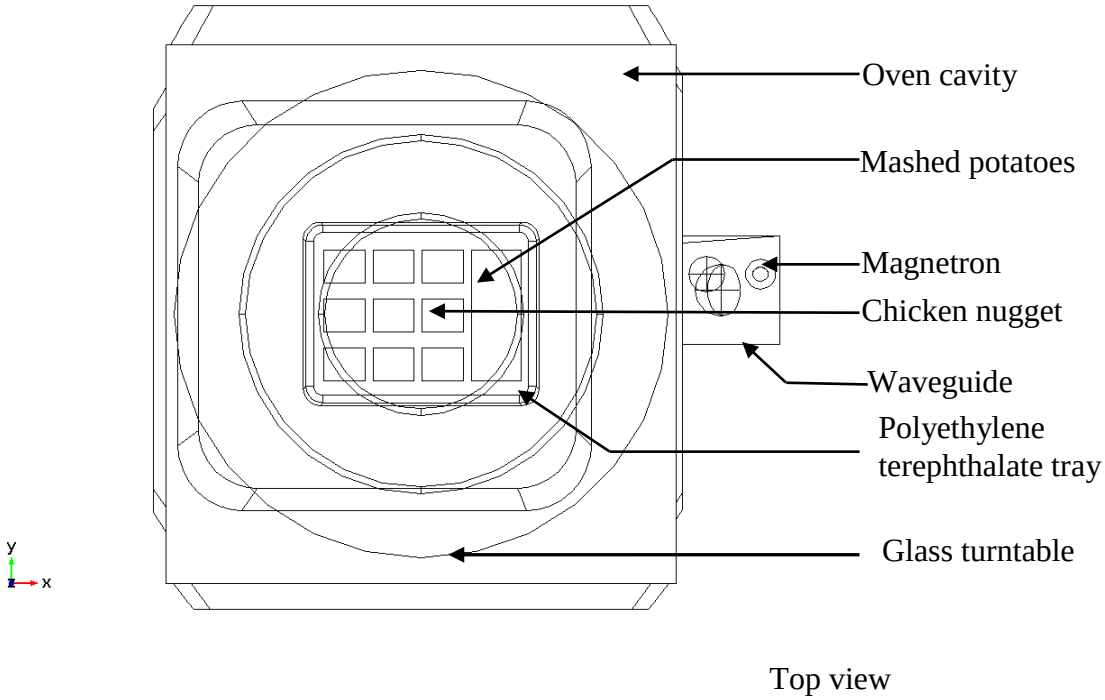

Figure 2. 1. Geometric model of 1200 W rated power microwave oven **(**Model no: NN-SD767W, Panasonic Corporation) with magnetron as coaxial feed source.

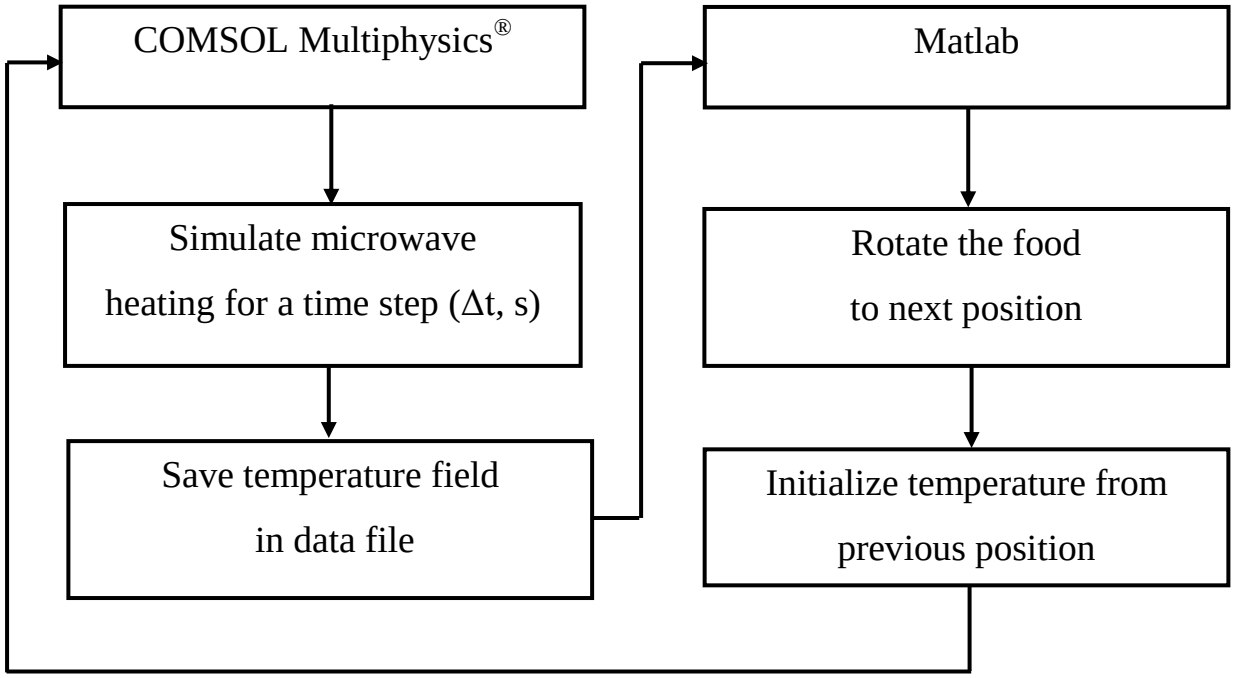

Figure 2. 2. COMSOL-MATLAB interface depicting simulation strategy for rotating food in the turntable.

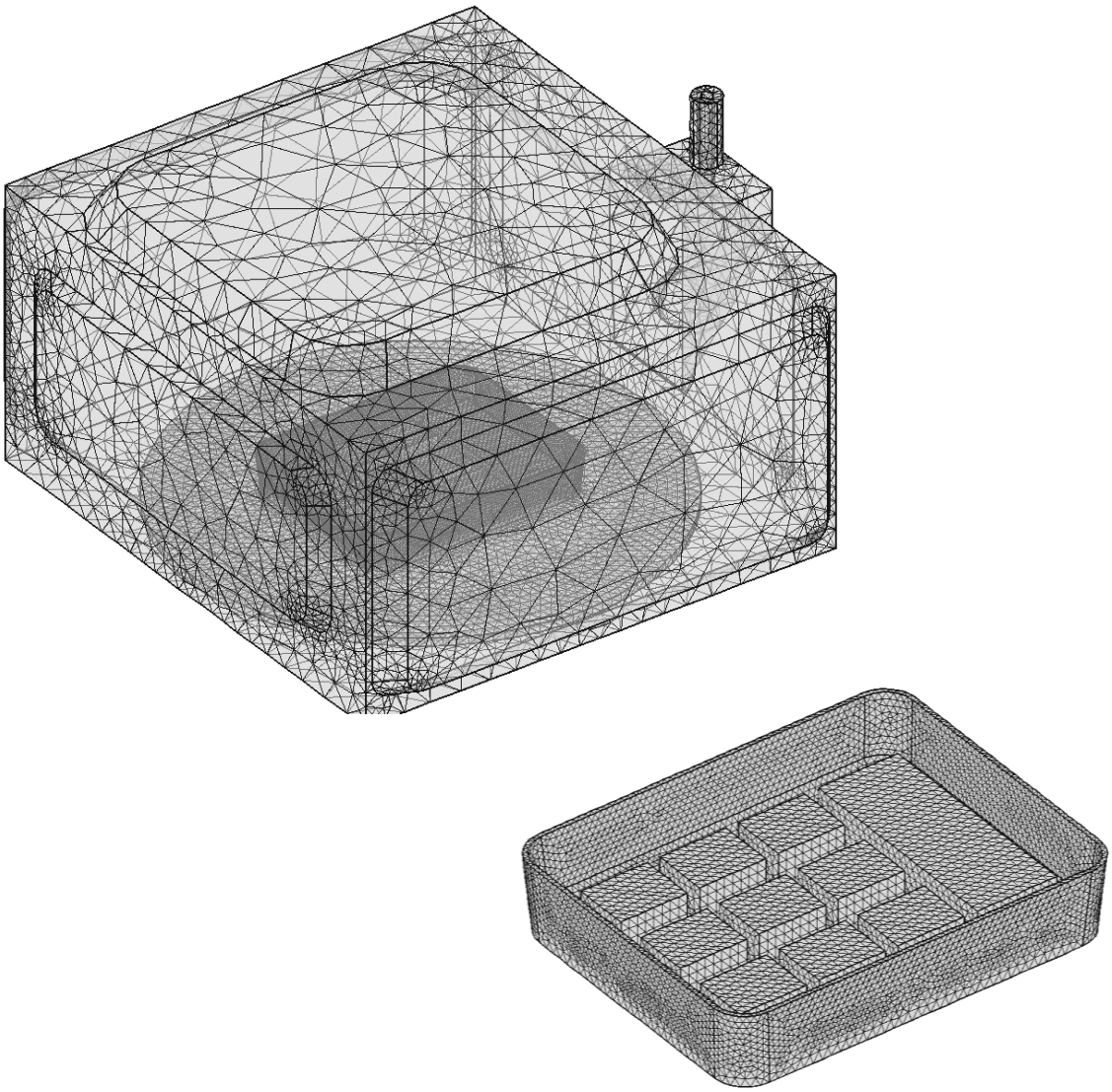

Figure 2. 3. Meshing scheme implemented for the oven cavity and multi-component meal tray.

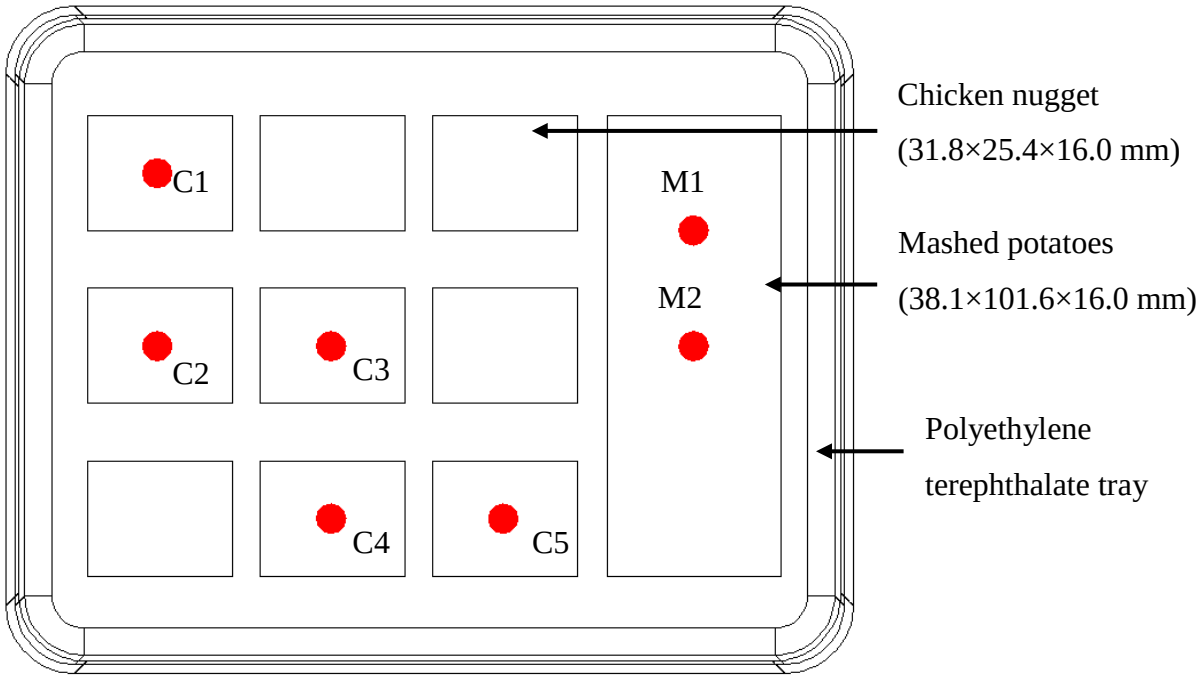

Figure 2. 4. Location of the fiber-optic sensors in food components (all sensors inserted 8 mm from the top surface and diameter of the sensors is 1.7 mm).

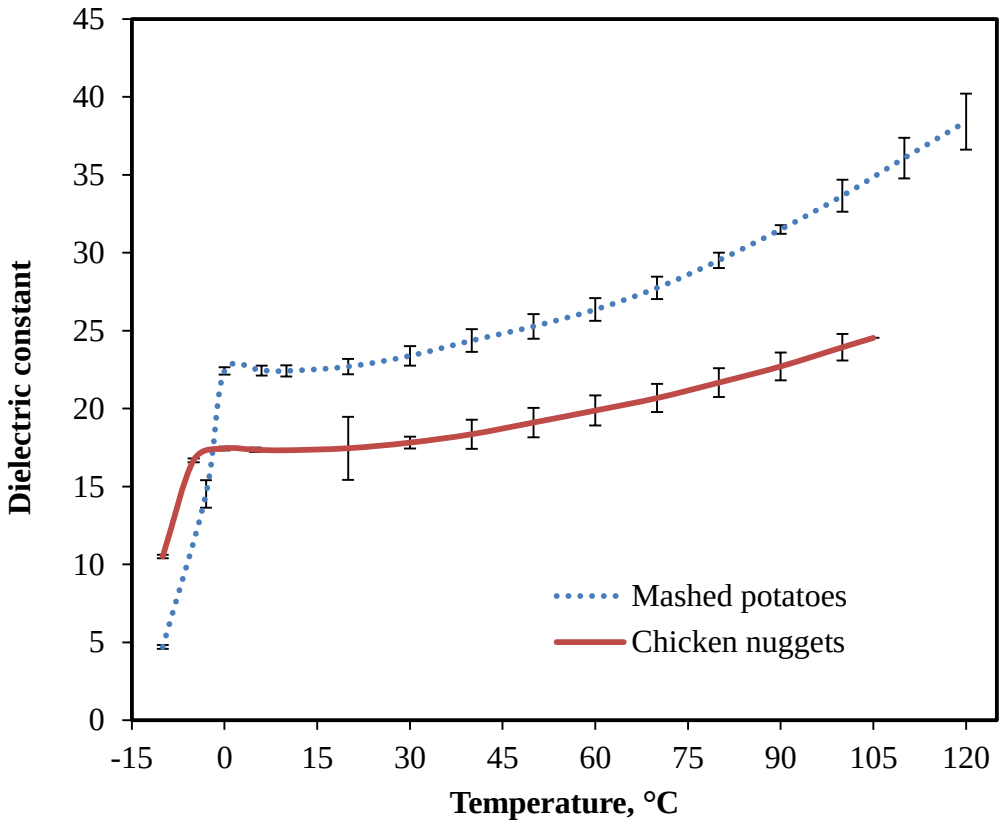

Figure 2. 5. Temperature-dependent dielectric constant of chicken nuggets and mashed potatoes measured at 2.45 GHz frequency.

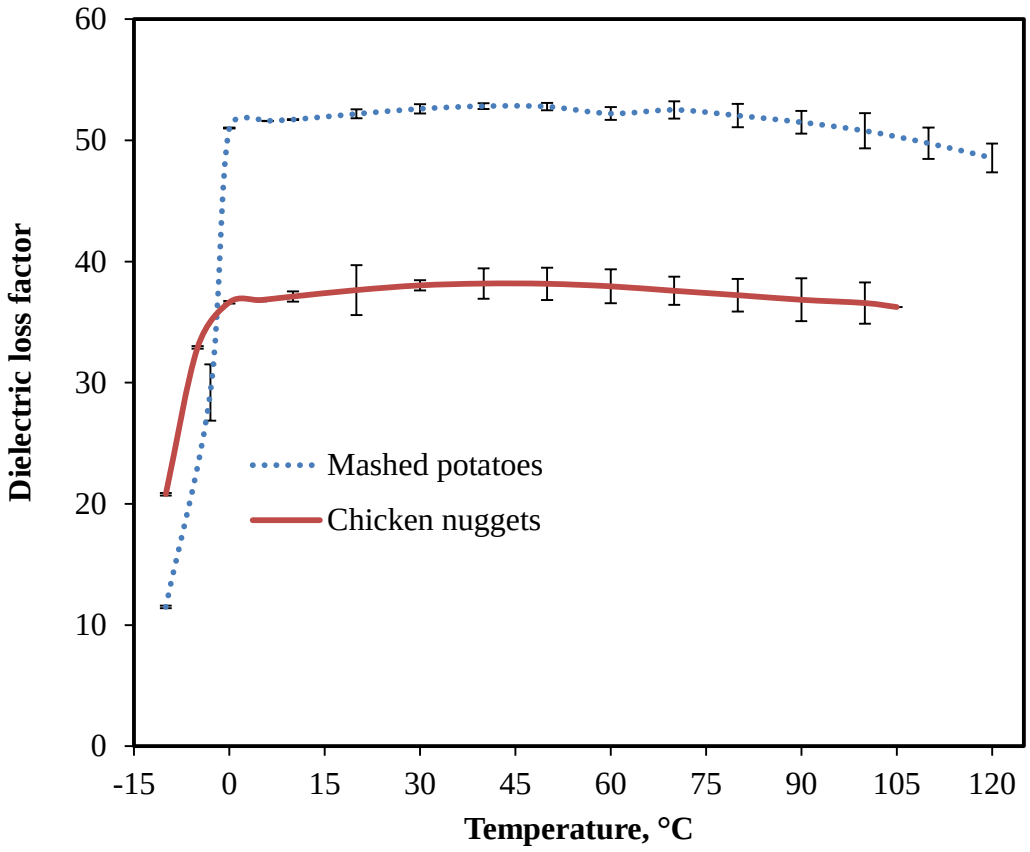

Figure 2. 6. Temperature-dependent dielectric loss factor of chicken nuggets and mashed potatoes measured at 2.45 GHz frequency.

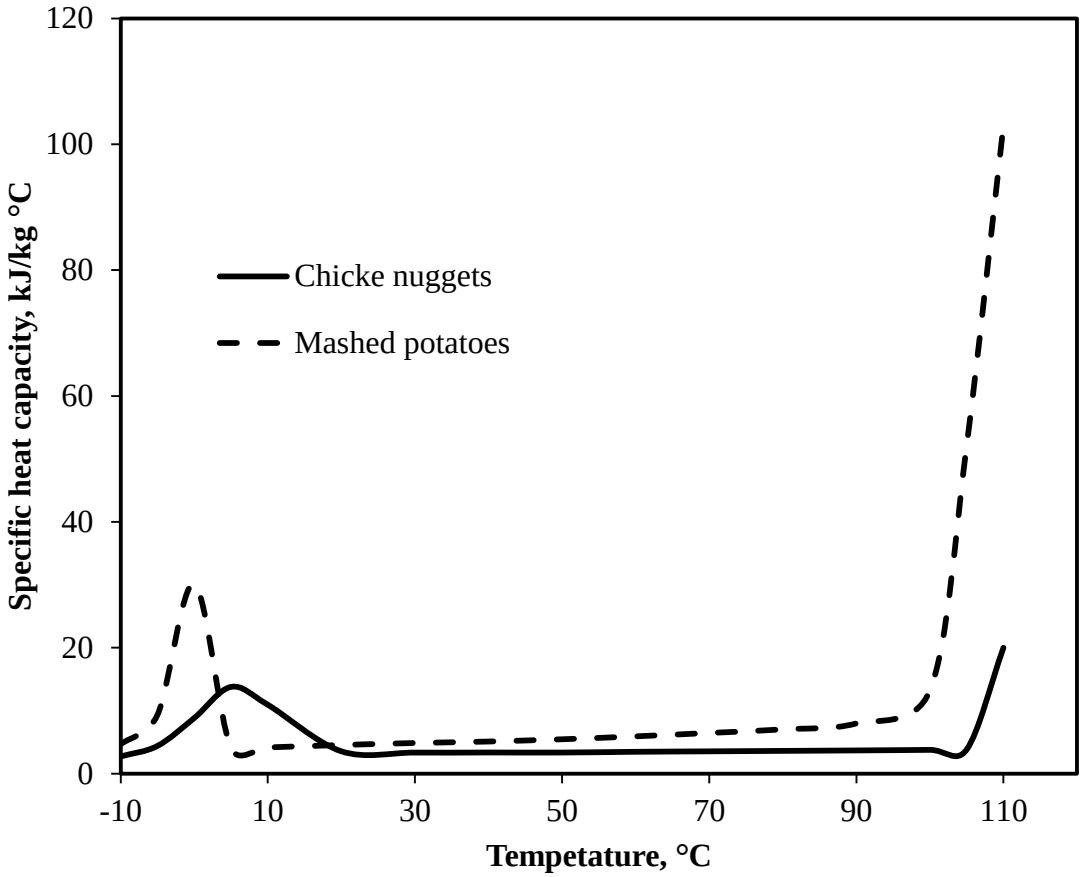

Figure 2. 7. Specific heat capacity of chicken nuggets and mashed potatoes as a function of temperature.

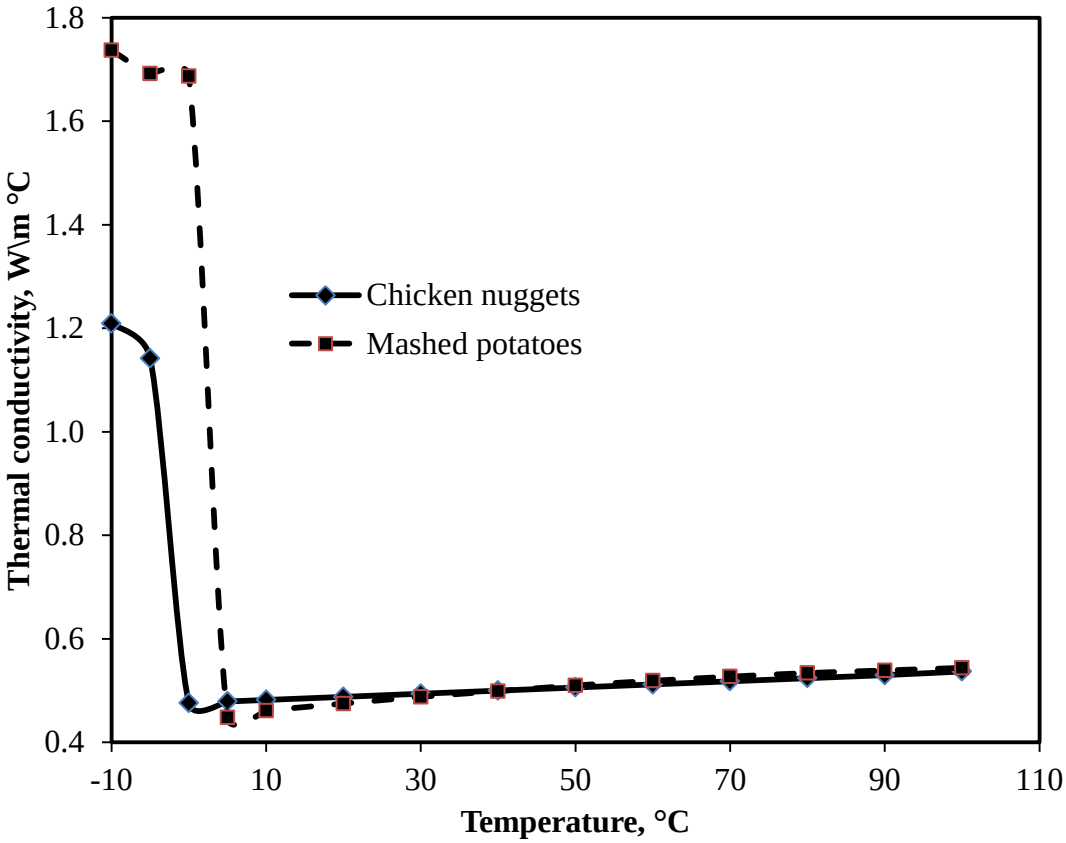

Figure 2. 8. Temperature-dependent thermal conductivity of chicken nuggets and mashed potatoes.

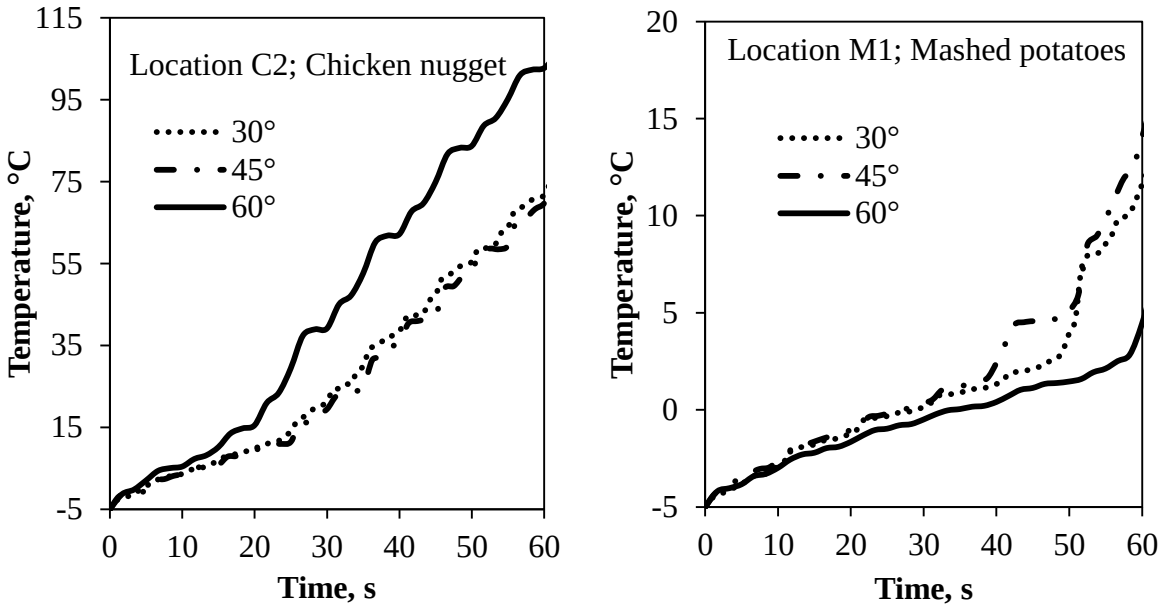

Figure 2. 9. Effect of food rotation angle on simulated temperature (Refer locations in Figure 2.4).

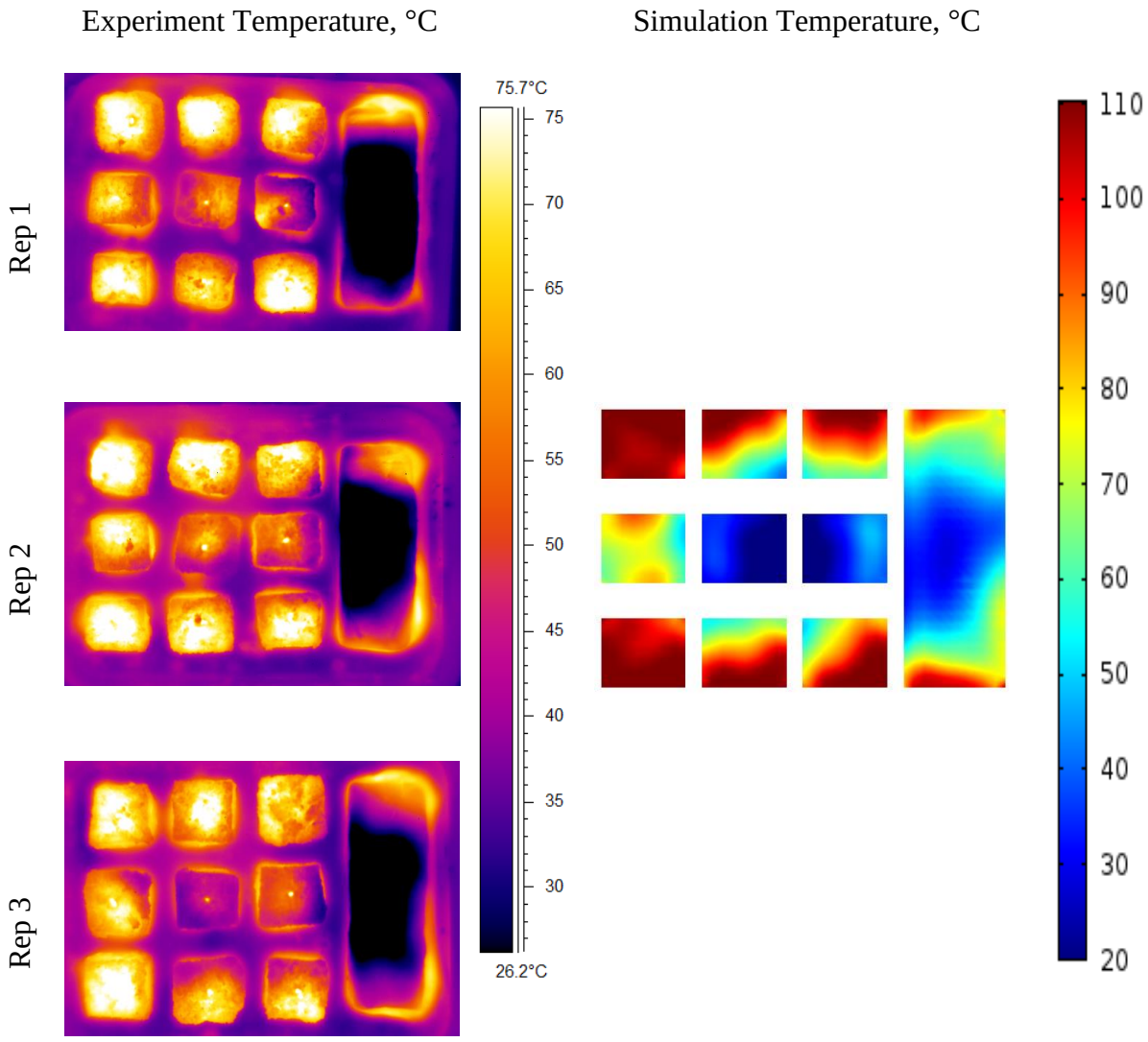

Figure 2. 10. Comparison of simulated and experiment surface temperature profile of multi-component meal subjected to 90 s heating in a 1200 W microwave oven.

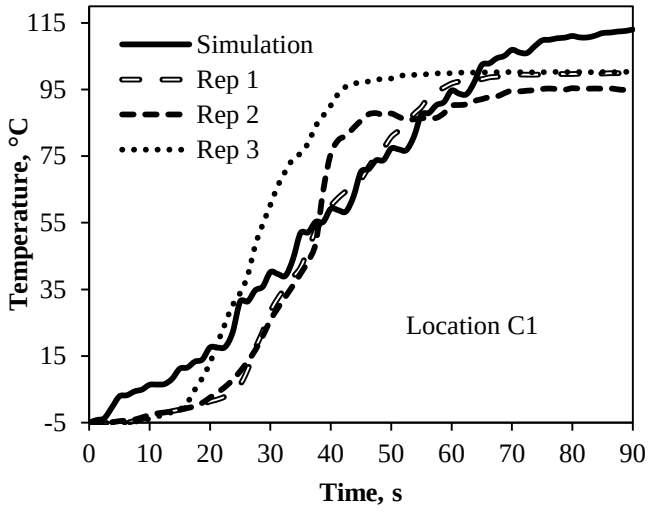
Simulation
Rep 1
Rep 2
Rep 3
Location C1
Temperature, °C
Time, s
115
95
75
55
35
15
-5
0
10
20
30
40
50
60
70
80
90

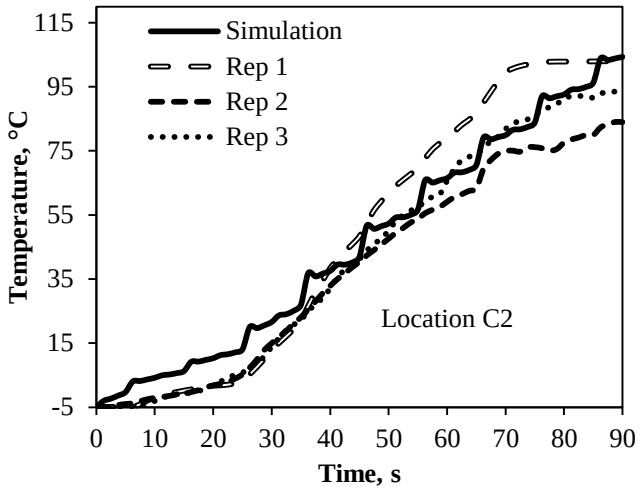
Simulation
Rep 1
Rep 2
Rep 3
Location C2
Temperature, °C
Time, s
115
95
75
55
35
15
-5
0
10
20
30
40
50
60
70
80
90

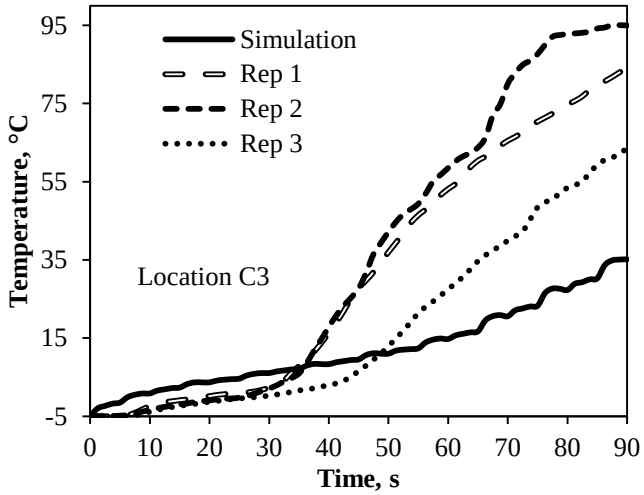
Simulation
Rep 1
Rep 2
Rep 3
Location C3
Temperature, °C
Time, s
95
75
55
35
15
-5
0
10
20
30
40
50
60
70
80
90

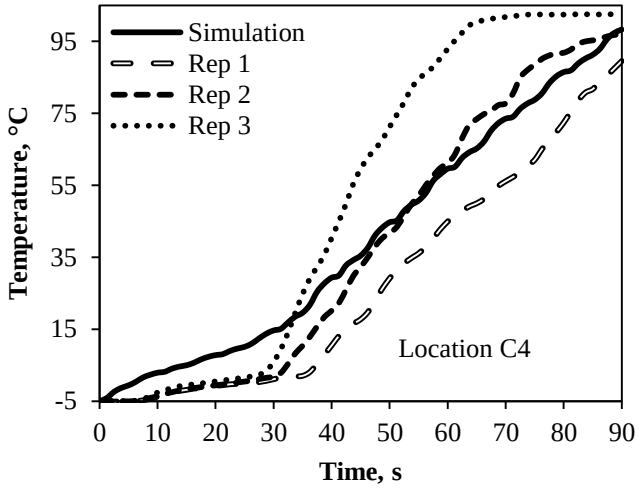
Simulation
Rep 1
Rep 2
Rep 3
Location C4
Temperature, °C
Time, s
95
75
55
35
15
-5
0
10
20
30
40
50
60
70
80
90

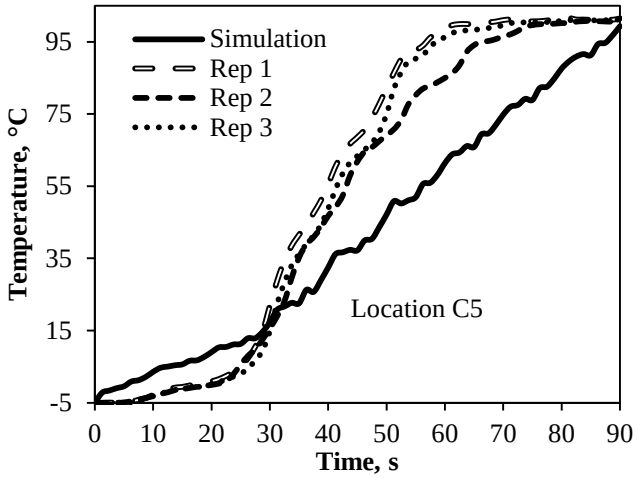
Simulation
Rep 1
Rep 2
Rep 3
Location C5
Temperature, °C
Time, s
95
75
55
35
15
-5
0
10
20
30
40
50
60
70
80
90

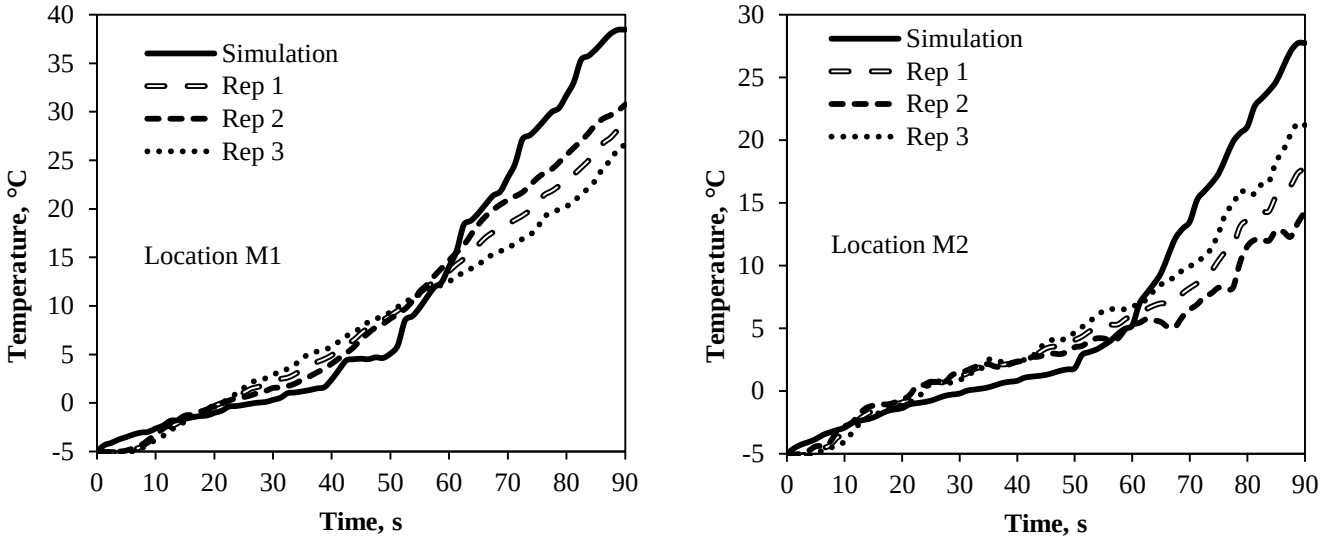

Figure 2. 11. Simulated and three replicates experimental time-temperature profile at seven locations of multi-component meal subjected to 90 s heating in a 1200 W microwave oven (Refer locations in Figure. 2.4).

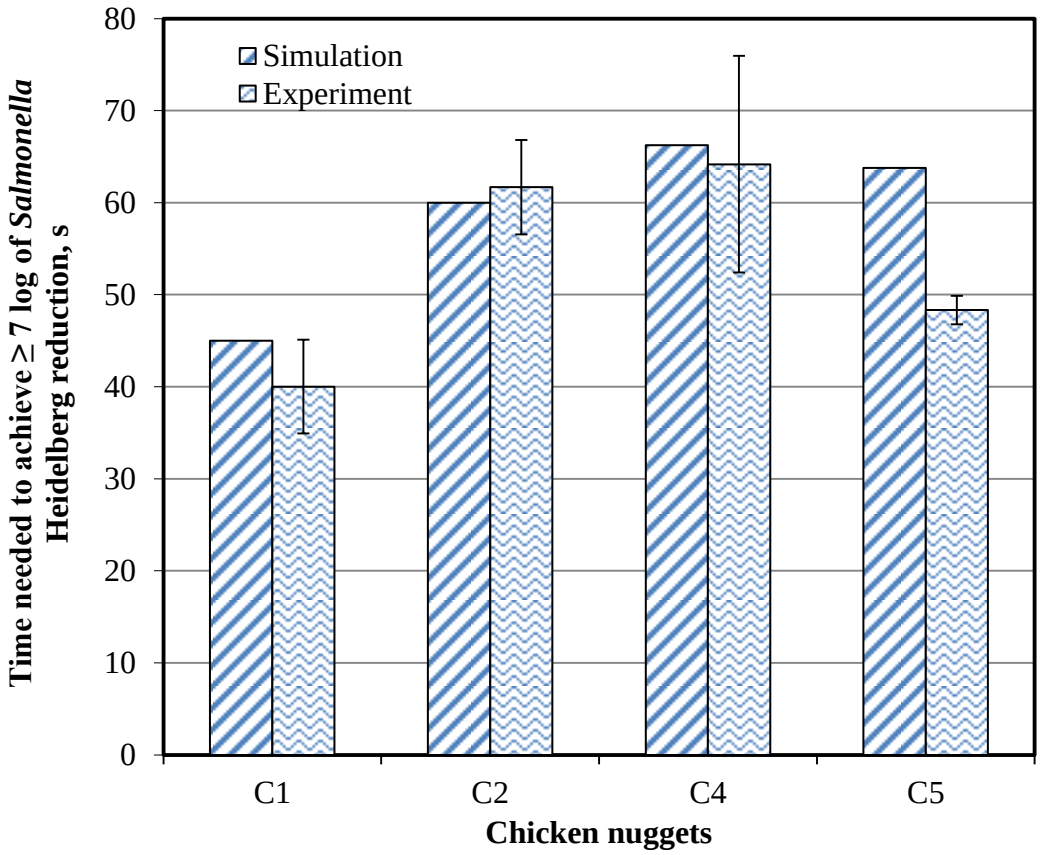

Figure 2. 12. Comparison of time needed to achieve ≥ 7 log reduction of *Salmonella* Heidelberg calculated from simulated and experimental time-temperature profile of chicken nuggets subjected to 90 s heating in a 1200 W microwave oven.

Table 2. 1. Summary of initial conditions and material properties applied in the model.

Parameter	Domains	Value
Initial temperature, °C	Air	20
	Glass turntable	20
	Chicken nuggets and mashed potatoes	-5
Dielectric constant, (ε')	Air	1
	Glass turntable	4
	Chicken nuggets and mashed potatoes	Fig. 5
Dielectric loss factor, (ε'')	Air	0
	Glass turntable	0
	Chicken nuggets and mashed potatoes	Fig.6
Specific heat capacity, (Cp, kJ Kg^{-1} °C^{-1})	Chicken nuggets and mashed potatoes	Fig.7
Density, (ρ, kg m^{-3})	Glass turntable	2050
	Chicken nuggets	1100
	Mashed potatoes	1050
Thermal conductivity, (k, W m^{-1} °C^{-1})	Chicken nuggets and mashed potatoes	Fig.8
Heat transfer coefficient, (h, W m^{-2} °C^{-1})	Food-Air	10

Table 2. 2. Root mean square error and end temperature difference of simulation and averaged experiment temperature profiles after 90 s of microwave heating.

Food component	Sensor ID (Refer Fig. 2.4)	RMSE (°C)	$T_{simulation}$ (°C)	Average $T_{experiment}$ (°C)	End temperature difference, ΔT (°C)
Chicken nuggets	C1	10.2	*113.5*	*98.5*	*15.0*
	C2	6.4	*107.9*	*93.6*	*14.2*
	C3	26.2	35.1	80.8	-45.7
	C4	5.8	*99.3*	*96.3*	*3.0*
	C5	16.9	100.1	101.1	-0.9
Mashed potatoes	M1	4.7	*38.4*	*28.6*	*9.7*
	M2	4.3	*27.7*	*17.7*	*10.0*

$\Delta T = (T_{simulation}-T_{experiment})_{final}$; italicize numbers denotes over-prediction; normal numbers denotes under-prediction.

CHAPTER III

MULTIPHYSICS MODELING OF MICROWAVE HEATING OF A FROZEN HETEROGENEOUS MEAL ROTATING ON A TURNTABLE

Krishnamoorthy Pitchai [a, b], Jiajia Chen [b], Sohan Birla [c], David Jones [b], Ric Gonzalez [c], and Jeyamkondan Subbiah [a, b, *]

[a] *Department of Food Science and Technology, University of Nebraska-Lincoln, NE – 68583*

[b] *Department of Biological Systems Engineering, University of Nebraska-Lincoln, NE – 68583*

[c] *ConAgra Foods, Inc., Omaha, NE – 68102*

*Corresponding author: Jeyamkondan Subbiah, Kenneth E. Morrison Distinguished Professor of Food Engineering, Departments of Food Science & Technology and Biological Systems Engineering, 212 L.W.Chase Hall, East Campus, University of Nebraska-Lincoln, Lincoln, NE-68583-0726, Ph. No: 402-472-4944, Fax No: 402-472-6338, Email: jeyam.subbiah@unl.edu.

Citation: Pitchai, K., Chen, J., Birla, S., Jones, D., Gonzalez, R., Subbiah, J. 2015. Multiphysics modeling of microwave heating of a frozen heterogeneous meal rotating on a turntable. Journal of Food Science. In journal review.

3.1. Abstract

Computer simulation is a highly desirable tool to understand the interactions of microwaves with food components in frozen heterogeneous meals during heating in domestic microwave ovens. The objective of this study was to develop and validate a 3-D finite element multiphysics model to predict spatial and temporal temperature profiles in frozen lasagna during microwave cooking. A multiphase porous media model combining the electromagnetic heat source with heat and mass transfer, and incorporating phase change of melting and evaporation was developed using a finite element method. The model simulated for six minutes of microwave cooking of a 450 g frozen lasagna tray kept at the center of the turntable in a 1200 W domestic microwave oven. For simulating microwave heating of a rotating lasagna tray, discrete rotation at every 30° angles was implemented. Temperature-dependent dielectric and thermal properties of lasagna ingredients were measured and provided as inputs to the model. Simulated temperature profiles were compared with experimental temperature profiles obtained using a thermal imaging camera and fiber-optic sensors. The total moisture loss in lasagna was predicted and compared with the experimental moisture loss during cooking. The simulated spatial temperature patterns predicted at the top layer was in good agreement with the corresponding patterns observed in thermal images. Predicted point temperature profiles at six different locations within the meal were compared with experimental temperature profiles and RMSE values ranged from 6.6 to 20.0 °C. The predicted total moisture loss matched well with an RMSE value of 0.54 g.

Keywords: microwave heating, heat and mass transfer, computer simulation model, multi-component, frozen lasagna.

3.2. Introduction

Domestic microwave ovens are used extensively by consumers for cooking frozen meals. Microwave heating of a heterogeneous meal is highly non-uniform. Non-uniform heating in microwave heating is due to (a) non-uniform distribution of microwaves within the cavity (Pitchai and others 2012), (b) differences in dielectric and thermal properties of various food components leading to differences in microwave power absorption, heat dissipation and diffusion (Chamchong and Datta 1999b), (c) thawed regions absorbing more energy than frozen regions leading to thermal run-away heating (Tilford and others 2007), and (d) differences in physical properties (size, shape and location of the food) leading to different heating rates (Zhang and Datta 2000). Improving heating uniformity of the products at the end of microwave cooking is essential to achieve high quality.

Some of the frozen microwavable meals are available in the market as not-ready-to-eat (NRTE) meals, meaning that the meal has to be cooked thoroughly to ensure food safety. A frozen NRTE meal containing poultry products must be heated to a minimum target temperature of 73.9 °C throughout food to inactivate pathogens (USDA-FSIS 2014); when doing so, some locations within the meal may become overcooked. Therefore, uniformity of heating is important not only for food safety but also food quality. The microwaveable product development process is very time-consuming and expensive. Ryynanen and Ohlsson (1996) have experimentally studied microwave heating uniformity of chilled multicomponent ready meals consisting of meat patties, carrots, and mashed potato. Experimental techniques alone sometimes are insufficient for optimizing food product design to achieve uniform heating, due to the complex

interactions of microwaves with various food components; therefore, predictive simulation is desirable.

A computer-based simulation of microwave cooking is a promising tool that offers insights into microwave interactions with food components and can save a tremendous amount of time in food product development (Celuch and Kopyt 2009). The most commonly applied numerical methods to solve electromagnetic and heat and mass transfer equations are Finite Difference Time Domain (FDTD) and Finite Element Method (FEM). Researchers have developed a computer simulation model using FDTD method to calculate the electromagnetic and heat transfer field distribution in horizontally moving packages that are heated in a microwave assisted thermal sterilization (MATS) system (Chen and others 2008; Resurreccion and others 2013). In most cases, FDTD method-based solvers are limited in simulation application because of their inability to handle irregular geometries. Alternatively, FEM-based solvers have been used extensively in simulating microwave heating that includes complex geometries (Lin and others 1995; Geedipalli and others 2007; Liu and others 2008; Pitchai and others 2014). Solving coupled electromagnetic and heat and mass transfer equations in three-dimensional space and time requires a great amount of computational resources.

In the past, many studies developed microwave heat transfer models for various model food products such as phantom gel (DinCov and others 2004), raw potato (Geedipalli and others 2007), and gel (Wappling-Raaholt and others 2002). Ryynanen and others (2004) developed a numerical modeling of microwave heating of a multilayered hamburger consisting of meat patties and a bun. However, they did not consider the frozen foods in the model and did not validate their model results with the

experiment. In North America, most of the microwaveable meals are available in the market as frozen meals. Therefore, it is important to include the phase change (thawing, evaporation) characteristics of microwaveable foods in the model. In the literature, microwave heat transfer models were developed for thawing of foods. However, those models are limited in a realistic microwave heating scenario because they were developed with a simplistic approach in consideration, for example, of Lambert's law (Campañone and Zaritzky 2005), a single component food (Virtanen and others, 1997; Tilford and others 2007), 1-D or 2-D heat and mass transfer models (Chamchong and Datta 1999a; Campañone and Zaritzky 2010), and/or a simplified geometry of the oven cavity (Chamchong and Datta 1999b). There have not been any microwave heat transfer models developed for heterogeneous multicomponent meals going through a multiphase change (frozen to thawed to cooked). In our earlier work, we developed a 3-D FEM model for heating of a frozen two- component meal on a rotating turntable (Pitchai and others 2014). In that work, chicken nuggets and mashed potato were considered; each component was homogeneous and was not touching each other and mass transfer physics was not included in the model.

A multiphase porous media model combining the electromagnetic heat source with heat and mass transfer, and including phase change of water during evaporation, is needed to accurately describe the microwave heating process. A very few comprehensive multiphase porous media models have been developed to study various heating processes such as conventional cooking (Dhall and others 2012), frying (Halder and others 2007a, 2007b, 2011) and microwave puffing (Rakesh and Datta 2011, 2012). These models coupled different types of heating sources with heat and mass transfer for different food

processes. However, most of these models only considered 2-D problems. In our earlier work, we developed a 3-D multiphase porous media model for a frozen homogeneous mashed potato (Chen and others 2014). However, a 3-D multiphase porous media microwave heating models for a frozen heterogeneous food has not been reported.

Many researchers have modeled the domestic microwave oven cavity and waveguide as a simple geometry to reduce the number of mesh elements required to solve the equations (Geedipalli and others 2007; Ma and others 1995; Yakovlev 2001). Those special features of the microwave design, such as dents in the cavity and metal bumps in the waveguide, are incorporated for improving electric field distribution inside the cavity. Simplification of cavity geometry in the simulation model can introduce significant error in the prediction of the electric field distribution within the cavity. Pitchai and others (2012 & 2014) included all of these special features in the microwave cavity design and demonstrated improved accuracy in predicting hot and cold spot locations.

Microwave ovens are equipped with a turntable to rotate food during cooking. Geedipalli and others (2007) demonstrated using a FEM model for a homogenous food (raw potato) that the use of a turntable improved heating uniformity by 43%. Therefore, it is critical to simulate the rotation of food on the turntable. Chatterjee and others (2007) developed a model for microwave heating of a rotating containerized liquid. In their study, electromagnetic power loss inside the containerized liquid was calculated using Lambert's law, which considers planar electromagnetic waves on one direction. Most of the simulation models in the literature do not consider one or more of the following: (i) phase change from frozen to thawing, (ii) rotation of the turntable, (iii) detailed geometry of the cavity, (iv) temperature-dependent dielectric and thermal properties, (v)

heterogeneous food products, and (vi) mass transfer physics. In this study, we included all the aforementioned factors in the model. The main objective of this study was to develop a comprehensive 3-D FEM model for a heterogeneous lasagna meal to predict temperature and moisture while heating in a domestic microwave oven. Specific objectives of this study were to:

i) develop a coupled electromagnetic, heat and mass transfer model for a lasagna meal, and
ii) validate the multiphysics model using experimental measurements of temperature and moisture.

3.3. Model Development

3.3.1. Governing equations

The governing equations of Maxwell's equations, mass conservation equations, phase change of evaporation, and energy conservation equations were applied in this model as described by Chen and others (2014). Chen and others (2014) developed a multiphase porous media model for a homogeneous fresh mashed potato. The same model was extended to incorporate the heterogeneity of food and phase change of melting.

3.3.2. Electromagnetic field distribution

The electromagnetic energy distribution inside an oven cavity is governed by a set of four Maxwell's equations (Pitchai and others 2012). Solution of the combined waveform of Maxwell's equations gives the estimated electromagnetic field strength ($\vec{\mathbf{E}}$) at any point in the computational domain (Li 2010):

$$\nabla\times\mu_r^{-1}\left(\nabla\times\vec{\mathbf{E}}\right)-\left(\frac{2\pi f}{c}\right)^2\left(\varepsilon'-i\varepsilon''\right)\vec{\mathbf{E}}=0 \qquad (3.1)$$

where f is the microwave frequency of the magnetron in GHz, c is the speed of light (3.0×10^8 m·s^{-1}), $\vec{\mathbf{E}}$ is the electric field strength in V·m^{-1}, ε', ε'' and μ_r are the dielectric constant, dielectric loss factor, and electromagnetic permeability of the dielectric material (food), respectively.

Electromagnetic energy is dissipated as thermal energy in food. The electromagnetic power loss density (Q_m) in W·m^{-3} is calculated as (Datta 2001):

$$Q_m = \pi f\varepsilon_0\varepsilon''\left|\vec{\mathbf{E}}\right|^2 \qquad (3.2)$$

3.3.3. Mass conservation and phase change of evaporation

The lasagna can be recognized as a mixture of the solid phase, the liquid phase of water, and the gaseous phase of water vapor and air. The lasagna was considered as a single phase of solid from -10 °C to 10 °C (porosity = 0). Above 10 °C, the thawed lasagna was assumed to be porous product including solid, liquid (water), and gas (vapor and air) phases. The porosity of the each component of lasagna (pasta, ricotta cheese, and meat sauce) was calculated based on the moisture content and the values are reported in Table 3. 1. The transport of species (liquid water, water vapor, and air) inside the food product during the microwave heating process is described by a multiphase porous media model. The mass conservation equation included the diffusion term (Fick's law), convection term (Darcy's law) and reaction term (phase change of evaporation) (Stocker 2011):

$$\frac{\partial C_i}{\partial t}+\nabla\cdot\left(-D_i\nabla C_i+\mathbf{u_i}C_i\right)=\pm r_i \qquad (3.3)$$

where C_i is the concentration of each species in $mol \cdot m^{-3}$, D_i is the diffusion coefficient of each species in $m^2 \cdot s^{-1}$, $\mathbf{u_i}$ is the Darcy's velocity of each species $m \cdot s^{-1}$ which is calculated by Darcy's law, r_i is the reaction term describing the production or consumption of each species ($mol \cdot s^{-1} \cdot m^{-3}$) ("-" sign used for liquid water, "+" sign used for vapor, r = 0 for air, as the air is neither generated nor converted to another species).

The reaction term (phase change of evaporation term) can be calculated for liquid water and water vapor (Halder and others 2007a):

$$r = \frac{K(p_{v,eq} - p_v)}{RT} \qquad (3.4)$$

where K is a rate constant of evaporation in s^{-1}, p_v is the vapor pressure in Pa which can be calculated from the ideal gas law ($p_v = C_v RT$) where C_v is concentration of vapor in mol/m^3, $p_{v,eq}$ is the equilibrium water vapor pressure in Pa calculated from isotherm data, R is the ideal gas constant (8.314 $J \cdot K^{-1} \cdot mol^{-1}$) , and T is the temperature in °C.

3.3.4. Energy conservation

The energy conservation equation consisted of convection, diffusion, conduction, water evaporation (Eq. 3.4) and microwave heat source (Eq. 3.2), which can be described as (Delgado 2011):

$$\frac{\partial}{\partial t}\left(\rho_{eff} C_{p,eff} T\right) + \nabla \cdot \left(\sum_{i=w,v,a} \rho_i C_{p,i} \mathbf{u_i} T\right) = \nabla \cdot (k_{eff} \nabla T) - \lambda r M_w + Q_m \qquad (3.5)$$

where ρ_{eff} is the effective density in $kg \cdot m^{-3}$, $C_{p,eff}$ is the specific heat capacity in $kJ \cdot kg^{-1} \cdot °C^{-1}$, $\mathbf{u_i}$ is the Darcy's velocity of each species in $m \cdot s^{-1}$, λ is the latent heat of

vaporization of water (2.26×10^6 J·kg^{-1}), T is the temperature in K, and M_w is the molecular weight of the water vapor (18 g/mol).

Because, the mass transfer phenomenon was insignificant below 10 °C, the measured apparent specific heat capacity and thermal conductivity from -10 to 10 °C were used in the model. Above 10 °C, the effective thermal conductivity, density and specific heat capacity were considered. The domains are discretized and defined for each ingredient, as shown in the Figure 3. 1. Choi and Okos (1986) equations were used for determining thermal conductivity of each proximate component (fat, carbohydrate, protein) as a function of temperature; however those equations were developed using the experimental data up to 40 °C. Thermal conductivity of fat component in Choi and Okos (1986) equation becomes negative value above 60 °C temperature. Therefore, we assumed a constant thermal conductivity of fat component of 0.01 W. m^{-1}. K^{-1} above 60 °C temperature.

The effective thermal conductivity was calculated based on weighted average of the phase (solid, liquid, and gas) compositions (Choi and Okos 1986):

$$k_{eff} = (1-\Phi)k_s + \Phi[S_w k_w + S_g(\omega_v k_v + \omega_a k_a)] \qquad (3.6)$$

where ω_i is the mass fraction of vapor or air in gaseous phase.

Chen and others (2014) considered a constant density for the homogeneous mashed potato. However, the density changes when some moisture evaporates. Therefore, we considered the effective density, which was calculated at each time step based on porosity, and gas saturation (S_g) and water saturation (S_w). The effective

density was calculated based on the weighted average of volume fraction of phase compositions (Choi and Okos 1986):

$$\rho_{eff} = (1- \Phi)\rho_s + \Phi[\rho_w S_w + \rho_v S_g + \rho_a S_g] \quad (3.7)$$

Chen and others (2014) used constant specific heat capacity for solids (dry matter), water, vapor, and air and then estimated the effective specific heat capacity based on mass fractions in each finite element for heating of homogeneous mashed potato. Mass transfer calculations changed mass fraction of water and water vapor at each time step. This study considered the thawing of frozen lasagna. For the frozen region (from -10 to 10 °C), mass transfer was considered to be zero and apparent specific heat capacity determined from DSC was used to incorporate latent heat of melting (Figure 3. 3). After 10 °C, the same approach used by Chen and others (2014) was used in this study. The effective specific heat capacity was calculated based on the weighted average of mass fraction of phase components (Choi and Okos 1986).

$$C_{p,eff} = m_s C_{p,s} + m_w C_{p,w} + m_v C_{p,v} + m_a C_{p,a} \quad (3.8)$$

where m_i is the mass fraction of each phase (soid, liquid, and gas) to the total mass of three phases.

The thermal conductivity of solid portion, k_s in each component of lasagna is calculated based on volume fraction of proximate composition ignoring water, while the specific capacity of solid in each lasagna component is calculated based on mass fraction of proximate composition ignoring water (Choi and Okos 1986).

3.3.5. Boundary and initial conditions

The perfect electric conductor condition at the cavity boundary, vapor flux from the food surface to the ambient air by convection and diffusion, mass flux due to convective heat transfer, and outward normal heat flux boundary conditions were applied in this model as described by Chen and others (2014). It was considered that on the bottom of the lasagna tray, there was no mass flux or heat flux, because of the sealing of the tray bottom. The initial conditions of temperature, water concentration, vapor concentration and air concentration are listed in the input parameters table (Table 3. 1).

The fan in the oven circulated the air inside the cavity. At the lasagna tray surface, we considered a convective natural heat flux boundary at the food-air interface. Chamchong and Datta (1999a) used the heat transfer coefficient (h) values from 0.0001 to 30 W. m^{-2}. K^{-1} to evaluate the sensitivity of h values on thawing time in microwave heating. They found that h values were not sensitive to the thawing time. Therefore, it was recommended that any values can be chosen from the range of 0.0001 to 30 W. m^{-2}. K^{-1}. In our study, we used the reported value of 20 W. m^{-2}. K^{-1} (Ni and others 1999). The fan in the oven continuously circulated outside air into the cavity, and therefore the initial air temperature of 20 °C was assumed to remain constant during heating.

3.3.6. Geometric model

Microwave heating of lasagna was performed in a 1200 W rated power (1100 W available power measured using IEC 60705 method) microwave oven (Model no: NN – SD767W; Panasonic Corporation, Shanghai, China). An inclusive and detailed geometry model of the oven was created in commercial software COMSOL Multiphysics 4.3b (COMSOL, Burlington, MA). The geometry of the 500 g lasagna was created in

commercial software Solidworks 2011 (Solidworks, Waltham, MA) and imported into COMSOL Multiphysics v4.3b. In this study, we included the magnetron as a coaxial power source feeding microwave energy into the waveguide located at the center of the right side of the cavity wall. The geometric model of the microwave oven and layers of multi-components of lasagna is shown in Figure 3. 1. A summary of the initial conditions and material properties applied in the model is given in Table 3. 1.

3.3.7. Simulation strategy

Solving coupled non-linear electromagnetic wave and heat transfer equations requires an iterative solver to perform the simulation. A Generalized Minimal Residual (GMRES) method based iterative solver was used to solve electromagnetic and heat transfer equations. The simulation was performed on a Dell Precision T7500 workstation with an 72 GB DDR3 RAM running on two quad-core Intel Xeon X5570 2.93 GHz processor.

The turntable rotates at 6 rpm and therefore one complete rotation of the turntable takes 10 s. Within that short time, the dielectric properties did not change significantly (Liu and others 2013). Therefore, dielectric properties can be assumed to be constant within each rotation. In the COMSOL Multiphysics® v4.3b and earlier versions, the rotation of a 3-D non-symmetric object cannot be implemented in the Radio Frequency module for solving electromagnetic equations and there were issues in coupling with the Arbitrary Lagrangian-Eulerian algorithm for moving mesh during rotation (Pitchai and others 2014). A custom MATLAB routine was written to simulate microwave heating of the rotation of an object and was then interfaced with COMSOL using MATLAB livelink. Figure 3. 2 shows the pseudo-code of this custom routine to enable rotation.

Instead of continuous rotation of the lasagna tray on the turntable, the model considered discrete positions with 12 locations during one complete rotation (360°) to take into account the variability in electromagnetic field at various positions. For each position, electromagnetic field was determined using a newton method based stationary solver in the frequency domain (Eq. 3.1). The 12 electromagnetic field data correspond to 12 positions of the tray along the rotation path during one complete rotation. To calculate the averaged electromagnetic field of 12 locations, the Cartesian coordinates of different locations were rotated back to the initial position. Geometric transformation (Pitchai and others 2014) was used to rotate the electromagnetic results of all positions to the initial position. As mesh coordinates did not match, the values were linearly interpolated to the initial position and were then averaged.

The custom-routine written in MATLAB then passes the average EM field to COMSOL Multiphysics® v4.3b for solving coupled heat and mass transfer physics for one complete rotation (10 seconds of actual microwave heating). At the end of the first rotation, the temperature field was used to update the dielectric properties and then Maxwell's equations (Eq. 3.1) were solved to determine electromagnetic fields separately for the 12 discrete locations. This cyclic process continued until a complete cooking time of 6 min was reached.

3.3.8. Meshing scheme

The meshing scheme was adapted to each domain (air, glass turntable, and food) based on the mesh size described in Chen and others 2014 to achieve mesh independent results. Air, glass turntable and lasagna domains were assigned with four-node unstructured tetrahedral elements with the quadratic shape functions. Two meshes with

different refinement levels were enforced for tetrahedral elements (i.e., normal: air domain, size: 8 mm; finer: glass turntable and lasagna domains, size: 2 mm). In all the domains, minimum element quality was ensured to be > 0.02, which is recommended for faster convergence in the COMSOL Multiphysics (COMSOL 2013). Three dimensional meshes created about 387,000 total elements, out of which 212,000 elements comprised the lasagna and glass turntable.

3.4. Materials and Methods

3.4.1. Sample preparation

The lasagna consisted of multiple layers of ricotta cheese, pasta and meat sauce. The ricotta cheese was prepared by mixing 80% of ricotta cheese (Crystal Farms, Lake Mills, WI) and 20% of distilled water. Meat sauce procured from ConAgra Foods Inc. consisted of 85.3% of marinara sauce (45.0% water, 42.0% tomato, 5.7% onions, 1.5% sugar, 2.3% starch, 2.0% garlic, and 1.5% spices) and 14.7% ground beef. Dry pasta sheet (Barilla Lasagna, Barilla America, Inc., Bannockburn, IL) was cooked for 8 min in boiling water and then the cooked pasta was rinsed with cold water. The cooked pasta was manually layered in the tray with ingredients of meat sauce and ricotta cheese and then the prepared lasagna trays were covered with polythene sheet and stored at -10 °C until further use.

3.4.2. Dielectric properties

The dielectric properties of lasagna components were measured using a multi-point temperature calibration and reported in Chen and others (2015). The reported temperature- dependent dielectric properties were used in this model.

3.4.3. Thermal properties

The specific heat capacity of the lasagna food components was measured using a differential scanning calorimeter (DSC 822, Mettler Toledo, Columbus, OH) in accordance with the ASTM standard E1269-01. Measurements were carried out using a Pyris 1 DSC system equipped with an Intracooler 1P refrigeration unit (Perkin-Elmer, Inc., Norwalk, CT, USA). Nitrogen gas was used to flush the sample holder unit. Three individual (25 mg) samples were scanned from -10 °C to 20 °C at a heating rate of 5 °C min^{-1} placed in 40 µl aluminum crucibles (Model no: ME-27331, Perkin-Elmer Corp., Norwalk, CT, USA) covered with a lid. An empty aluminum crucible was used as a reference.

The thermal conductivity of the lasagna food components were measured, as a function of temperature from -10 to 10 °C using a KD2 Pro thermal properties analyzer (Decagon Devices, Inc., Pullman, WA, USA). Before each experiment, the calibration of the TR-1 thermal conductivity probe was verified using an acetal plastic standard. Samples were filled in a 30 mm diameter copper tube and immersed in a hot water bath and maintained at a desired temperature. The TR-1 probe was used to measure thermal conductivity of 5 °C and 10 °C. The TR-1 probe was also inserted into samples maintained at a frozen temperature prior to recording; the sample was drilled using a mechanical drill bit of 2 mm in order to easily insert the TR-1 probe into samples.

3.4.4. Experimental validation

The lasagna samples were maintained at -10 °C in the freezer. The transient temperature at six locations was recorded using fiber-optic sensors (8-channel signal conditioner, FISO Technologies Inc., Quebec, Canada). To place the sensors, lasagna

was drilled to a depth of 15 mm using a mechanical drill bit (dia – 2mm) at six locations as shown in Figure 3. 6. G. Because the product was cooked for a long time (6 min), steam that is developed inside the product can move the fiber-optic sensors. The fiber-optic sensors have a sturdy plastic wrap surrounding the sensor at the lowest portion for 20 mm length, which gets inserted into the product. Above that plastic wrap, the sensor cable is flexible. To keep them straight during cooking, we inserted a small plastic tube (dia - 3mm; length - 90 mm) around the sensors above the sturdy plastic wrap. This tube does touch the product. It stays above the product. This improved the consistency of location of the sensor during cooking. The lasagna sample was cooked in a 1200 W domestic microwave oven for 6 min. After microwave heating, a thermal image of the top surface of the lasagna was immediately captured using an infrared camera (SC640, 640 × 480 pixels accuracy ± 2 °C, FLIR systems, Boston, MA). Temperature profiles were measured in five replications and reported in this study.

3.4.5. Model accuracy measurement

Model accuracy measurement was determined by comparing the deviation between the simulated and experimental temperatures at different points during heating and root mean square error (RMSE) was calculated.

3.5. Results and Discussion

3.5.1. Thermal properties

The specific heat capacities of all three food components from -10 °C to 10 °C are shown in Figure 3. 3. From -10 to 0 °C, the specific heat capacities of meat sauce, ricotta cheese and pasta increased from 3.6 to 23.2 and 3.6 to 24.4 and 2.3 to 19.3 $kJ\cdot kg^{-1}\cdot °C^{-1}$,

respectively. The increase in the apparent specific heat capacity is due to phase change. The latent heat of fusion was calculated by integrating the area under the curve from -10 to 10 °C using the trapezoidal rule; the baseline curve area between -10 and 10 °C was subtracted to remove sensible heat due to change in temperature from -10 to 10 °C. The latent heat of fusion was determined as 144.22, 134.97 and 108.77 $kJ\cdot kg^{-1}$ for meat sauce, ricotta cheese and pasta, respectively. The latent heat of fusion of meat sauce and ricotta cheese was higher than that of pasta, which can be attributed to the higher moisture content of meat sauce and ricotta cheese. Above 10 °C, the effective specific heat capacity was calculated based on different species (solid, water, air, vapor) concentration in the sample.

The thermal conductivities of all three components as a function of temperature from -10 to 10 °C are shown in Figure 3. 4. The thermal conductivities of all three components were decreased drastically from the temperature of -10 to 0 °C, and then remained relatively constant around 0.45 $W\cdot m^{-1}\cdot °C^{-1}$. However, in meat sauce, the thermal conductivity value at -10 °C was lower than that of the thermal conductivity value at -5 °C. This variation in trend might be attributed to the fact that the TR-1 probe was designed to measure the thermal conductivity of solid material and there may be more experimental error in measuring meat sauce, when compared to cheese and pasta. All three components have higher thermal conductivity values at frozen temperatures than those at thawed temperatures, as the thermal conductivity of ice is higher than that of liquid water. Above 10 °C, the effective thermal conductivity was calculated based on different species (solid, water, air, vapor) concentration in the sample.

3.5.2. Spatial temperature profile

The simulated spatial temperature profile of a frozen lasagna was compared with five replicates of experimental temperature profiles obtained using a thermal imaging camera (Figure 3. 5). Five replicates of experimental temperature profiles consistently showed the locations of hot and cold patterns in the frozen lasagna. A center portion of lasagna had a cold spot and remained at ~30 °C even after 6 min of microwave heating. Similarly, the simulated temperature distribution in lasagna showed a cold spot in the center portion of lasagna and the temperature stayed around 10 °C. Thermal images show that the temperature at the edges of the lasagna was 80 °C, whereas the simulated temperature was 90 °C at the edges of the lasagna. Non-uniform heating persisted even after rotating the lasagna during heating. Rotation primarily makes the heating more uniform along the circumference of rotation and make the heating pattern more symmetric; however non-uniform heating persisted across the radius of rotation. For instance, Pitchai and others (2012) showed the simulation profiles of a stationary object, and the temperature pattern were not symmetric resulting in more non-uniform heating. Liu and others (2013) also reported edge heating in microwave heating of rotating foods. Edge heating is prominent in microwave cooking, because microwaves incident on the edges from the multiple directions resulting in faster heating. Overall, simulated spatial temperature distribution profiles were in good agreement with the experimental thermal images in predicting hot and cold spot patterns.

3.5.3. Transient-temperature profile

Transient temperature profiles of five experimental replicates at six points were compared with the simulated temperature profiles in Figure 3. 6. The simulated transient

temperature profiles showed a phase-change effect in their trend (change in slope around the thawing region) similar to experimental profiles. The phase change involves larger latent heat and therefore phase change has a considerable effect on the accuracy of the model. Electromagnetic energy is the heat source, which determines the heating rate of frozen lasagna. Accurate electromagnetic field prediction is one of the key factors influencing the model prediction accuracy. Even though we included detailed geometry and temperature-dependent dielectric properties to improve the accuracy of electric field prediction, some other factors, such as discrete rotation steps, complexity in food products geometry and single microwave frequency can influence the model prediction considerably. Due to rapid microwave heating, the temperature of food product can dramatically change with very small changes in spatial locations. This presents a major challenge in real-time temperature measurement during microwave cooking using fiber-optic probes, because a small movement or change of location of the probes in the lasagna might result in substantial changes in the measured temperature. The steam pocket developed during heating could also push the probe and cause errors in experimental measurement. To account the experimental variations during lasagna cooking, the root mean square error was calculated using time-temperature profile of each replication and averaged time-temperature profiles of five replications. As shown in Figure 3. 7, root mean square error of model predictions falls within the root mean square error of experimental variations except locations 4 and 6. At locations 4 and 6, root mean square error of experimental variations was only 2.1 °C and 3.5 °C, respectively. Average root mean square error of six locations of experimental variations was 9.1 °C as compared to 11.8 °C of root mean square error of model predictions. Even though the

root mean square error from predicted time-temperature profiles of six locations was 11.8 °C, which was close to the experimental variations root mean square error of 9.1 °C.

Except at center location 4 and 6, the predicted temperature falls within variations in five experimental replicates. On average, it took about 2-3 min to thaw the frozen lasagna. The root mean square error (RMSE) was calculated using averaged experimental time-temperature profiles in comparison with simulated time-temperature profiles for each location. The RMSE values ranged from 6.6 to 20.0 °C. As shown in Figure 3. 6, the simulated transient temperature profiles at the center (location 4) under-predicted the temperature in comparison to all five replications. At location 4, the simulation showed that the product did not thaw at the center, while the experiments showed thawing. Experiments showed that all locations are completely thawed. To determine the extent of errors, Figure 3. 6. H shows the frozen regions at the central plane predicted by the model. About 1.24% by volume of the total products was frozen (had temperatures less than or equal to 0 °C). Predicting phase change is a challenge and the errors in prediction may be attributed to the fact that most of mass transfer properties were used from the available literature for this study. Chamchong and Datta (1999a) also observed that tylose with 3% salt heated for 3 min with 90% of microwave power did not thaw in both simulations and experiments.

3.5.4. Moisture profile

Moisture loss is significant at longer heating times. The total moisture loss profile comparison between simulation and experiment during the six minutes microwave heating of lasagna is shown in Figure 3. 8. The predicted total moisture loss showed a good agreement with observed result with the RMSE of 0.54 g. Until 1 min of heating,

the total moisture loss was not observed in experiments. After 1 min of heating, the total moisture loss linearly increased with increasing temperature and predicted total moisture loss falls within the five experimental variations. After 6 minutes of heating, the lasagna sample was lost about 28 g of water.

Mass transfer of liquid water and water vapor is driven due to pressure-driven flow described by Darcy's law and concentration driven flow described by Fick's law of diffusion. Mass transfer physics (Eq. 3.3) takes the evaporate rate from phase change (Eq. 3.4) as input and provides concentrations of gas (vapor and air) and water in each element as output. To understand mass transfer, the slice plot of temperature, vapor pressure ($p_v = C_vRT$, Pa), vapor concentration distribution ($C_{v,}$ mol/ m^3), and water concentration ($C_{w,}$ mol/ m^3) at the end of 6 minutes of heating time are plotted in Figure 3. 9. Vapor species were generated from water species inside the lasagna, especially at the bottom of tray leads to higher temperature. Higher the vapor pressure inside the food product pushes the vapor move upwards and convective out from the top surface of the tray. Vapor pressure was more at the bottom and side of the tray, because of dominant edge heating where the water started to convert to vapor at much faster rate and the vapor cannot convective out from the shield bottom. Because of higher vapor pressure at the bottom of the tray, the temperature at the bottom pasta layer was higher. As shown in Figure 3. 10, volume average temperature of bottom pasta layer was 82 °C and the volume average temperature reduced to 69 °C at the top of the tray (top meat sauce). There is a difference of about 13°C of volume average temperature from bottom of tray to top of the tray. To achieve the uniform heating, it must be important to leave lasagna for standing time after microwave cooking. The maximum and minimum temperature at

each component was shown in Figure 3. 10. B. It is also evident that maximum and minimum temperature at the bottom pasta layer was higher as compared to the other components. As shown in Figure 3. 10. B, the portion of lasagna was still close to the frozen or around thawing temperature (bottom meat sauce to top meat sauce). The vapor concentration showed discrete values for each layer of components, because of different porosity values at each component layer. Generally, the water concentration at the bottom of the tray was lower which corresponds to the higher water evaporation at the bottom of the tray. At the top of the tray where the tomato sauce domain present had a higher water concentration because of lower water evaporation and higher moisture content in the tomato sauce.

3.6. Conclusions

An electromagnetic and heat and mass transfer model was developed to simulate rotation of lasagna on the turntable. A discrete rotation of lasagna tray at every 30° angles was implemented using geometric transformation of mesh coordinates every 1.25 s of microwave heating. The model was validated with experimental measurements. The simulated spatial temperature profile obtained from the mono-frequency of 2.45 GHz was found to be in good agreement with experimental spatial temperature profile. The root mean square error values ranged from 6.6 °C to 20.0 °C. The predicted total moisture loss matched well with the experimental result and RMSE value of 0.54 g. The validated model is a useful tool to explore various package shapes and layout of the ingredients for improving heating uniformity for both food safety and quality.

Acknowledgements

The authors gratefully acknowledge the financial support provided by the ConAgra Foods, Inc., and USDA CSREES – NIFSI Grant (Project Number: 2008-51110-04340).

Nomenclature

$\vec{\mathbf{E}}$	electric field strength, $V \cdot m^{-1}$
f	frequency, GHz
c	speed of light, 3.0×10^8 $m \cdot s^{-1}$
Q_m	electromagnetic power dissipation density, $W \cdot m^{-3}$
C_i	concentration of each species, $mol \cdot m^{-3}$
D_i	diffusion coefficient of each species, $m^2 \cdot s^{-1}$
$\mathbf{u_i}$	Darcy's velocity of each species, $m \cdot s^{-1}$
$\mathbf{u_{i=v}}$	Darcy's velocity of vapor in m. s^{-1}
r	water evaporation rate in mole, $mol \cdot m^{-3} \cdot s^{-1}$
M_w	molecular weight of the water vapor (18 g/mol).
K	evaporation rate constant, s^{-1}
p_v	vapor pressure, Pa
$p_{v,eq}$	equilibrium vapor pressure, Pa
S_g	gas saturation
R	universal gas constant, 8.314 $J \cdot K^{-1} \cdot mol^{-1}$
$C_{p,eff}$	effective specific heat capacity, $kJ \cdot kg^{-1} \cdot °C^{-1}$
k_{eff}	effective thermal conductivity, $W \cdot m^{-1} \cdot °C^{-1}$
T	temperature, °C
RMSE	root mean square error, °C

T_s	simulated point temperature, °C
T_e	experimental point temperature, °C
$k_{in,v}$	intrinsic permeability of vapor, m^2
$k_{r,v}$	relative permeability of vapor
P	total pressure, Pa

Greek symbols

μ_r	relative electromagnetic permeability
ε'	dielectric constant
ε''	dielectric loss factor
ε_0	free space permittivity, 8.854×10^{-12} F·m^{-1}
Φ	porosity
ρ_{eff}	effective density, kg·m^{-3}
λ	latent heat of vaporization, 2.26×10^{6} J·kg^{-1}
ω_i	mass fraction of vapor or air in gaseous phase
μ_v	dynamic viscosity of vapor, Pa.s

3.7. References

Blackham DV, Pollard RD. 2002. An improved technique for permittivity measurements using a coaxial probe. IEEE Transactions on Instrumentation and Measurement 46(5):1093-1099.

Campañone LA, Zaritzky NE. 2005. Mathematical analysis of microwave heating process. Journal of Food Engineering 69(3): 359-368.

Campañone LA, Noemi EZ. 2010. Mathematical modeling and simulation of microwave thawing of large solid foods under different operating conditions. Food and Bioprocess Technology 3(6): 813-825.

Celuch M, Kopyt P. 2009. Modeling microwave heating in foods. In M.W. Lorence, P. S. Pesheck (Eds.), Development of packaging and products for use in microwave ovens. (First edn., pp. 305-346). CRC Press LLC, Boca Raton, FL.

Chamchong M, Datta AK. 1999a. Thawing of foods in a microwave oven: I. Effect of power levels and power cycling. The Journal of Microwave Power and Electromagnetic Energy: a publication of the International Microwave Power Institute 34(1): 9-21.

Chamchong M, Datta AK. 1999b. Thawing of foods in a microwave oven: II. Effect of load geometry and dielectric properties. The Journal of Microwave Power and Electromagnetic Energy: a publication of the International Microwave Power Institute 34(1): 22-32.

Chatterjee S, Basak T, Das SK. 2007. Microwave driven convection in a rotating cylindrical cavity: A numerical study. Journal of Food Engineering 79(4):1269-1279.

Chen H, Tang J, Liu F. 2008. Simulation model for moving food packages in microwave heating processes using conformal FDTD method. Journal of Food Engineering 88(3): 294-305.

Chen J, Pitchai K, Birla S, Gonzalez R, Jones D, Subbiah J. 2013. Temperature-dependent dielectric and thermal properties of microwaveable model foods. Transactions of the ASABE 50(6):1457-1467.

Chen J, Pitchai K, Birla S, Negahban M, Jones D, Subbiah J. 2014. Heat and mass transport during microwave heating of mashe dpotato in domestic oven- model development, validation, and sensitivity analysis. J. Food Sciecne 79(10):1991-2004.

Chen J, Pitchai K, Birla S, Gonzalez R, Jones D, Subbiah J. 2015. Development of a multi-temperature calibration method for the measurement of dielectric properties applied to microwaveable food. IEEE Transaction on Dielectrics and Electrical Insulation. Accepted.

Choi Y, Okos MR. 1986. Physical and chemical properties of food. American Society of Agricultural Engineers, St. Joseph, Mich.

Dincov DD, Parrott KA, Pericleous KA. 2004. A new computational approach to microwave heating of two-phase porous materials. International Journal of Numerical Methods for Heat & Fluid Flow 14(6): 783-802.

Datta AK. 2001. Fundamentals of heat and moisture transport for microwaveable food product and process development. In: Datta AK, Anantheswaran R. Handbook of microwave technology for food application. ISBN: 0-8247-0490-8.

Delgado JMPQ. 2011. Heat and mass transfer in porous media, Davanced sturctured materials. Springer.

Dhall A, Halder A, Datta AK. 2012. Multiphase and multicomponent transport with phase change during meat cooking. J. Food Eng. 113(2), 299–309.

Geedipalli SSR, Rakesh V, Datta AK. 2007. Modeling the heating uniformity contributed by a rotating turntable in microwave ovens. Journal of Food Engineering, 82(3):359-368.

Halder A, Dhall A, Datta AK, 2007a. An improved, easily implementable, porous media based model for deep-fat frying: part i: model development and input parameters. Food Bioprod. Process. 85(3), 209–219.

Halder A, Dhall A, Datta AK. 2007b. An improved, easily implementable, porous media based model for deep-fat frying: Part II: results, validation and sensitivity analysis. Food Bioprod. Process. 85(3), 220–230.

Halder A, Dhall A, Datta AK. 2011. Modeling transport in porous media with phase change: applications to food processing. J. Heat Transfer 133(3), 31010.

International Electrotechnical Commission (IEC). 1999. Household microwave ovens - methods for measuring performance. IEC publication, 60705.

Li D. 2010. Numerical simulation of the time-harmonic Maxwell equations and incompressible magnetohydrodynamics problems. Dissertation at the University of British Columbia, Vanvouver, Canada.

Lin Y, Anantheswaran R, Puri V.1995. Finite element analysis of microwave heating of solid foods. Journal of Food Engineering 25(1): 85-112.

Liu S, Fukuoka M, Sakai N. 2013. A finite element model for simulating temperature distributions in rotating food during microwave heating. Journal of Food Engineering 115(1):49-62.

Ni H, Datta AK, Torrance KE. 1999. Moisture transport in intensive microwave heating of biomaterials: a multiphase porous media model. Int. J. Heat Mass Transf. 42, 1501–1512.

Pitchai K, Birla S, Subbiah J, Jones D, Thippareddi H. 2012. Coupled electromagnetic and heat transfer model for microwave heating in domestic ovens. Journal of Food Engineering 112(1-2): 100-111.

Pitchai K, Chen J, Birla S, Gonzalez R, Jones D, Subbiah J. 2014. A microwave heat transfer model for a rotating multi-component meal in a domestic oven: Development and validation. Journal of Food Engineering 128: 60-71.

Rakesh V, Datta AK. 2011. Microwave puffing: Determination of optimal conditions using a coupled multiphase porous media–Large deformation model. J. Food Eng. 107(2), 152–163.

Rakesh V, Datta AK. 2012. Transport in deformable hygroscopic porous media during microwave puffing. AIChE J. 59(1), 33–45.

Resurreccion Jr F, Tang J, Pedrow P, Cavalieri R, Liu F, Tang Z. 2013. Development of a computer simulation model for processing food in a microwave assisted thermal sterilization (MATS) system. Journal of Food Engineering 118(4): 406-416.

Ryynänen S, Ohlsson T. 1996. Microwave heating uniformity of ready meals as affected by placement, composition, and geometry. Journal of Food Science 61(3): 620-624.

Ryynänen S, Risman P, Ohlsson T. 2004. Hamburger composition and microwave heating uniformity. Journal of Food Science 69(7): 187-196.

Stocker, T. 2011. Introduction to climate modelling. Springer. ISBN: 978-3-642-00772-9.

Tilford T, Baginski E, Kelder J, Parrott K, Pericleous K. 2007. Microwave modeling and validation in food thawing applications. The Journal of microwave power and electromagnetic energy: a publication of the International Microwave Power Institute 41(4): 30-45.

USDA-FSIS. 2014. Safe minimum internal temperature chart. http://www.fsis.usda.gov/wps/portal/fsis/topics/food-safety-education/get-answers/food-safety-fact-sheets/safe-food-handling/safe-minimum-internal-temperature-chart/ct_index

Virtanen A, Goedeken D, Tong C. 1997. Microwave assisted thawing of model frozen foods Using Feed-back Temperature Control and Surface Cooling. Journal of Food Science, 62(1):150-154.

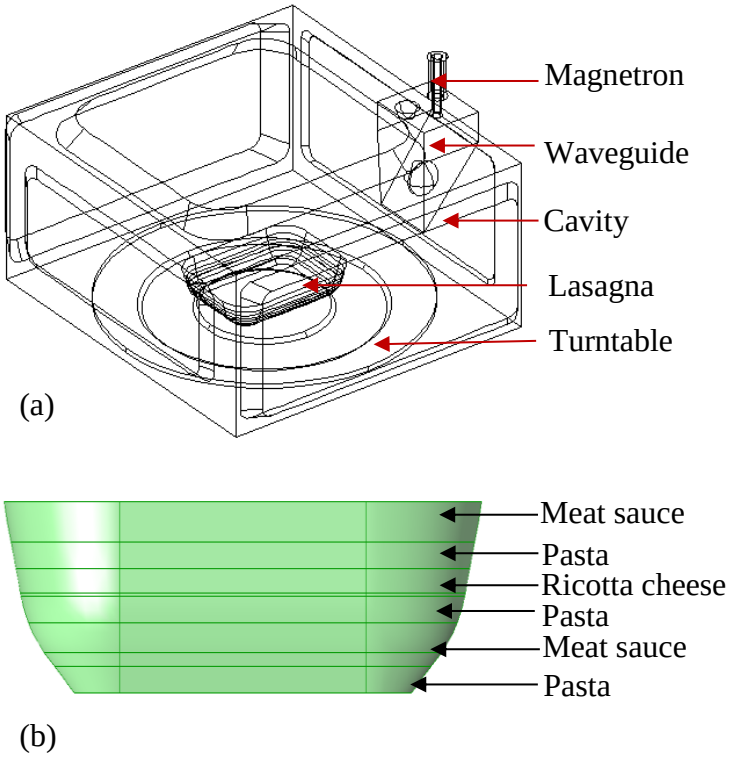

Figure 3. 1. Geometric model of a 1200 W rated domestic microwave oven (Model No: NN-SD767W, Panasonic Corporation, Shanghai, China) (a) and layers of food components of lasagna (b).

```
for i = 1: 36 (number of turntable rotations to complete the full cooking time)

        Determine EM field for food at 12 discrete locations separately along its
        rotation in COMSOL;

Pass the EM field data to Matlab;

        Rotate EM field data from all 12 locations to initial position;

        Interpolate electromagnetic field data at all angles to initial coordinates;

        Average EM field of 12 locations;

Pass the average EM field to COMSOL;
```

Figure 3. 2. Pseudo code depicting strategies to simulate microwave heating of rotating frozen lasagna.

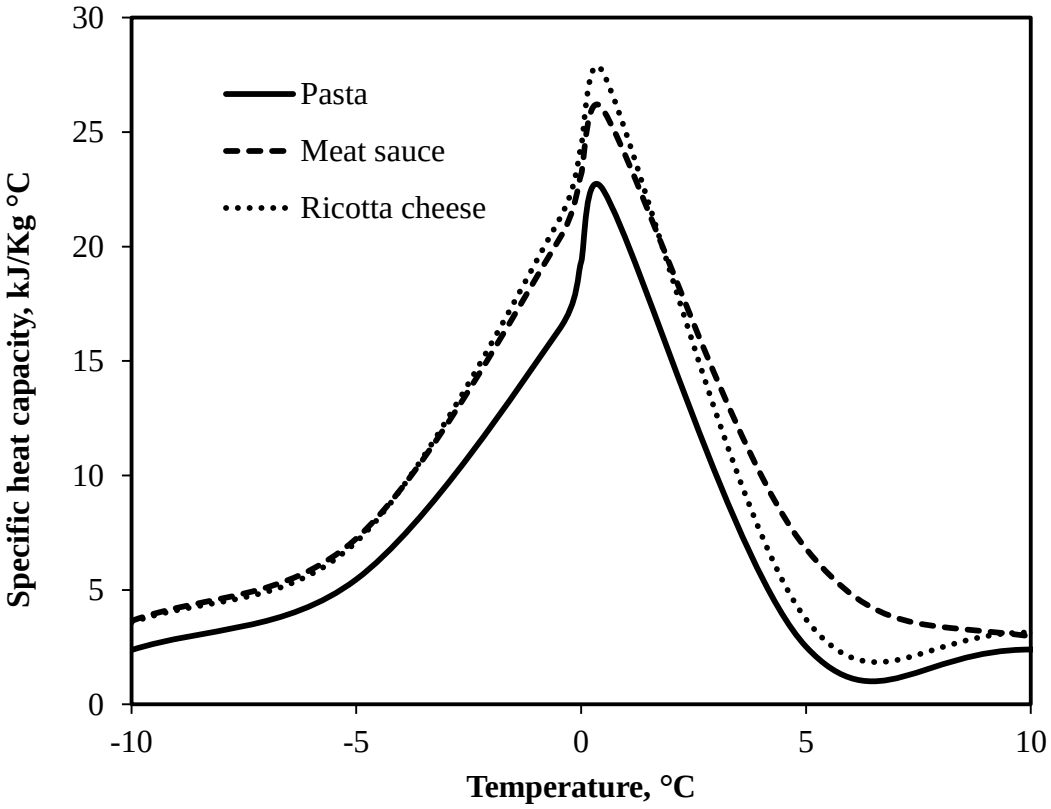

Figure 3. 3. Specific heat capacity of lasagna food components as a function of temperature.

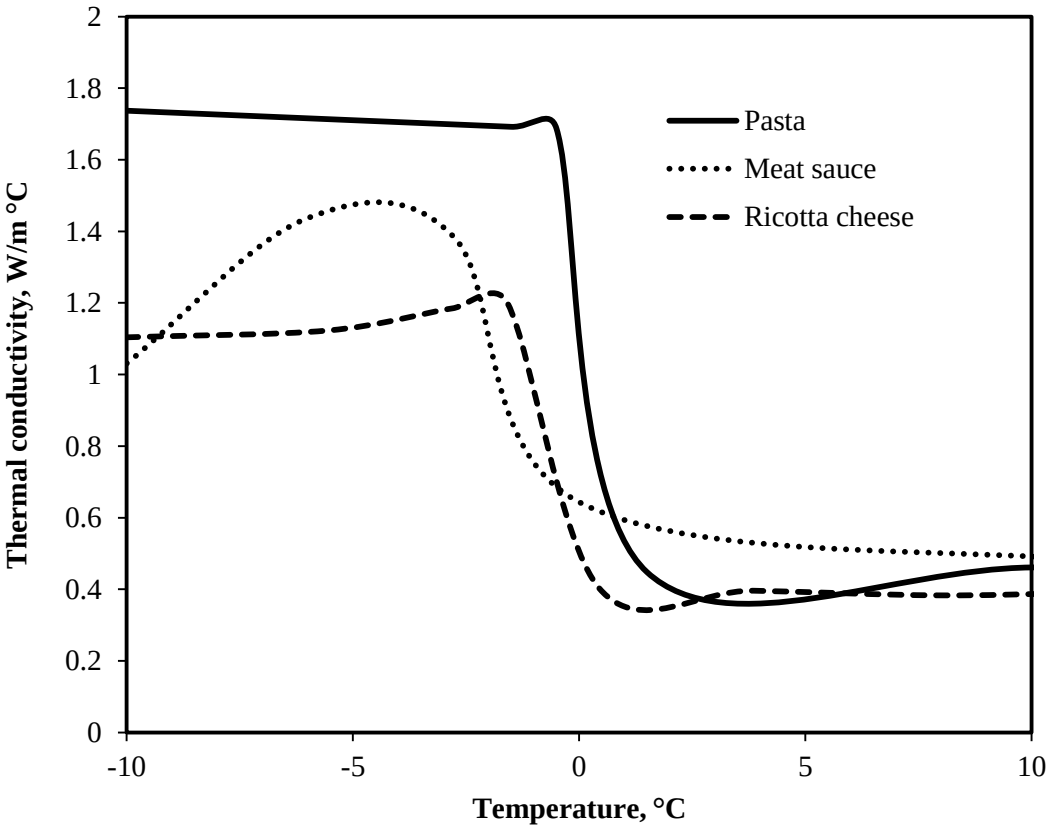

Figure 3. 4. Thermal conductivity of lasagna food components as a function of temperature.

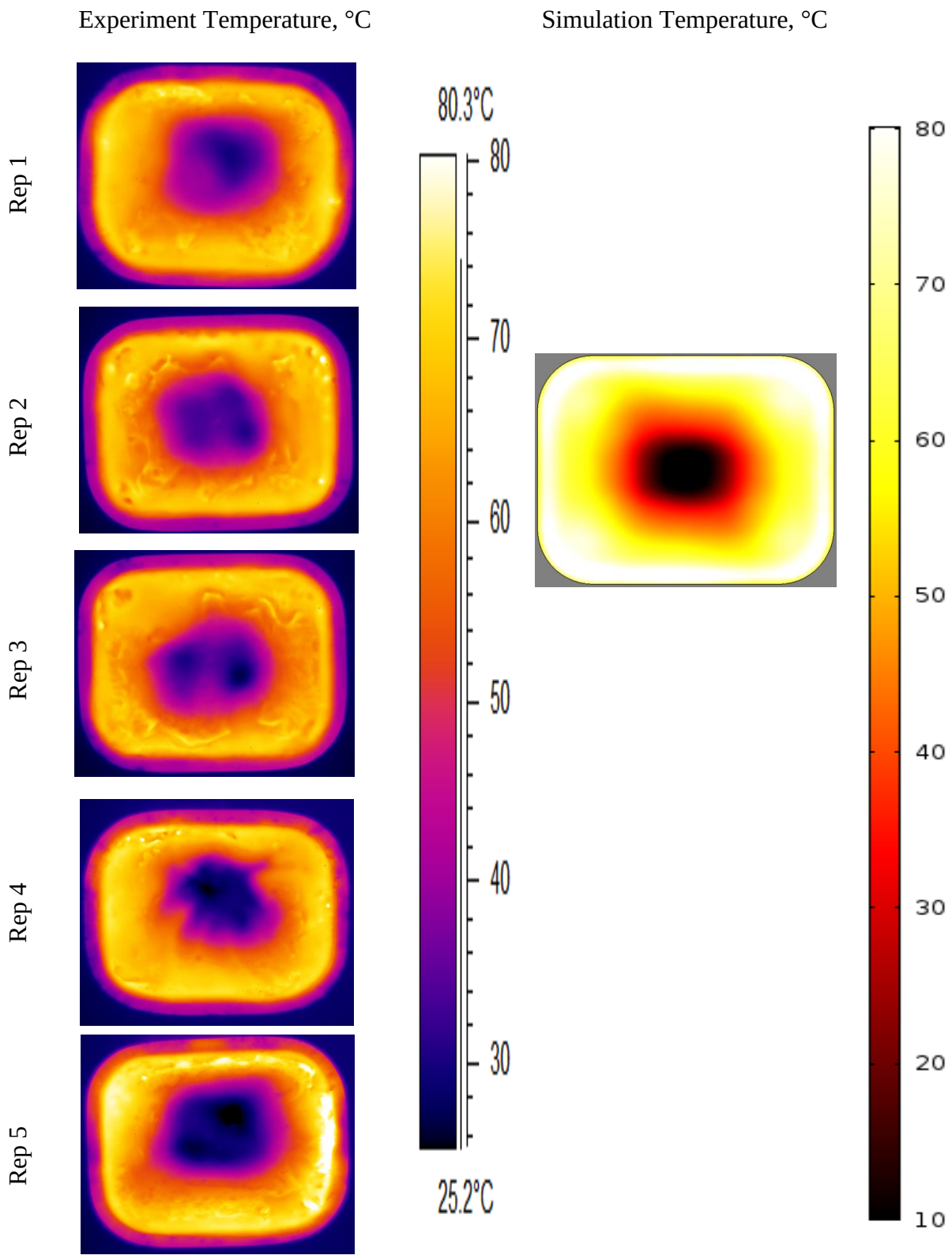

Figure 3. 5. Comparison of simulated and experimental surface temperature profiles.

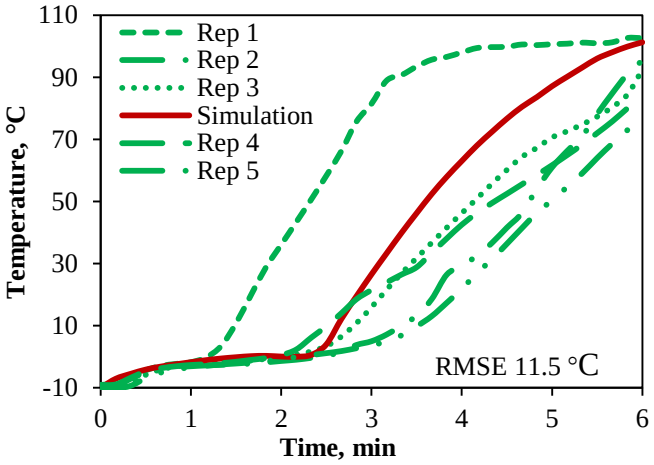

A. Location 1

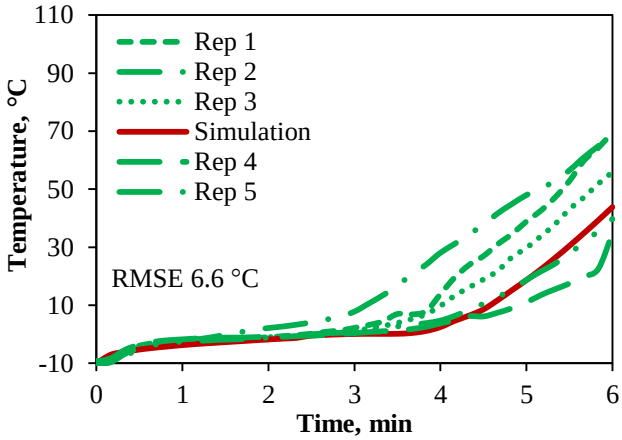

B. Location 2

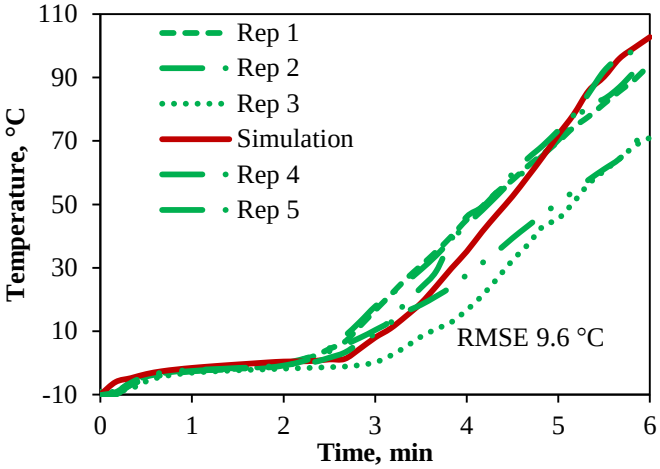

C. Location 3

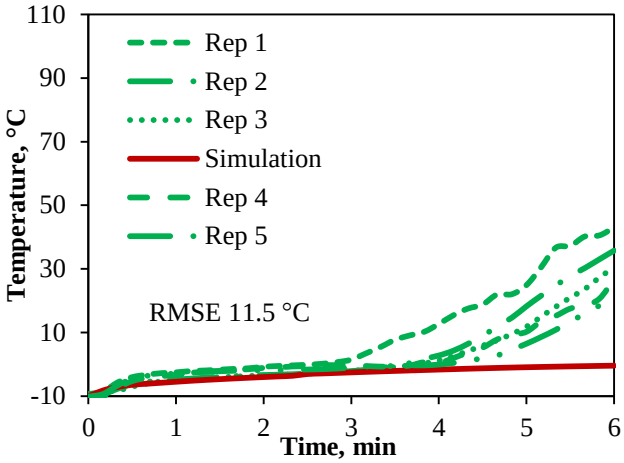

D. Location 4

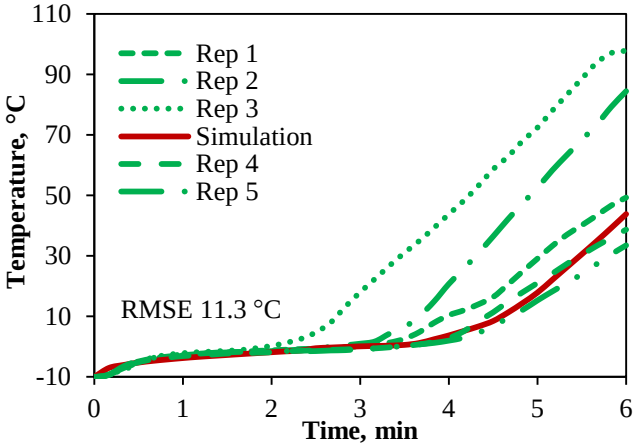

E. Location 5

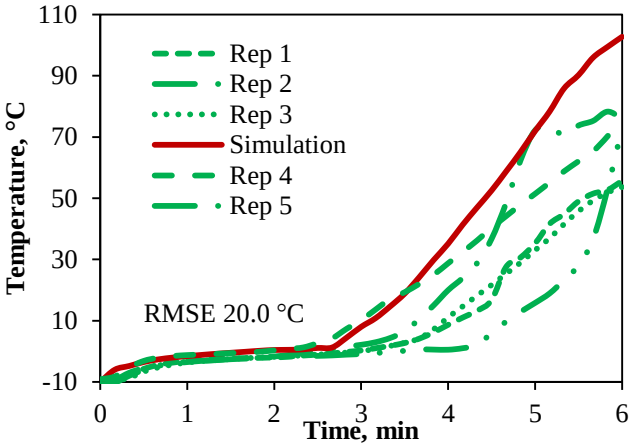

F. Location 6

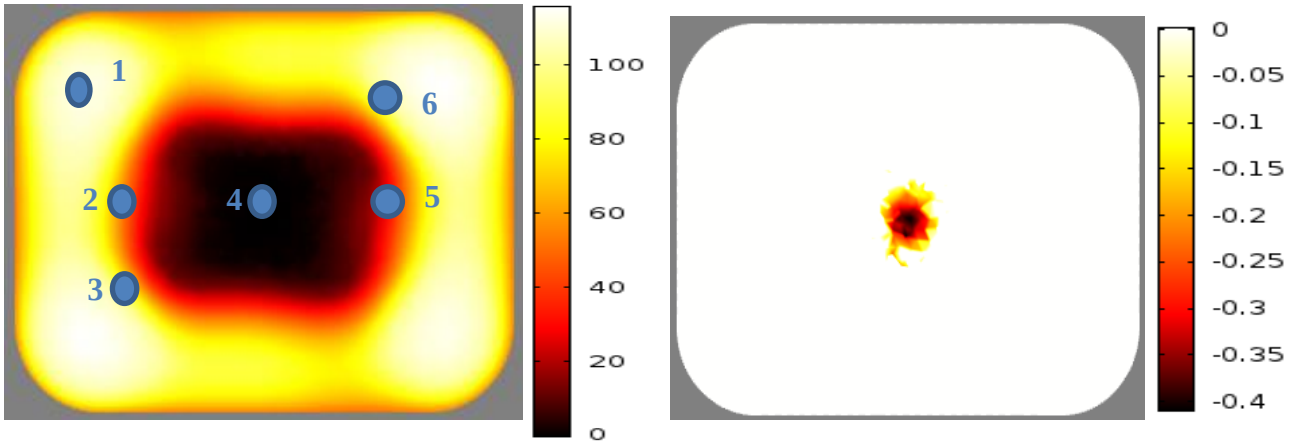

G. Sensors location in center plane H. Frozen region in center plane

Figure 3. 6. Comparison of simulated and experimental transient temperature profiles at six points.

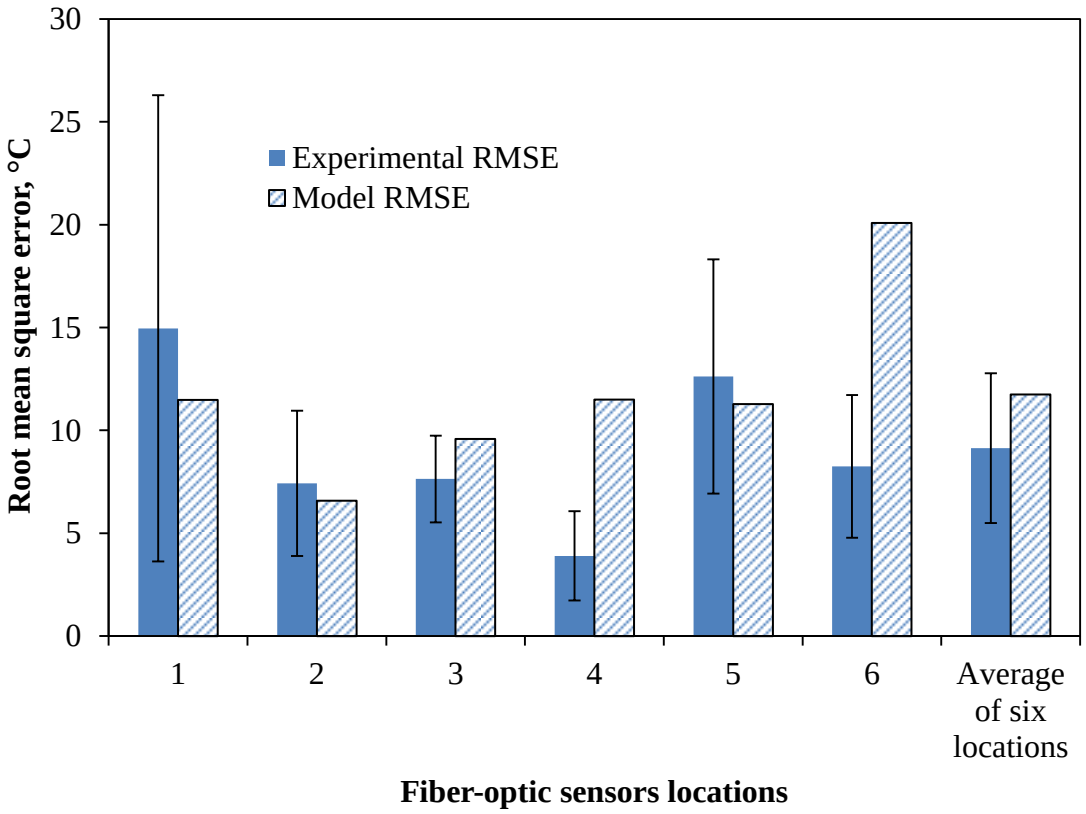

Figure 3. 7. Root mean square error comparison of experimental variations and model prediction.

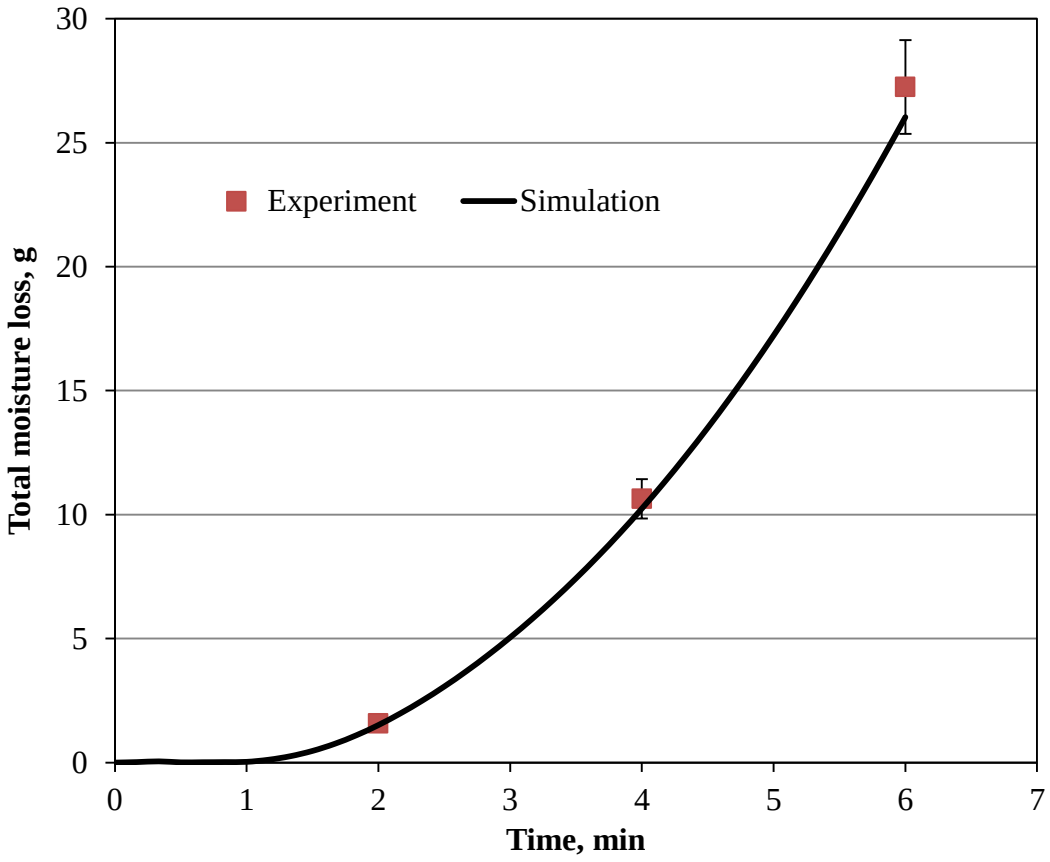

Figure 3. 8. Total moisture loss profile comparison between the simulation and the experimental results during 6 minutes of microwave heating of lasagna.

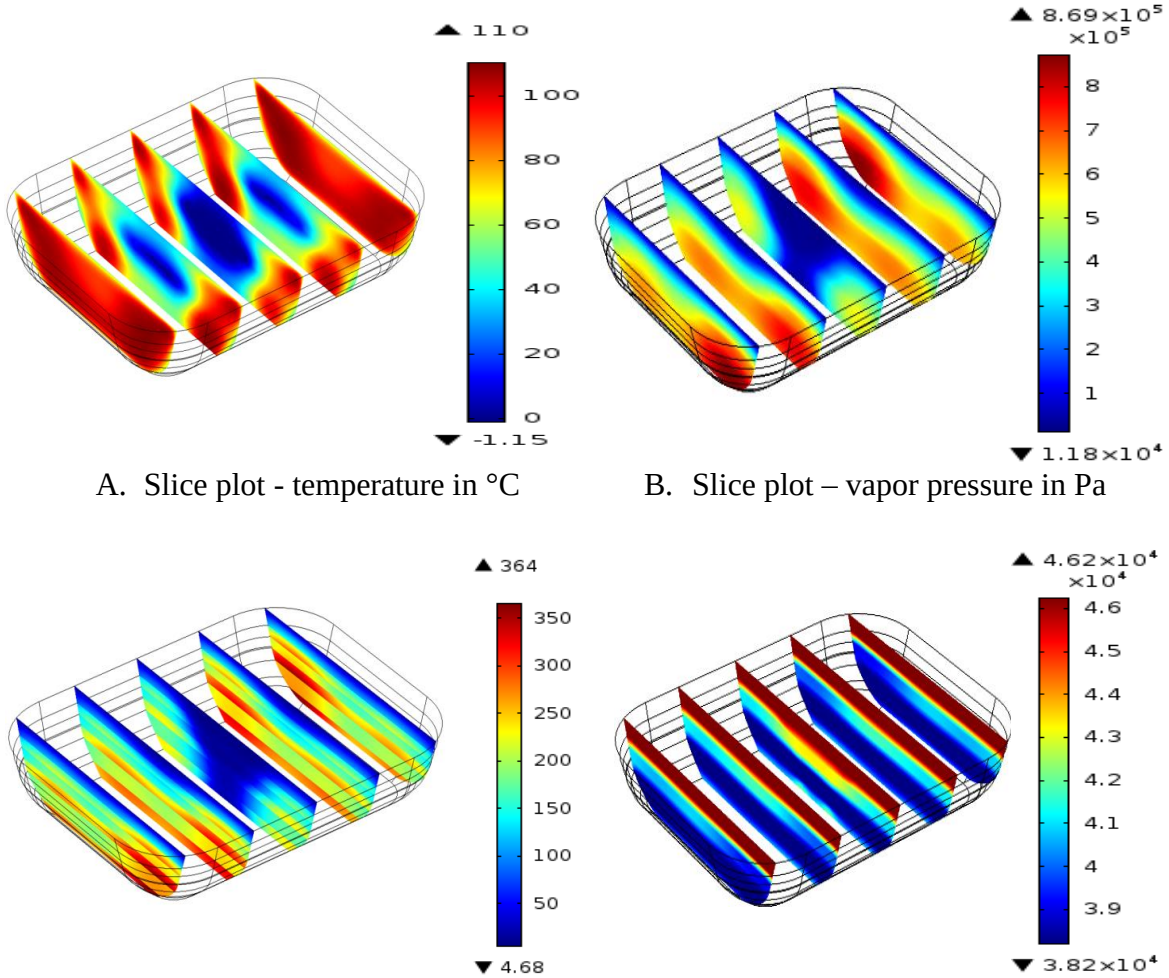

A. Slice plot - temperature in °C

B. Slice plot – vapor pressure in Pa

C. Slice plot - vapor concentration normalized to porosity in mol/m^3

D. Slice plot – water concentration in mol/m^3

Figure 3. 9. Slice plot of vapor pressure, vapor concentration, and water concentration distribution at the end of 6 minutes heating time.

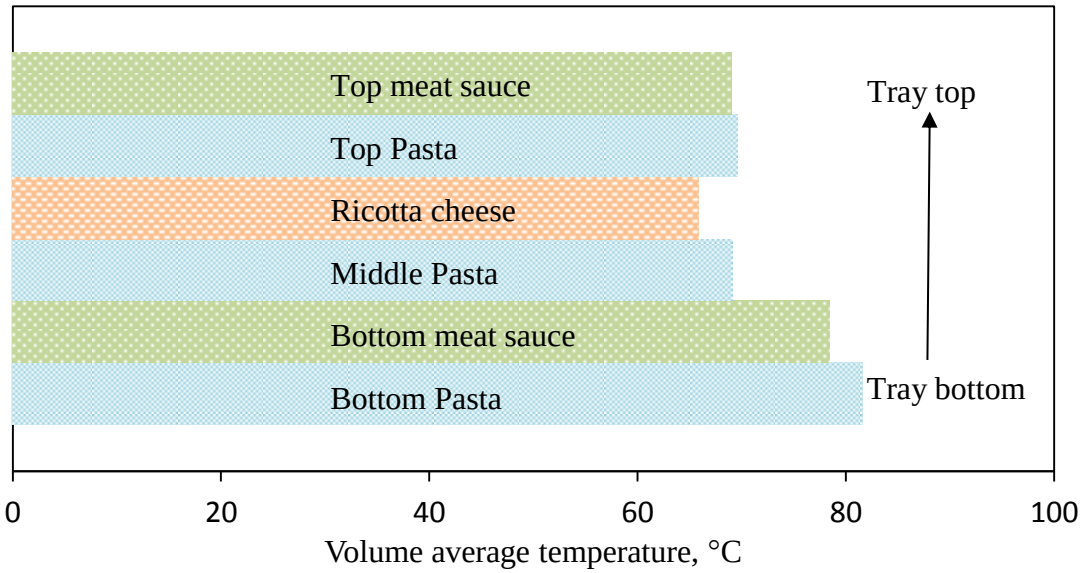

A. Volume average temperature at different lasagna components

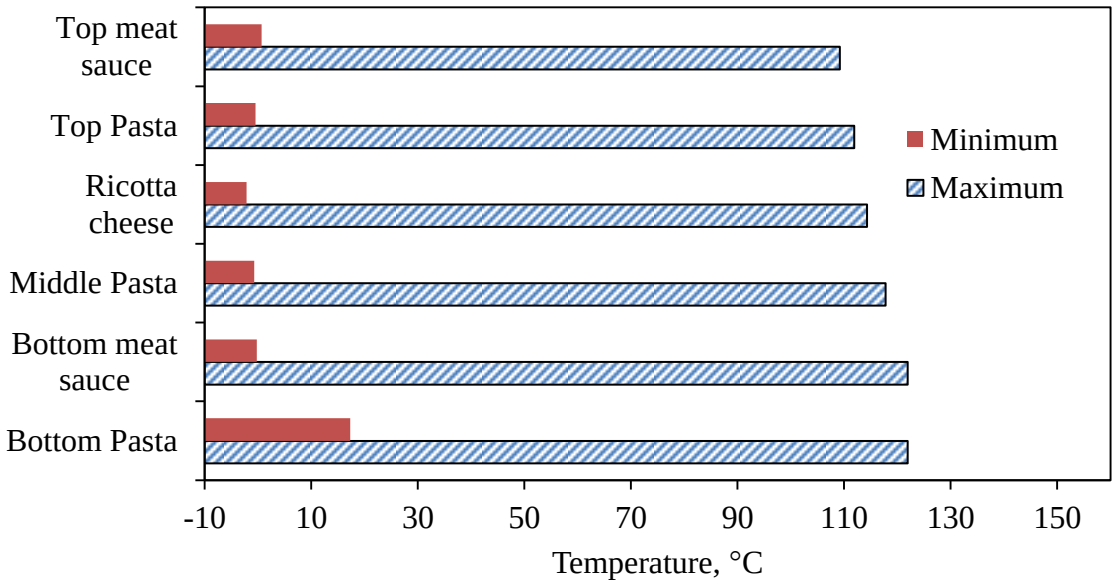

B. Maximum and minimum temperatures at different lasagna components

Figure 3. 10. Volume average, maximum, and minimum temperatures at the end of 6 minutes heating time at different lasagna components.

Table 3. 1. Summary of material properties.

Parameter	Symbol	Value	unit	Source/Remarks
Initial conditions				
Water saturation	S_{w0}	0.99		Model assumption
Gas saturation	S_{g0}	0.01		Model assumption
Water concentration				
Pasta	C_{w0}	36501	$mol \cdot m^{-3}$	Calculated from S_{w0} and porosity
Meat sauce		49620		
Ricotta cheese		46107		
Porosity				
Pasta	Φ	0.665		Calculated from the volume fraction of water
Meat sauce		0.904		
Ricotta cheese		0.840		
Vapor concentration				
Pasta	C_{v0}	2.1×10^{-3}	$mol \cdot m^{-3}$	Calculated from S_{g0} and porosity
Meat sauce		2.9×10^{-3}		
Ricotta cheese		2.7×10^{-3}		
Air concentration				
Pasta	C_{a0}	0.27	$mol \cdot m^{-3}$	Calculated from S_{g0} and porosity
Meat sauce		0.37		
Ricotta cheese		0.34		
Ambient pressure	P_{amb}	101325	Pa	
Density				
Pasta	ρ_s	1488	$kg \cdot m^{-3}$	Choi and Okos (1986)
Meat sauce		1170	$kg \cdot m^{-3}$	Choi and Okos (1986)

Ricotta cheese		1499	$kg \cdot m^{-3}$	Choi and Okos (1986)
Water	ρ_w	998	$kg \cdot m^{-3}$	Choi and Okos (1986)
Vapor	ρ_v	Ideal gas	$kg \cdot m^{-3}$	
Air	ρ_a	Ideal gas	$kg \cdot m^{-3}$	
Ambient vapor density	$\rho_{v,amb}$	0.02	$kg \cdot m^{-3}$	
Specific heat capacity				
Pasta		1664	$J \cdot kg^{-1} \cdot K^{-1}$	Choi and Okos (1986)
Meat sauce	Cp_s	1674	$J \cdot kg^{-1} \cdot K^{-1}$	Choi and Okos (1986)
Ricotta cheese		1912	$J \cdot kg^{-1} \cdot K^{-1}$	Choi and Okos (1986)
Water	Cp_w	4178	$J \cdot kg^{-1} \cdot K^{-1}$	Choi and Okos (1986)
Vapor	Cp_v	2062	$J \cdot kg^{-1} \cdot K^{-1}$	Choi and Okos (1986)
Air	Cp_a	1006	$J \cdot kg^{-1} \cdot K^{-1}$	Choi and Okos (1986)
Thermal conductivity				
Pasta		0.217	$W \cdot m^{-1} \cdot K^{-1}$	Choi and Okos (1986)
Meat sauce	k_s	0.219	$W \cdot m^{-1} \cdot K^{-1}$	Choi and Okos (1986)
Ricotta cheese		0.169	$W \cdot m^{-1} \cdot K^{-1}$	Choi and Okos (1986)
Water	k_w	0.57	$W \cdot m^{-1} \cdot K^{-1}$	Choi and Okos (1986)
Vapor	k_v	0.026	$W \cdot m^{-1} \cdot K^{-1}$	Choi and Okos (1986)
Air	k_a	0.026	$W \cdot m^{-1} \cdot K^{-1}$	Choi and Okos (1986)
Intrinsic permeability				
Water	$k_{in,w}$	1×10^{-15}	m^2	Ni and others (1999)
Gas	$k_{in,g}$	1×10^{-14}	m^2	Ni and others (1999)
Diffusion coefficient				
Water	D_w	$1.0 \times 10^{-7} e^{(-2.8+2M)}$		Rakesh and Datta (2011)
Gas	D_g	2.6×10^{-5}	$m^2 \cdot s^{-1}$	Ni and others (1999)
Viscosity				
Water	μ_w	9.88×10^{-4}	$Pa \cdot s$	Rakesh and Datta (2012)

Gas	μ_g	1.80×10^{-5}	Pa·s	Rakesh and Datta (2012)
Latent heat of vaporization	λ	2.26×10^{6}	$J \cdot kg^{-1}$	Rakesh and Datta (2012)
Evaporation rate constant	K	50	s^{-1}	Model assumption
Mass transfer coefficient	h_m	0.011	$m \cdot s^{-1}$	Ni and others (1999)
Heat transfer coefficient	h	20	$W \cdot m^{-2} \cdot C^{-1}$	Ni and others (1999)
Dielectric constant	ε’	measured		Chen and others (2015)
Dielectric loss factor	ε”	measured		Chen and others (2015)
Molecular weight of vapor	M_w	18	g/mol	

CHAPTER IV

A MICROWAVE HEAT TRANSFER MODEL FOR THAWING OF A FROZEN PIZZA USING SUSCEPTOR IN A DOMESTIC OVEN

Krishnamoorthy Pitchai [a, b], Jiajia Chen [b], Sohan Birla [b], Mehrdad Negahban[c], David Jones [b], and Jeyamkondan Subbiah [a, b, *]

[a] *Department of Food Science and Technology, University of Nebraska-Lincoln, NE – 68583*

[b] *Department of Biological Systems Engineering, University of Nebraska-Lincoln, NE – 68583*

[b] *Department of Mechanical and Materials Engineering, University of Nebraska-Lincoln, NE – 68588*

*Corresponding author: Jeyamkondan Subbiah, Kenneth E. Morrison Distinguished Professor of Food Engineering, Departments of Food Science & Technology and Biological Systems Engineering, 212 L.W.Chase Hall, East Campus, University of Nebraska-Lincoln, Lincoln, NE-68583-0726, Ph. No: 402-472-4944, Fax No: 402-472-6338, Email: jeyam.subbiah@unl.edu.

Citation: Pitchai, K., Chen, J., Birla, S., Jones, D., Subbiah, J. 2015. A microwave heat transfer model for thawing of a frozen pizza using susceptor in a domestic oven. Journal of Food Engineering. In review.

4.1. Abstract

Susceptors are used in microwavable food packages to facilitate preferential heating. A heat transfer model is needed to understand microwave interactions with food and susceptor package. The objective of this study was to develop and validate a 3-D finite element model for predicting microwave heating of frozen pizza placed on a susceptor tray in a domestic oven. Temperature-dependent dielectric and thermophysical properties of frozen pizza components were measured from -10 °C to 110 °C and provided as input to the multiphysics model. Electrical conductance of susceptor film was measured as a function of temperature using a split post dielectric resonator attached to a network analyzer. Transition boundary condition was used to model susceptor, which is geometrically thin but not electrically thin. The susceptor was considered as a highly conductive layer and the boundary heat source was applied in the heat transfer analysis to calculate the temperature in the susceptor film. The model simulated a stationary frozen pizza kept at the center of the turntable in a 1250 W domestic microwave oven for a 130 s microwave heating. Simulated temperature profiles and experimental temperature profiles obtained using a thermal imaging camera and fiber-optic sensors were in good agreement. The root mean square error values of transient temperature profiles of five locations ranged from 5.0 °C to 12.6 °C. The root mean square error of experimental variations between the replications ranged from 2.6 to 10.6 °C at different location, with an average value of 5.9 °C. The validated model can be used for optimizing the layout and food system/package modification for improved heating uniformity.

Keywords: Susceptor-assisted microwave heating, transition boundary condition, microwave heat transfer modeling, finite element modeling, electrical conductivity of susceptor film, validation.

4.2. Introduction

Susceptors have been used as active package materials since the late 1970s (Cesnek et al. 2003) for providing preferential surface heating. Susceptors are typically very thin metal layers deposited onto microwaveable food packages. Susceptors absorb electromagnetic energy (Risman, 2009). Microwave susceptor packaging can be handy to overcome the lack of browning and crispiness in food products that otherwise would become soggy and not brown in conventional packaging. In spite of more than 40 years of uses of the susceptor, microwave interaction of it with food has not been extensively studied. Modeling of susceptor and food interaction in microwave ovens is an opportunity to bridge the knowledge gap and better understand the role of microwave food packages.

A computer-based simulation of microwave cooking is a promising tool that offers insights into microwave interactions with food components and packages. It can also save a tremendous amount of time in food product development (Celuch and Kopyt, 2009). A few researchers have attempted to develop susceptor-assisted microwave heat transfer models (Celuch et al. 2008; Soltysiak et al. 2008). Celuch et al. (2008) and Soltysiak et al. (2008) used finite-difference time domain (FDTD) based software, QuickWave 3D, to solve the susceptor- assisted microwave heating of a water container placed inside a cavity. For susceptor material, the authors created a 1-mm thick layer of

surrogate materials whose properties were adjusted to mimic the susceptor film. The authors studied the effect of conductance on power absorption in water, but they did not validate their approach by experimental methods. Pitchai et al. (2011) developed a 3-D Finite Element Method (FEM) based computer model to simulate microwave interactions with a model food (1% gellan gel) and susceptor placed on top of a model food. There has not been any microwave heat transfer models developed for susceptor-assisted microwave heating of a multi-component food going through a change (frozen to thaw). Most of the simulation models in the literature do not consider one or more of the following: (i) phase change from frozen to thawing, (ii) detailed geometry of the cavity, (iii) temperature-dependent dielectric and thermal properties, (iv) multi-component food products, and (v) including susceptor. In this study, all the aforementioned factors are included in the model development. The main objective of this study was to develop and validate a microwave heat transfer model to simulate microwave interaction with a multi-component frozen food and a thin susceptor film. Specific objectives of this study were to:

i. measure electrical conductivity of susceptor film as a function of temperature using split post dielectric resonator,
ii. develop a coupled electromagnetic and heat transfer model to simulate microwave interaction with a susceptor film and a frozen pizza, and
iii. validate the electromagnetic and heat transfer model by comparing the temperature predictions with experimental measurements.

4.3. Model Development

4.3.1. Governing equations

Electromagnetic field strength (**E**) at any point in the computational domain is governed by set of Maxwell's equations. The combined wave form of Maxwell's equation is expressed as (Chen et al. 2014):

$$\nabla\times\mu_r^{-1}(\nabla\times\mathbf{E})-(\frac{2\pi f}{c})^2\left(\epsilon_r-i\,\epsilon''\right)\mathbf{E}=0 \qquad (4.1)$$

where f is frequency in 2.45 GHz, c is the speed of light in 3×10^8 m/s, ϵ'' is the dielectric loss factor, and ϵ_r and μ_r are relative dielectric constant, and permeability of the material respectively.

Electromagnetic power density (Q) is the function of frequency and loss factor and square of the electric filed strength.

$$Q = \pi f\epsilon_o\epsilon''\,|\vec{\mathbf{E}}|^2 \qquad (4.2)$$

where ϵ_0 is the free space permittivity 8.854×10^{-12} F/m.

Dissipated power is diffused in the food and governed by Fourier's heat transfer equation.

$$\rho C_p\frac{\partial T}{\partial t} = \nabla.(k.\nabla T) + Q \qquad (4.3)$$

where ρ is the density in kg/m^3, C_p is the specific heat capacity at constant pressure in J/kg °C, k is the thermal conductivity in W/m °C, T is the transient temperature in °C.

4.3.2. Boundary conditions

The wall of the oven was assumed to be a perfect electrical conductor, where electric field strength is zero. In this study, transition boundary condition was used for resolving the power absorption in the susceptor film. The transition boundary condition is used on interior boundaries to model susceptor film that is geometrically thin but not electrically thin. It represents a discontinuity in the tangential electric field. Mathematically, it is described by a relation between the tangential electric field strength ($E_{t,}$ V/m) discontinuity and the induced surface current density (J_s, A/m):

$$J_{s1} = \frac{(Z_s E_{t1} - Z_T E_{t2})}{Z_s^2 - Z_T^2} \quad (4.4)$$

$$J_{s2} = \frac{(Z_s E_{t2} - Z_T E_{t1})}{Z_s^2 - Z_T^2} \quad (4.5)$$

$$Z_s = \frac{-j\omega\mu}{\varphi} \frac{1}{\tan(\varphi d)} \quad (4.6)$$

$$Z_T = \frac{-j\omega\mu}{\varphi} \frac{1}{\sin(\varphi d)} \quad (4.7)$$

$$\text{where } \varphi = \omega \sqrt{(\epsilon + \frac{\sigma}{j\omega})\mu}$$

where indices 1 (above the susceptor) and 2 (below the susceptor) refer to the different sides of the susceptor film, Z is the surface impedance in Ω/m, σ is the electrical conductivity in S/m of the susceptor film, and d thickness of the film in m. Thus, wave number defined as number of wave cycles per unit distance (φ), is directly related to electrical conductivity of the film and the surface impedance of the film is inversely

proportional to wave number and therefore the electrical conductivity. The surface impedance determines the induced surface current density in the film.

The susceptor film thickness was set to 0.1 mm. Thickness of the susceptor film was measured using a precision micrometer (Model no: 49-60; Testing machines, Inc., Amityville, New York). The actual thickness of the film was 0.127 mm. Electrical conductivity was adjusted such that the surface conductance of the 0.1 mm film used in the model is equal to that of the 0.127 mm film used in the experiments. The transition boundary condition was applied on the bottom of the frozen pizza where the susceptor film is physically present. At the frozen pizza surface, a convective natural heat flux boundary was considered at the food-air interface. The surface of the frozen pizza (both top surface and the circumference of pizza which is exposed to air) exchanges heat with surrounding air by convection expressed as:

$$-k \frac{\partial T}{\partial n} = h\,(T-T_a) \qquad (4.8)$$

The fan in the oven circulated the air inside the cavity. Heat exchange between air and the frozen pizza was approximated by assuming a heat transfer coefficient value of 20 W/m^2 °C. The fan in the oven continuously circulated ambient air into the cavity, and therefore the initial temperature of 20 °C was assumed to remain constant during heating. In the heat transfer analysis, the boundary heat source ($Q_b, \frac{W}{m^2}$) was applied in the bottom of the frozen pizza. The boundary heat source in the bottom of the frozen pizza is expressed as:

$$-n.(-k\,\nabla T) = Q_b \qquad (4.9)$$

The boundary heat source is calculated by multiplying surface current density (J_s, A/m) with tangential electric strength ($E_{t,}$ V/m):

$$Q_b = J_s \times E_t \qquad (4.10)$$

4.3.3. Geometric model

Susceptor assisted microwave heating of a frozen pizza was performed in a 1250 W rated power (1200 W available power measured using IEC 60705 method) microwave oven (Model no: NN–SD967S; Panasonic Corporation). An inclusive and detailed geometry of the oven was created in COMSOL Multiphysics v4.4 (COMSOL, Burlington, MA). In this study, we included the magnetron as a coaxial power source feeding microwave energy into the waveguide located at the center of the right side of the cavity wall. The geometric model of the microwave oven and frozen pizza is shown in Figure 4. 1.

4.3.4. Model assumptions

Following assumptions were considered in the model development.

i. In the retail pack, frozen pizza was placed inside a paperboard box (177×177×35 mm). The paperboard box top peeled along the perforations and the frozen pizza removed from the paperboard box and plastic overwrap. The paperboard box top fully folded around the bottom of the paperboard box. Now, the susceptor film surface faced up and creating a platform to place the frozen pizza on top. The cooking instructions recommended that the frozen pizza needs to be placed on the top of platform and cooked. The validation studies considered frozen pizza placed and cooked on top of platform. The paperboard box does not interact with

electromagnetic waves because it has very low dielectric constant. Therefore, the paperboard box was not considered in both electromagnetic and heat transfer analysis. However, the frozen pizza was raised to a height of 35 mm from the turntable in the computational domain to account for the physical position of the frozen pizza on top of a platform.

ii. A partial-coupling method was used to solve electromagnetic and heat transfer equations, meaning that heat transfer equations were solved for a defined time (Δt = 10 s). Based on the temperature at the end of 10 s, the dielectric constant and loss factor values of frozen pizza components and electrical conductivity of susceptor film were updated in the model to calculate the new electromagnetic power density for the next time step.

iii. The initial temperature of the frozen pizza was considered as homogeneous and isotropic (-10 °C).

iv. The mass transfer physics was not included in the model.

v. Simulation was performed by considering a 2.45 GHz magnetron frequency.

vi. The frozen pizza consisted of three food components: bread crust, tomato sauce, and mozzarella cheese. All three components were considered as a solid domain and not going through any deformation during heating.

4.3.5. Simulation strategy

A Generalized Minimal Residual (GMRES) method based iterative solver was used to solve electromagnetic and heat transfer equations (COMSOL, 2013). Electric field strength was calculated by solving Maxwell's electromagnetic wave equation (Eq. 4.2) to calculate dissipated power density. In heat transfer analysis, dissipated power

density is updated in Eq. 4.3 to calculate temperature field. Thermal and dielectric properties of the food and electrical conductivity of susceptor are updated with respect to changes in the temperature field. Electric field is then solved and the cycle is repeated until the cooking time is completed.

4.3.6. Meshing scheme

Air, glass turntable, and frozen pizza domains were discretized using four-node unstructured tetrahedral elements with the quadratic shape functions. Different mesh refinement levels were enforced for different domains (i.e., air, size: 30 - 2 mm; glass turntable, size: 6 - 3 mm; mozzarella cheese, size: 4 - 1 mm; bread crust and tomato sauce, size: 4 - 2 mm). The boundary layer elements were created in the bottom of the pizza to facilitate accurate calculation of boundary heat source and temperature in susceptor (number of boundary layers = 8). In all the domains, average element quality, which is a dimensionless quantity between 0 and 1, where 1 represents a perfectly regular element, and 0 represents a degenerated element, was ensured to be > 0.02 (COMSOL, 2013). Three dimensional meshes created about 544,000 total elements, out of which 155,000 elements comprised the frozen pizza and 2,400 elements in susceptor (Figure 4. 2). The simulation was performed on a Dell Precision T7500 workstation with an 72 GB RAM running on two quad-core Intel Xeon X5570 2.93 GHz processor.

4.4. Materials and Methods

4.4.1. Frozen pizza sample

The frozen pizza was purchased from the local grocery store. The frozen pizza was removed from the package and drilled at five locations to a depth of 25 mm from the

top using a 2 mm drill bit. Plastic tubes (dia-2 mm; height-25 mm) were inserted in drilled holes and were re-frozen. Then, the frozen pizza was repacked and sealed and stored back in the freezer until usage.

4.4.2. Split post dielectric resonator

The electrical conductance of the susceptor film was measured using a split post dielectric resonator (SiPDR 2400 MHz fixture; QWED Sp. z o.o., Warsaw, Poland) connected with a 2-port vector network analyzer (model no: PNA-5230; Agilent Technologies, Inc., Santa Clara, CA). The spilt post dielectric resonator connected with high-temperature coaxial cable was placed inside a micro-climatic chamber (MCBH 1.2., Cincinnati Sub-Zero Products, Inc., Cincinnati, OH) to control the susceptor film temperature. The two parameters values (resonant frequency and Q-factors) in the presence and absence of susceptor film were recorded from 30 to 180 °C. The Q-factor in the susceptor (Q_s) was calculated using the following equation:

$$Q_s = \frac{1}{\left(\frac{1}{Q_t} - \frac{1}{Q_e}\right)} \qquad (4.11)$$

where Q_s is the Q-factor in the susceptor film, Q_t is the Q-factor with the presence of susceptor in the split post dielectric resonator, Q_e is the Q-factor with absence of susceptor in the split post dielectric resonator.

Using the resonant frequency shifts due to presence and absence of susceptor film and the Q-factor in the susceptor film, the electrical conductance in S was calculated (Krupka et al. 2007). The schematic diagram of experimental setup for measurement of electrical conductance of susceptor film is shown in Figure 4. 3. The theoretical

explanation for the calculation of electrical conductance of thin susceptor film is explained in detail in Krupka et al. (2007). The electrical conductance calculated from this procedure is the inverse of the sheet resistance. The electrical conductance was divided by the film thickness to calculate the electrical conductivity of the susceptor film in S/m (Perry and Lentz, 2009). The dielectric constant of the susceptor film was assumed to be 1.

4.4.3. Dielectric properties

All three frozen pizza components (mozzarella cheese, tomato sauce, and bread crust) were separated manually from pizza after letting the pizza thawing in room temperature. During separation, it was made sure that each of the components did not mix with other components. Then, each of the components was placed inside a sealed plastic box and re-frozen until usage for dielectric properties measurements. The dielectric properties of each pizza components were measured separately using a multi-point temperature calibration protocol outlined in Chen et al. (2013). Dielectric properties were measured in triplicate and the mean value was used in simulation.

4.4.4. Thermal properties

The specific heat capacity of the frozen pizza components was measured using a differential scanning calorimeter (DSC 822, Mettler Toledo, Columbus, OH) in accordance with the ASTM standard E1269-01. Measurements were carried out using a Pyris 1 DSC system equipped with an Intracooler 1P refrigeration unit (Perkin-Elmer, Inc., Norwalk, CT, USA). Nitrogen gas was used to flush the sample holder unit. Three individual (25 mg) samples were scanned from -10 °C to 20 °C at a heating rate of 5 °C min^{-1} placed in 40 µl aluminum crucibles (Model no: ME-27331, Perkin-Elmer Corp.,

Norwalk, CT, USA) covered with a lid. An empty aluminum crucible was used as a reference.

The thermal conductivity of the frozen pizza components were measured, as a function of temperature from -10 to 10 °C using a KD2 Pro thermal properties analyzer (Decagon Devices, Inc., Pullman, WA, USA). Before each experiment, the calibration of the TR-1 thermal conductivity probe was verified using an acetal plastic standard. Samples were filled in a 30 mm diameter copper tube and immersed in a hot water bath and maintained at a desired temperature. The TR-1 probe was used to measure thermal conductivity of 5 °C and 100 °C. The TR-1 probe was also inserted into samples maintained at a frozen temperature prior to recording; the sample was drilled using a mechanical drill bit of 2 mm in order to easily insert the TR-1 probe into samples.

4.4.5. Experimental validation

The frozen pizza samples were removed from the freezer and placed inside a micro-climatic chamber (MCBH 1.2, Cincinnati Sub-Zero Products, Inc., Cincinnati, OH) maintained at -10 °C. The transient temperature was recorded using fiber-optic sensors (8-channel signal conditioner, FISO Technologies Inc., Quebec, Canada) at five locations (Figure 4. 12.A). Before inserting the fiber-optic sensors into the product, the plastic tubes from the holes were removed. The pizza was cooked in a 1250 W microwave oven for 2 min 10 s. After microwave heating, a thermal image at the top surface was recorded using an infrared camera (SC640, 640 × 480 pixels accuracy ± 2 °C, FLIR systems, Boston, MA) and then immediately flipped upside down to record the bottom surface thermal image. We measured the temperature profiles in three replications and reported in this study.

4.5. Results and Discussion

4.5.1. Dielectric properties

The temperature-dependent dielectric constants of three pizza components (bread crust, tomato sauce, and mozzarella cheese) measured at 2.45 GHz are shown in Figure 4. 4. The dielectric constant of all three components increased exponentially from the frozen state (-10 °C) to the thawed state (0 °C). The dielectric constant of mozzarella cheese and tomato sauce rapidly increased from the lowest values of 5.9 and 6.3 at -10 °C to the highest values of 21.8 and 77.8 at 0 °C, and then values did not change considerably above 0 °C. The dielectric constant of bread crust increased from 5.9 at -10 °C to 47.6 at 0 °C, and then linearly decreased to 42.9 at 100 °C. In the entire measured temperature range, tomato sauce has the highest dielectric constant values among all three components. This may be due to higher moisture content in the tomato sauce, when compared to mozzarella cheese and bread crust.

The trend of dielectric loss factors of bread crust, tomato sauce, and mozzarella cheese as a function of temperature at 2.45 GHz is shown in Figure 4. 5. Similar to dielectric constant, the dielectric loss factors of all three food components exponentially increased from frozen to thawed state. Above 0 °C, the dielectric loss factors of all three components increased linearly. The tomato sauce had the higher slope of increase of dielectric loss factor with respect to temperature after thawing. The higher increase in dielectric loss factor with temperature can be attributed to the dominant ionic conduction as tomato sauce has higher salt content than the other two components.

4.5.2. Thermal properties

The specific heat capacities of all three food components from -10 °C to 110 °C are shown in Figure 4. 6. From -10 to 0 °C, the specific heat capacities of tomato sauce, mozzarella cheese, and bread crust increased from 3.5 to 21.9 and 4.5 to 17.5 and 4.0 to 14.4 kJ· kg^{-1}· $°C^{-1}$, respectively. The increase in the apparent specific heat capacity is due to phase change. The latent heat of fusion was calculated by integrating the area under the curve from -10 to 10 °C using the trapezoidal rule; the baseline curve area between -10 and 10 °C was subtracted to remove sensible heat due to change in temperature from -10 to 10 °C. The latent heat of fusion was determined as 130.39, 94.18 and 113.29 kJ· kg^{-1} for tomato sauce, mozzarella cheese and bread crust, respectively.

The thermal conductivities of all three components as a function of temperature from -10 to 10 °C are shown in Figure 4. 7. The thermal conductivities of all three components decreased drastically during the phase change from frozen to thawing, and then remained relatively constant above 0 °C. Above the thawing temperature of 0 °C, thermal conductivity of tomato sauce, mozzarella cheese, and bread crust stayed constant around 0.51, 0.45, and 0.59 W. m^{-1} $°C^{-1}$, respectively. All three components have higher thermal conductivity values at frozen temperatures than those at thawed temperatures, as the thermal conductivity of ice is higher than that of liquid water.

4.5.3. Electrical conductivity of susceptor film

The temperature-dependent electrical conductivity of susceptor film measured using a split post dielectric resonator attached with a vector network analyzer is shown in Figure 4. 8. The electrical conductivity gradually increases from 108.18 S/m at 30 °C to 282.77 S/m at 110 °C and then decreasing to 83.30 S/m at 180 °C. The electrical

conductivity increases with temperature until 110 °C. It is well known that the electrical conductivity of a thin material increase with temperature due to number of free electrons in the film vibrates at a faster rate leading to carry more current charge. The electrical conductivity plateaued at around 100-120 °C and then drops to low value. Dropping is due to fracturing of the susceptor film. The electrical conductivity of susceptor film decreased after 110 °C, because the susceptor started to fracture at high temperatures and leading to creation of resistive islands within the susceptor film. Risman (2009) observed similar fractures in microscopic image of 8 nm thick susceptor film after heating in a domestic microwave oven.

4.5.4. Transient power absorption and temperature in pizza and susceptor

Figure 4. 9 shows the simulated time-dependent electromagnetic power absorption and volumetric average temperature in pizza and susceptor. The susceptor is a thin metal layer that reflects, transmits, and/or absorbs a fraction of the incident energy. The susceptor material is usually designed to absorb more energy than reflecting and transmitting the incident energy. When including the susceptor in the computational model, after 10 s of heating, electromagnetic power absorption in susceptor was 310.63 W while the pizza was absorbed 491.94 W. As the susceptor has much smaller mass than the pizza, the temperature in the susceptor increased exponentially at the beginning and then gradually stabilizes. During heating, the susceptor continues to transfer heat to bread crust. Zuckerman and Miltz (1995) estimated the temperature profiles at susceptor/product interface during heating in a microwave oven. Authors observed the similar trend that temperature raised quickly to 100 °C within 30 s of heating and then gradually stabilizes at the end of 240 s of heating. In addition, the formation of resistive

islands reduced the power absorption, which reduced the rate of increase in temperature. As shown in Figure 4. 9, after 10 s of heating, a portion of susceptor reached quickly to 120 °C, while the average temperature was only 29.3 °C. Whereas, in pizza, volumetric average temperature reached only -6.18 °C after 10 s of heating. As shown in Figure 4. 9, after 10 s of heating, it was observed that there was a huge temperature variation in susceptor from right side to left side because the frozen pizza was kept stationary during heating. The right side of susceptor reached to higher temperature of 120 °C as it was close to the direction of microwave feed from magnetron. The frozen pizza initially absorbed slightly lower power of 491.94 W during first 10 s of heating, and then increased considerably to 630.9 W at the end of 20 s heating and then stabilized around 585 W. The lower electromagnetic power absorption at the beginning of microwave heating is because of the low dielectric loss factor of pizza components at frozen temperature. The increasing electromagnetic power absorption in pizza during heating can be attributed to the thawing of the pizza, which is related to the higher dielectric loss factor after thawing. The electromagnetic power absorption in susceptor was 310.63 W after 10 s heating leading to temperature raise in the susceptor layer rapidly and then conducts the heat to the frozen pizza. After 20 s of heating, the electromagnetic power absorption in susceptor layer sharply declined from 310.63 W to 63.52 W and then stayed constant at around 29 W. The sudden decrease in electromagnetic power absorption in susceptor can be attributed to reaching higher temperature within the short heating time and the susceptor layer becomes resistive to conduct heat due to fracture that leads to lower electrical conductivity in the higher temperature.

4.5.5. Spatial temperature profile

The simulated surface temperature profile of a frozen pizza was compared with three replicates of experimental surface temperature profiles at top and bottom layers obtained using a thermal imaging camera (Figure 4. 10 and Figure 4. 11). Three replicates of experimental surface temperature profiles acquired using thermal images of the top surface consistently showed the locations of hot and cold patterns. A center portion of frozen pizza showed a cold spot and remained at ~10 °C after 2 min 10 s of microwave heating. Similarly, the simulated temperature distribution showed a cold spot in the center of frozen pizza and the temperature stayed around 10 °C. It can also be corroborated from the digital images of replications 2 and 3 that a portion of mozzarella cheese in the center of the top surface did not melt. The hot spots on the left and right side can also be visibly seen in the simulated and experimental surface temperature profiles. There was a challenge is collecting consistent experimental surface temperature profiles at the top layer because the mozzarella cheese melted and flowed to other locations. As expected in microwave heating of any samples, there was a huge experimental variation due to microwave cooking performance and variation in pizza samples bought from the super market. The simulation profile just shows the topmost layer, which is the mozzarella cheese temperature, while the thermal images captured the mozzarella cheese layer and the underlying bread crust layer (note that the cheese layer does not completely cover the bread layer, refer Figure 4. 1.B). In the edges along the circumference of the pizza where the melted mozzarella cheese layer did not cover the bread layer, the experimental surface temperature profile showed hot spots, which was not observed in the simulated surface temperature profile. In case of simulation,

mozzarella cheese was considered as a single solid domain without liquid phase convection during heating. Therefore, hot spots along the circumference were not observed in the simulation. Overall, simulated spatial surface temperature distribution profile was in good agreement with the experimental thermal images in predicting hot and cold spots.

As shown in Figure 4. 11, at the bottom bread crust layer, three replicates of experimental surface temperature profiles consistently showed the locations of hot and cold patterns in the bread crust. Because the bottom bread crust was touching the susceptor during heating, the heat rapidly conducted from susceptor to the bread crust. Due to the conduction of heat from the susceptor, the bread crust reached the temperature close to 150 °C at the end of cooking and showed the browning effect. It can also be seen from the experimental surface temperature profile and simulated surface temperature profile that there was a small portion on the right corner reached 150 °C and rest of the portion reached close to 90 °C. As shown in the digital images of replications 2 and 3, the browning spot started to develop along the circumference of the bread crust edges, which can also be seen in the simulated surface temperature profile. Overall, the temperature variation at the bottom layer was lesser than the top layer due to the presence of susceptor at the bottom.

4.5.6. Transient-temperature profile

Transient temperature profiles of three experimental replicates at five points were compared with the simulated temperature profiles in Figure 4. 12. The simulated transient temperature profiles showed a phase-change effect in their trend (change in slope around the thawing region) similar to experimental profiles. To predict the

accuracy of model prediction, the root mean square error (RMSE) was calculated using averaged experimental time-temperature profiles in comparison with simulated time-temperature profiles for each location. The RMSE values ranged from 5.0 to 12.6 °C. Except at location 3 and 4, the predicted temperature falls within variations of three experimental replicates. On average, it took about 80 s to thaw the frozen pizza. The phase change involves larger latent heat and therefore phase change has a considerable effect on the accuracy of the model. Electromagnetic energy is the heat source, which determines the heating rate of frozen lasagna. Accurate electromagnetic field prediction is one of the key factors influencing the model prediction accuracy. Even though we included detailed geometry and temperature-dependent dielectric properties to improve the accuracy of electric field prediction, some other factors, such as complexity in food products geometry and single microwave frequency can influence the model prediction considerably. Due to rapid microwave heating, the temperature of food product can dramatically change with very small changes in spatial locations. This presents a major challenge in real-time temperature measurement during microwave cooking using fiber-optic probes, because a small movement or change of location of the probes in the frozen pizza might result in substantial changes in the measured temperature. The steam pocket developed during heating could also push the probe and cause errors in experimental measurement. To account the experimental variations during frozen pizza heating, the root mean square error was calculated using time-temperature profile of each replication and averaged time-temperature profiles of three replications. As shown in Figure 4. 13, root mean square error of experimental variations between the replications ranged from 2.6 to 10.6 °C at different location, with an average value of 5.9 °C.

4.5.7. Effect of susceptor on heat conduction to pizza

As shown in Figure 4. 14, maximum temperature of bottom bread crust layer was 190.4 °C, whereas tomato sauce and mozzarella cheese reached 117.9 °C and 117.7 °C, respectively. It can be inferred that bread crust reached 190.4 °C because of the heat conduction from susceptor film. It can also be seen that susceptor reached higher temperature as compared to three food components. Volume average temperature across the three food components varied from 48.1 °C to 63.4 °C. At the end of heating, volume average temperature in susceptor reached more than two times as compared to all three components. After 130 s heating, it can be observed that a portion of pizza was still not thawed.

The effect of susceptor was evaluated by comparing on the volumetric average temperature raise in all three pizza components and the whole pizza for heating in the presence and absence of susceptors (Figure 4. 15). By including the susceptor in the computational domain, it helped to raise the temperature considerably in the product that was in contact with the susceptor film. It can be observed that volumetric average temperature in bread crust with the presence of susceptor reached 48.1 °C, which is 22.6 °C more in bread crust without the susceptor. Volumetric average temperature was not considerably different in tomato sauce and mozzarella cheese irrespective of presence of susceptor, as those components were not in immediate contact with the susceptor. As the bread crust is the coldest component among all three components, the presence of susceptor almost improve the average temperature close to other two components resulting in more uniform cooking. Therefore, the susceptor is critical to achieve a good cooking performance of pizza. In the absence of the susceptor, the cold bread crust may

condense some of the steam resulting in sogginess of bread crust. Raising the temperature of bread crust will minimize condensation and the resulting sogginess. Also, the susceptor increased the overall temperature of the whole pizza (49.9°C, when compared to 32.4 °C without susceptor).

4.6. Conclusions

A partially coupled electromagnetic and heat transfer model was developed to simulate susceptor assisted microwave heating of frozen pizza. The temperature-dependent dielectric and thermal properties of frozen pizza components were measured and provided as inputs to the model. Electrical conductivity of susceptor film was measured as a function of temperature using a split post dielectric resonator attached with a network analyzer. The model was validated with experimental measurements. Simulated spatial temperature profile was found to be in good agreement with experimental spatial temperature profile. The root mean square error values of predicted transient temperature profiles ranged from 5.0 °C to 12.6 °C. The root mean square error of experimental variations between the replications ranged from 2.6 to 10.6 °C at different location, with an average value of 5.9 °C. The model can be used to identify cold spot locations and can be used by food product developers for optimizing food composition and package design to achieve more uniform heating.

Acknowledgements

The authors gratefully acknowledge the financial support provided by the USDA CSREES – NIFSI Grant (Project Number: 2008-51110-04340).

4.7. References

Celuch, M., Gwarek W., & Soltysiak M. (2008). Effective modeling of microwave heating scenarios including susceptors. In Proceedings of 08th International Conference on Recent Advances in Microwave Theory and Applications.

Celuch, M., & Kopyt, P. (2009). Modeling microwave heating in foods. In M. W. Lorence, P. S. Pesheck (Eds.), Development of packaging and products for use in microwave ovens. (First edn., pp. 305-346). CRC Press LLC, Boca Raton, FL.

Cesnek, J., Dobias, J., Housova, J., & Sedlacek, J. (2003). Properties of thin metallic films for microwave susceptors. Czech Journal of Food Sciences, 21(1), 34-40.

Chen J., Pitchai K., Birla S., Gonzalez R., Jones D., & Subbiah J. (2013). Temperature-dependent dielectric and thermal properties of whey protein gel and mashed potato. Transactions of the ASABE, 56(6), 1457-1467.

Chen, J, Pitchai, K, Birla, S, Negahban, M, Jones, D, & Subbiah, J. (2014). Heat and mass transport during microwave heating of mashe dpotato in domestic oven- model development, validation, and sensitivity analysis. Journal of Food Sciecne 79(10):1991-2004.

COMSOL. (2013). COMSOL Multiphysics manual v4.4.

Geedipalli, S.S.R., Rakesh, V., & Datta A.K. (2007). Modeling the heating uniformity contributed by a rotating turntable in microwave ovens. Journal of Food Engineering, 82(3), 359-368.

Krupka, J., Derzakowski, K., Zychowicz, T., Givot, B. L., Egbert, W. C., & David, M. M. (2007). Measurements of the surface resistance and conductivity of thin

conductive films at frequency about 1GHz employing dielectric resonator technique. Journal of the European Ceramic Society, *27*(8), 2823-2826

Liu, S., Fukuoka, M., & Sakai, N. (2013). A finite element model for simulating temperature distributions in rotating food during microwave heating. Journal of Food Engineering, 115(1), 49-62.

Perry, M.R., & Lentz, R.R.. (2009). Modeling microwave heating in foods. In M. W. Lorence, P. S. Pesheck (Eds.), Development of packaging and products for use in microwave ovens. (First edn., pp. 207-236). CRC Press LLC, Boca Raton, FL.

Pitchai, K., Chen, J., Birla, S., Gonzalez, R., Jones, D., & Subbiah, J. (2014). A microwave heat transfer model for a rotating multi-component meal in a domestic oven: Development and validation. Journal of Food Engineering, 128, 60-71.

Risman P.O. (2009). Modelling the effects of active packaging of microwaved foods. In M. W. Lorence, P. S. Pesheck (Eds.), Development of packaging and products for use in microwave ovens. (First edn., pp. 349-371). CRC Press LLC, Boca Raton, FL.

Soltysiak, M., Gwarek, W., Celuch, M., & Erle, U. (2010). FDTD modelling of plain susceptors for microwave oven applications. In Proceedings of 18th International Conference on Microwave Radar and Wireless Communications (MIKON).

Zuckerman, H., Miltz, J. (1995). Temperature profiles at susceptor/product interface during heating in the microwave oven. Journal of Food Processing and Preservation, 19(5), 385-398.

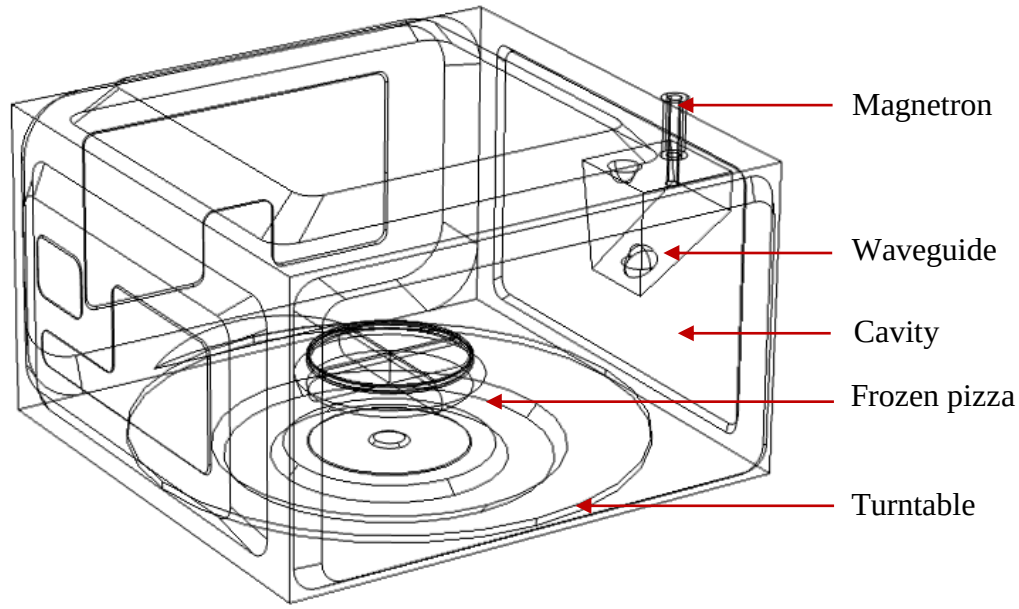

(A) Geometry of a 1250 W rated domestic microwave oven

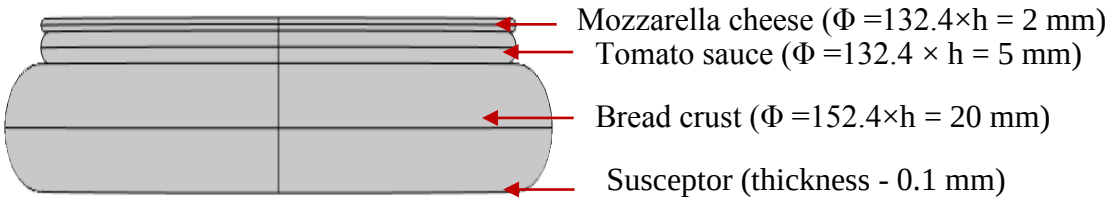

(B) Geometry of frozen pizza showing layers of food components (not to scale)

Figure 4. 1. Geometries of (A) microwave oven and (B) pizza used in the multiphysics model.

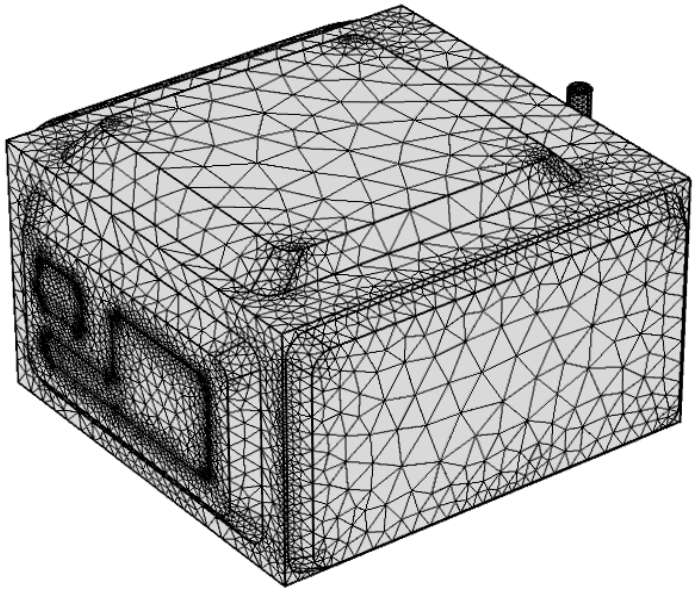

(A) Microwave oven cavity

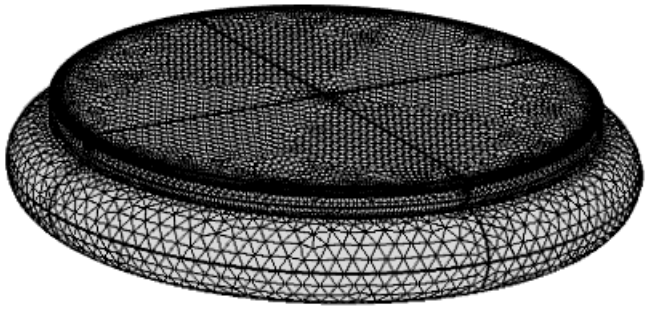

(B) Frozen pizza

Figure 4. 2. Meshing scheme of microwave oven cavity (A) and frozen pizza (B).

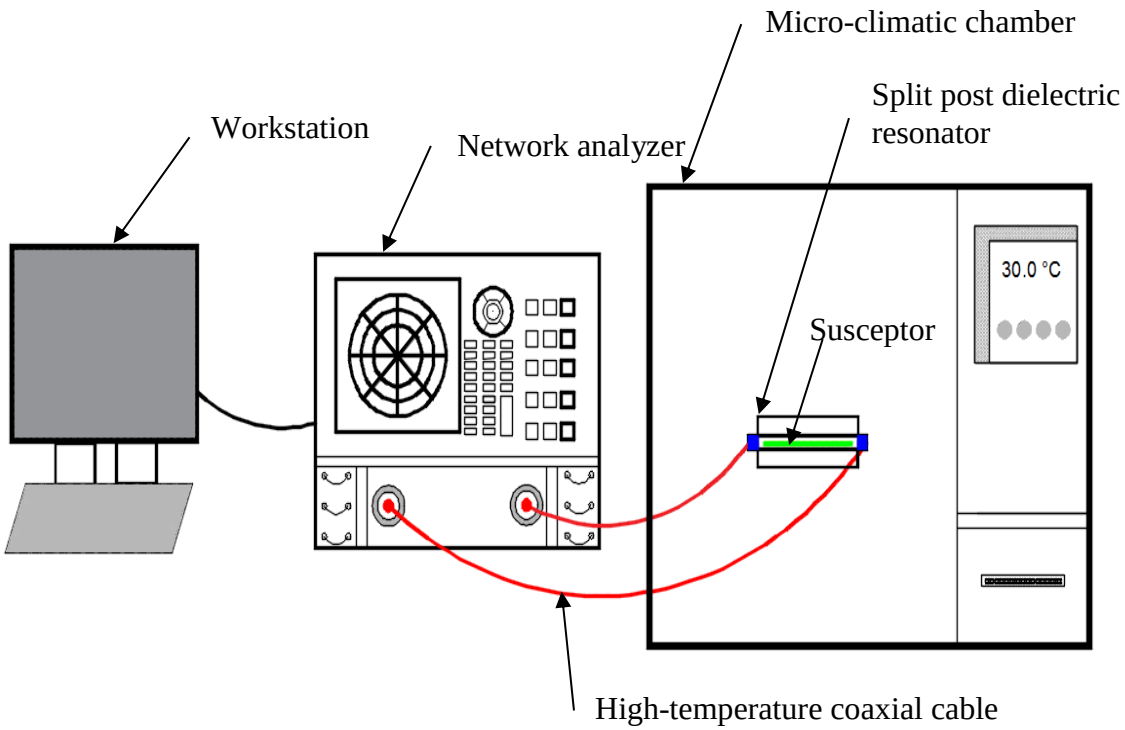

Figure 4. 3. Schematic diagram of experimental setup for measurement of electrical conductivity of susceptor film as a function of temperature.

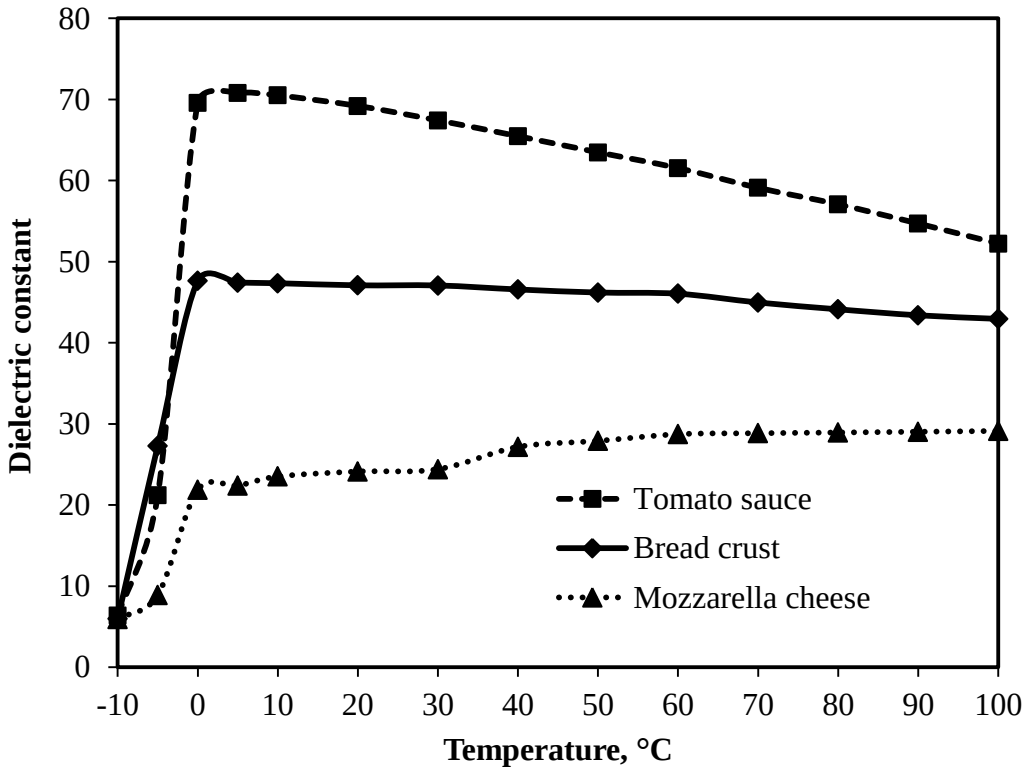

Figure 4. 4. Temperature-dependent dielectric constant of bread crust, tomato sauce, and mozzarella cheese measured at 2.45 GHz frequency.

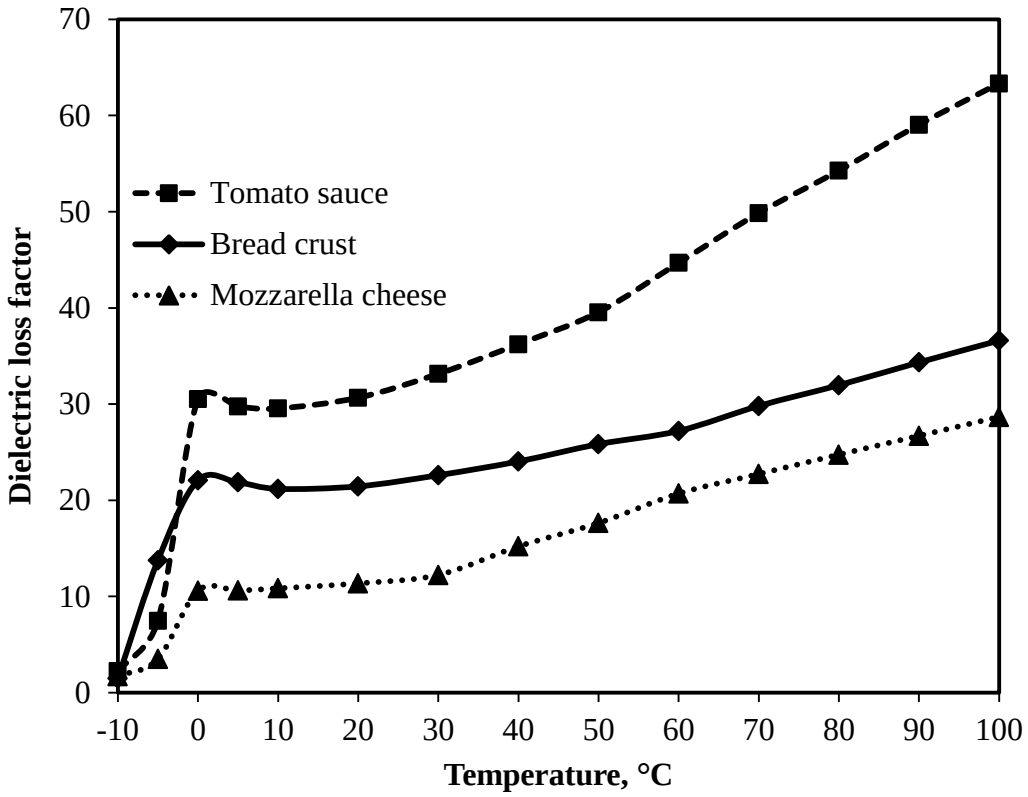

Figure 4. 5. Temperature-dependent dielectric loss factor of bread crust, tomato sauce and mozzarella cheese measured at 2.45 GHz frequency.

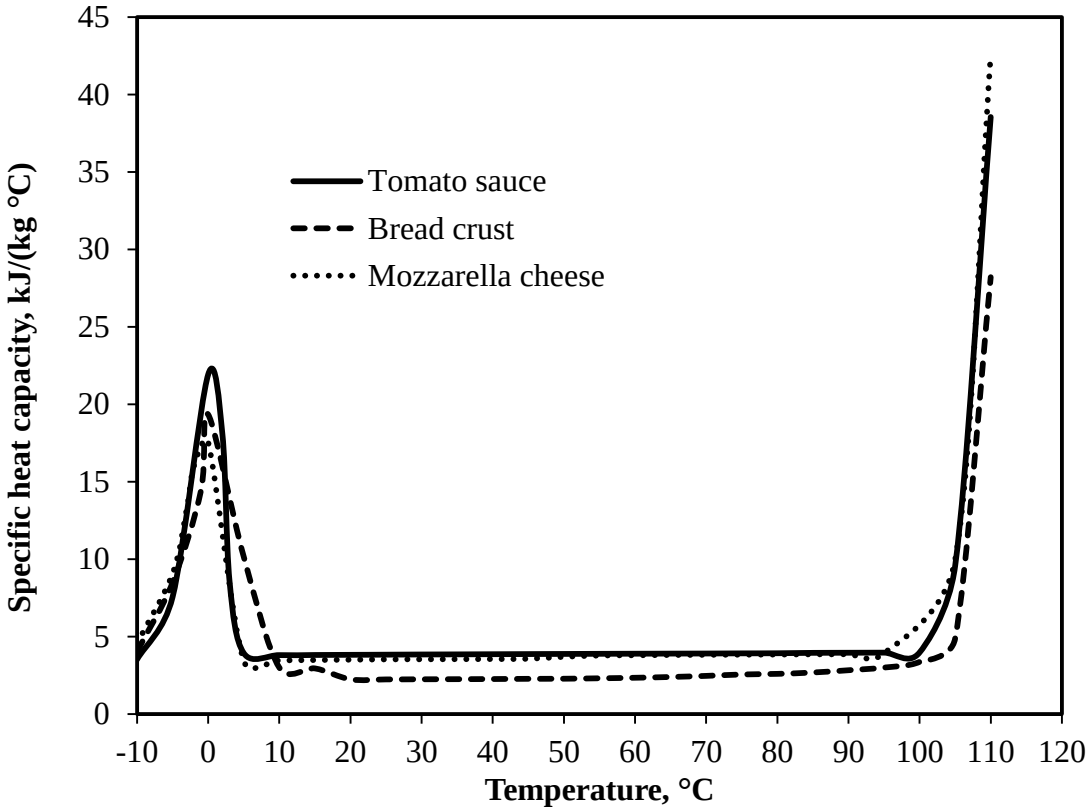

Figure 4. 6. Temperature-dependent specific heat capacity of bread crust, tomato sauce and mozzarella cheese measured using differential scanning calorimeter.

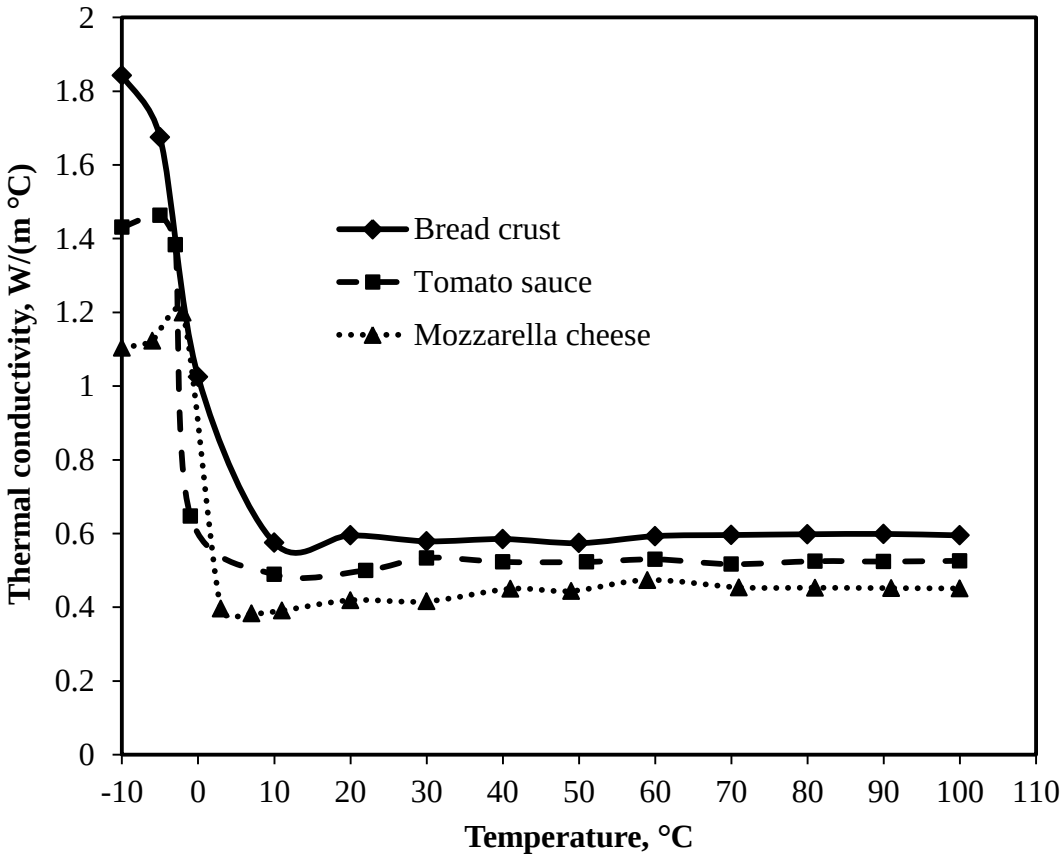

Figure 4. 7. Temperature-dependent thermal conductivity of bread crust, tomato sauce and mozzarella cheese measured using differential scanning calorimeter.

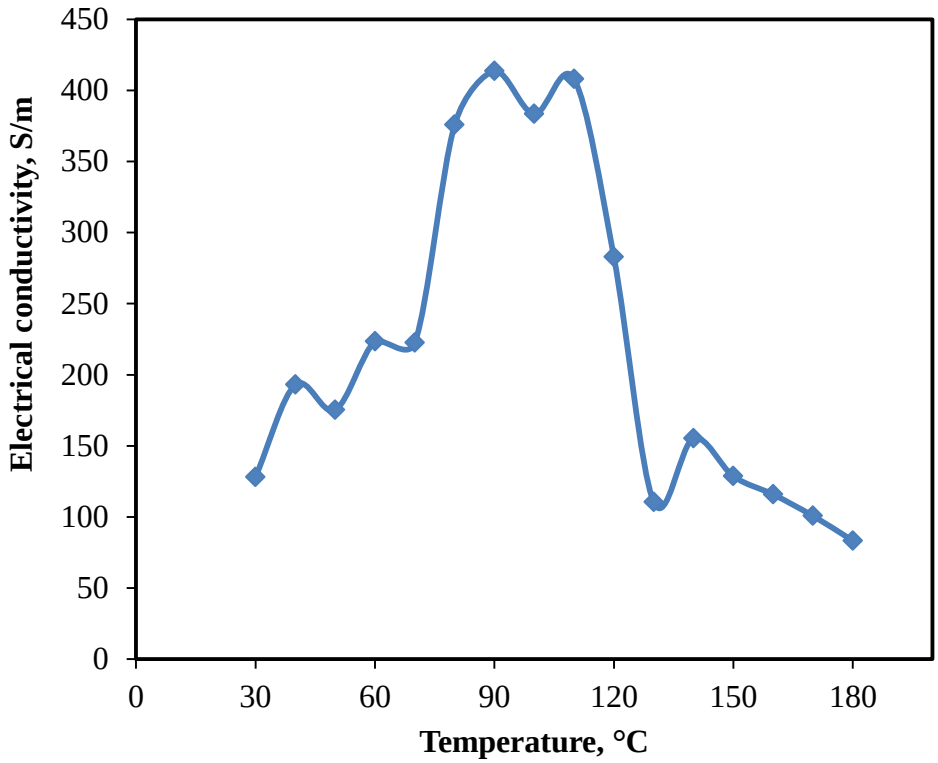

Figure 4. 8. Temperature-dependent electrical conductivity of the susceptor film.

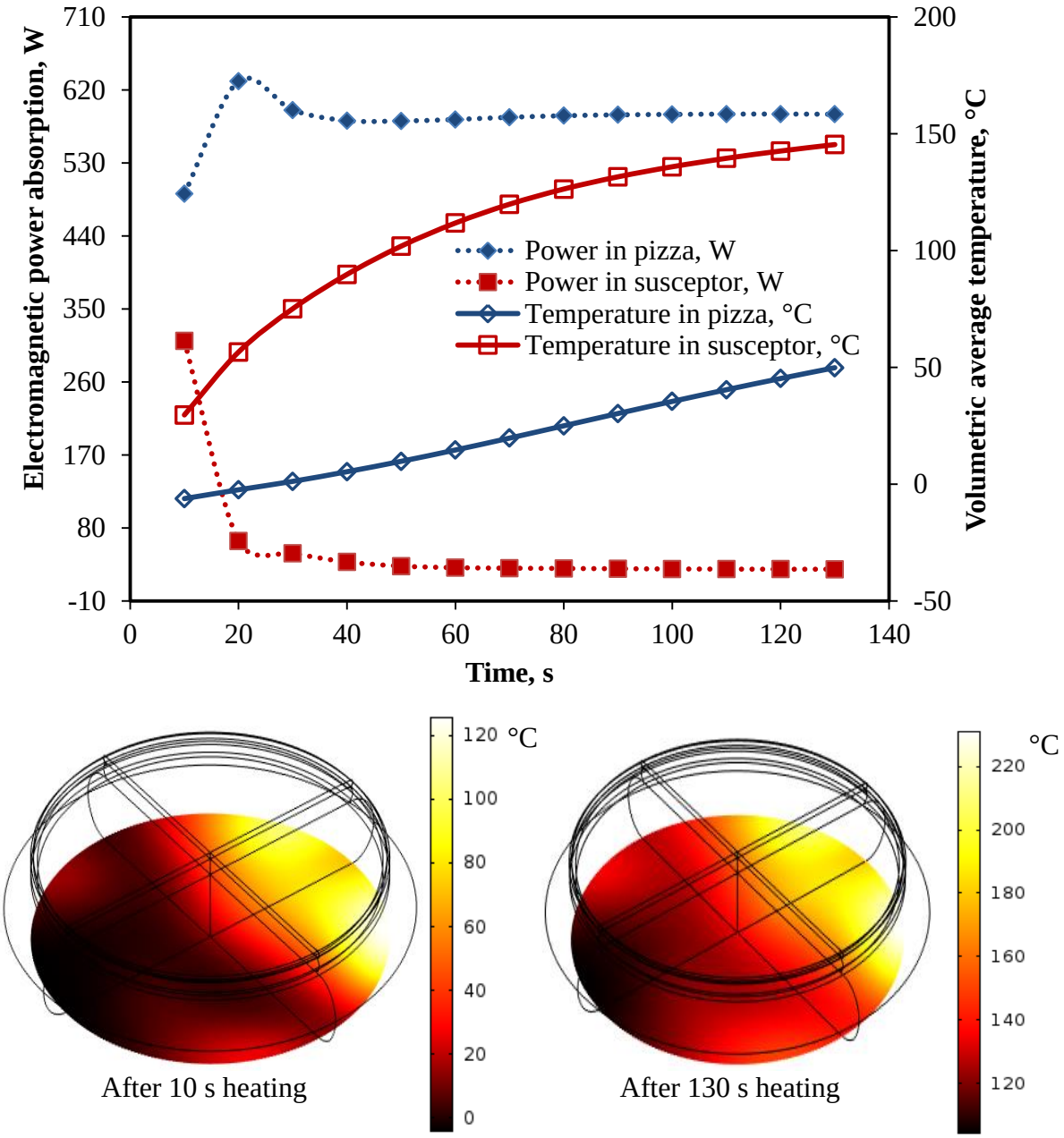

Figure 4. 9. Transient volumetric electromagnetic power absorption and volumetric average temperature in pizza and susceptor calculated through simulation and slice plot of temperature in susceptor after 10 and 130 s of stationary heating.

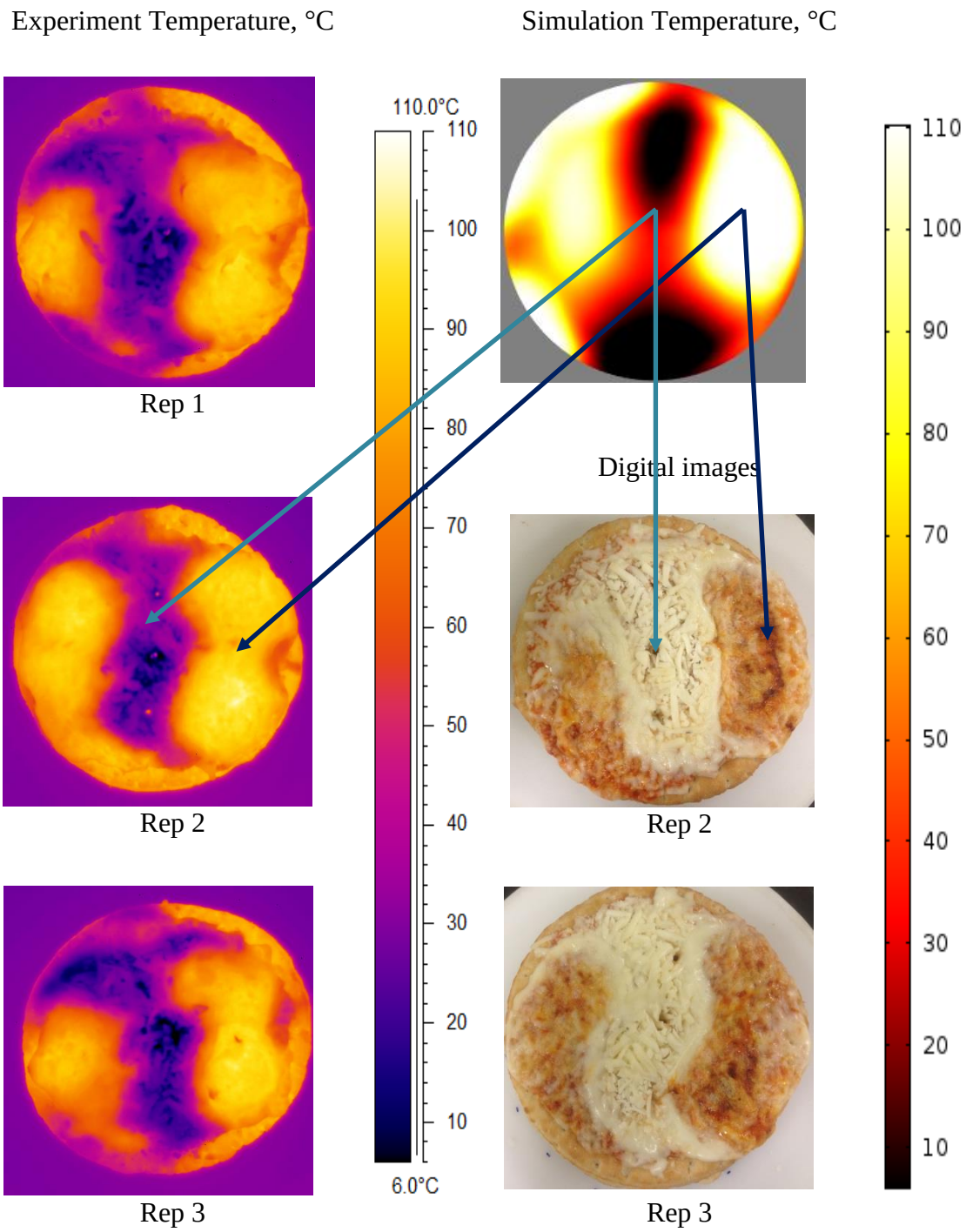

Figure 4. 10. Comparison of simulation temperature profile in the top layer with three experimental temperature profiles and digital images at the end of 130 s heating.

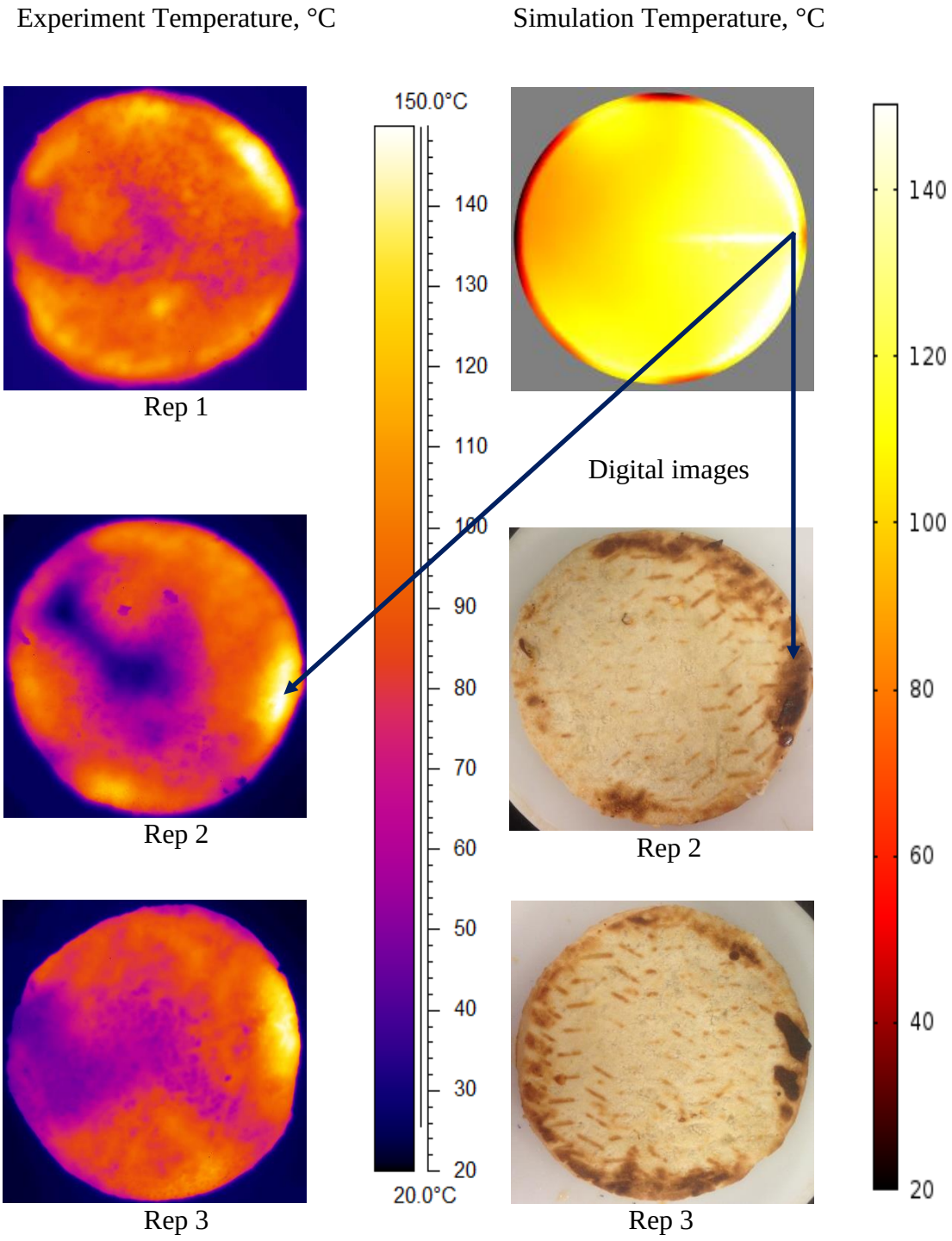

Figure 4. 11. Comparison of simulation temperature profile in the bottom layer with three experimental temperature profiles and digital images at the end of 130 s heating.

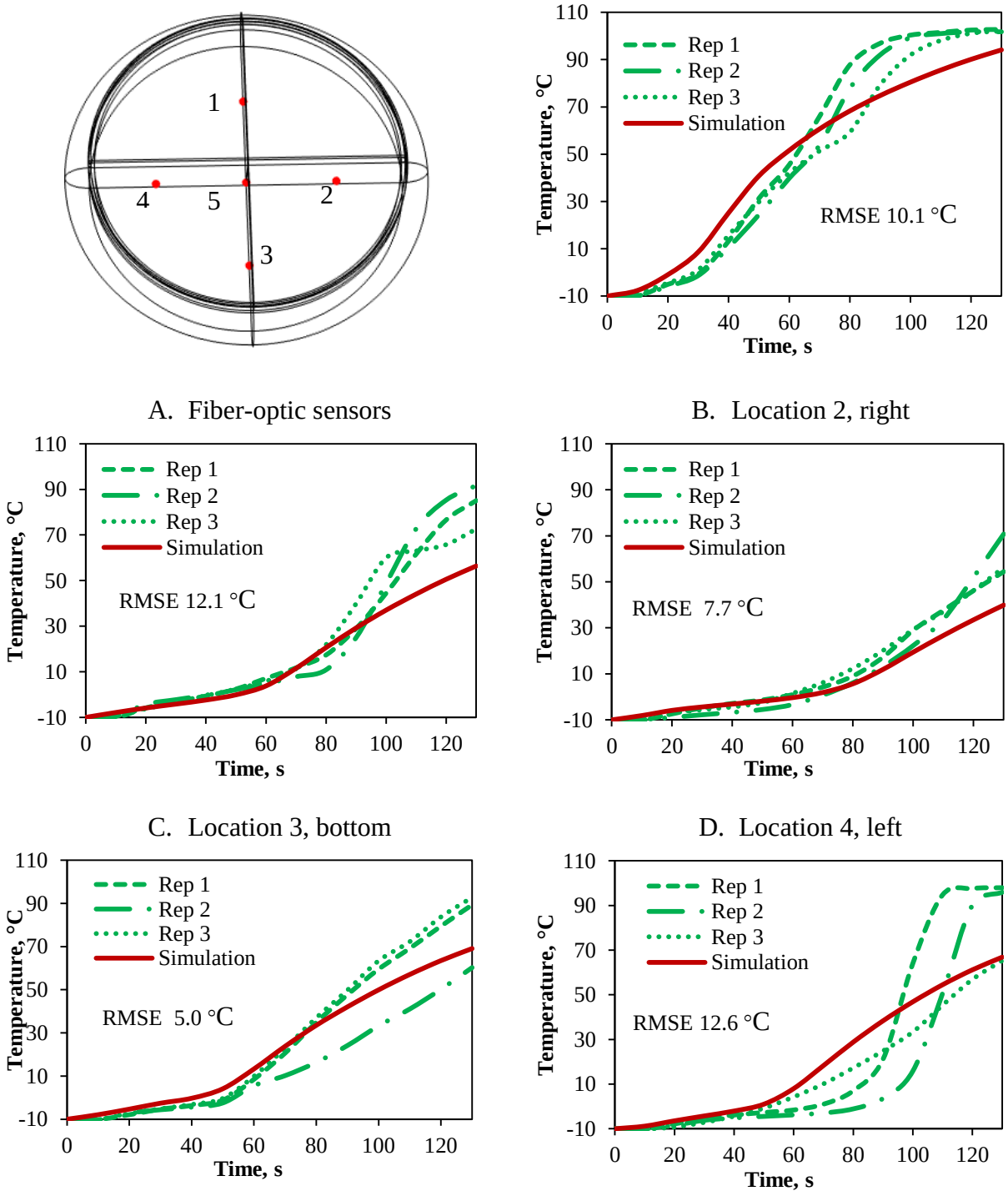

A. Fiber-optic sensors

B. Location 2, right

C. Location 3, bottom

D. Location 4, left

E. Location 5, center

F. Location 1, top

Figure 4. 12. Comparison of simulated and experimental transient temperature profiles at five locations and locations of fiber-optic sensors in pizza (all sensors are inserted 25 mm from the top surface).

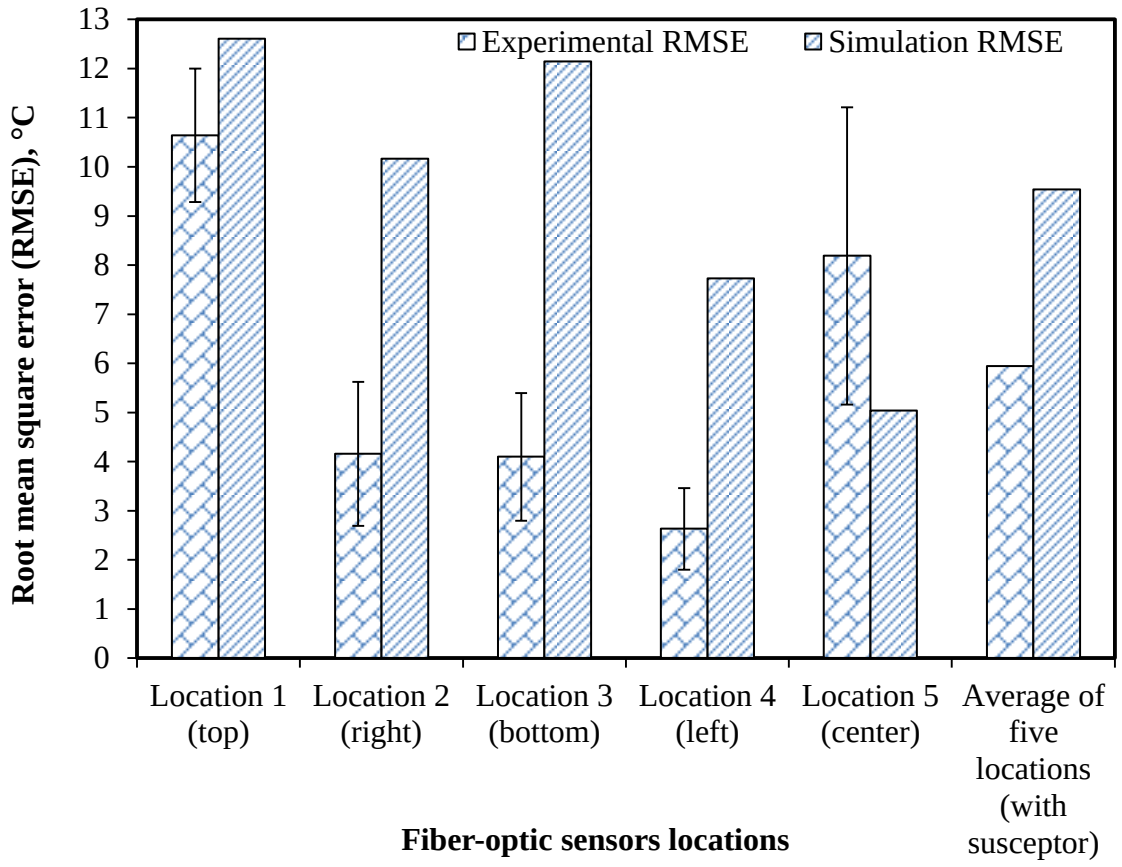

Figure 4. 13. Root mean square comparison of experimental variations and model prediction.

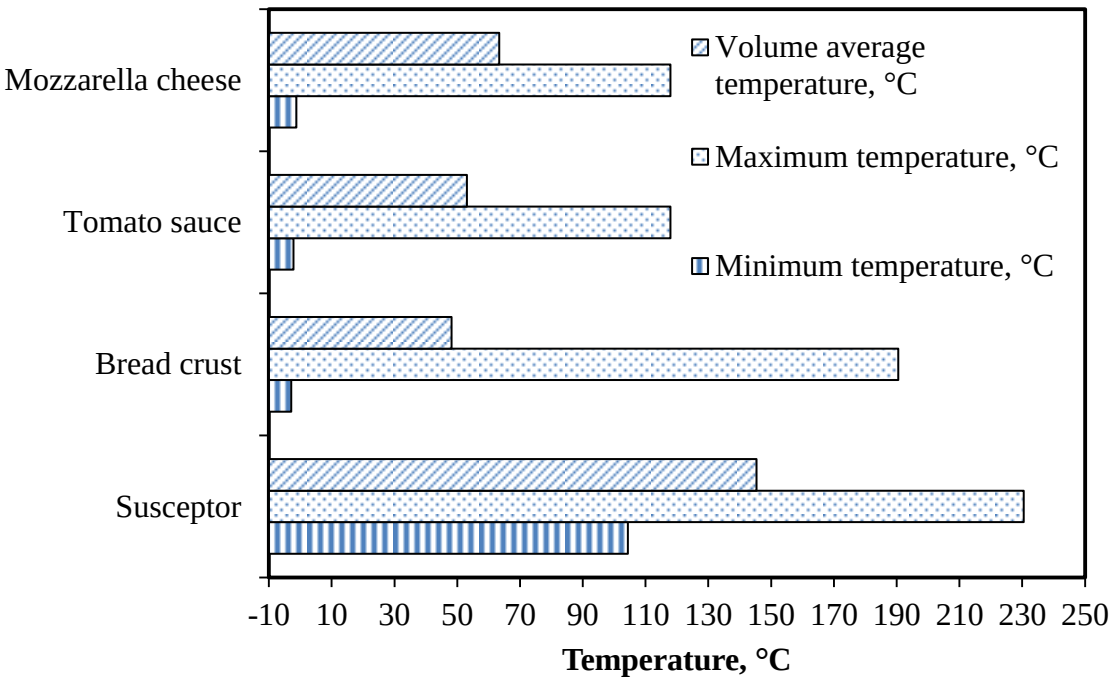

Figure 4. 14. Volume average, maximum, and minimum temperatures in three different food components compared at the end of 130 s heating.

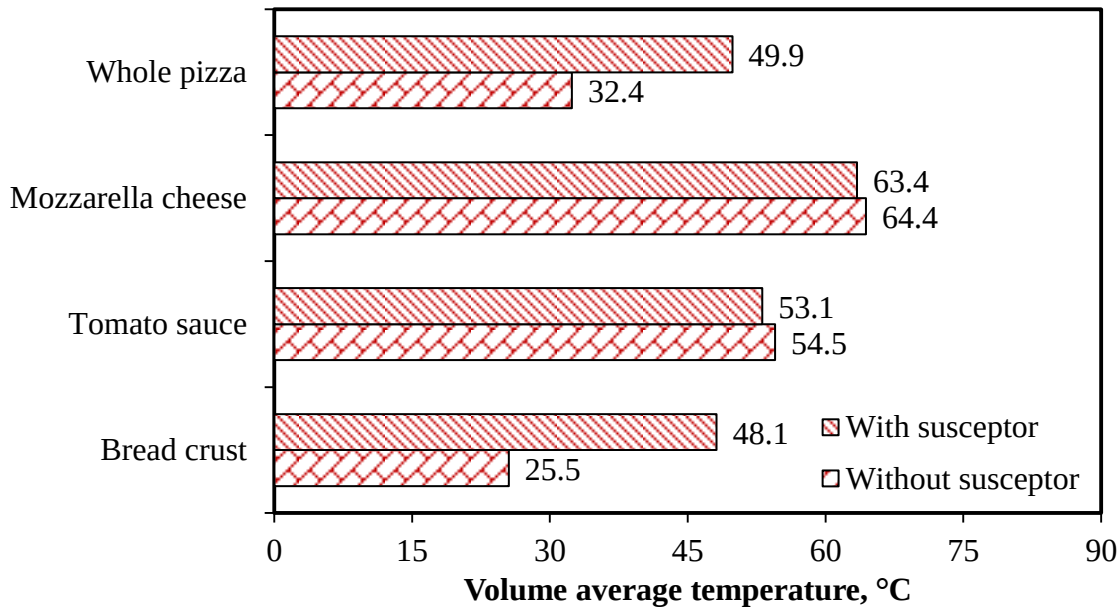

Figure 4. 15. Effect of with susceptor and without susceptor on volume average temperatures in three different food components (Mozzarella cheese, tomato sauce, and bread crust) and the whole pizza at the end of 130 s heating.

CHAPTER V

MODELING MICROWAVE HEATING OF FROZEN MASHED POTATO IN A DOMESTIC OVEN INCORPORATING ELECTROMAGNETIC FREQUENCY SPECTRUM

Krishnamoorthy Pitchai [a, b], Jiajia Chen [b], Sohan Birla [b], David Jones [b], and Jeyamkondan Subbiah [a, b, *]

[a] *Department of Food Science and Technology, University of Nebraska-Lincoln, NE – 68583*

[b] *Department of Biological Systems Engineering, University of Nebraska-Lincoln, NE – 68583*

*Corresponding author: Jeyamkondan Subbiah, Kenneth E. Morrison Distinguished Professor of Food Engineering, Departments of Food Science & Technology and Biological Systems Engineering, 212 L.W.Chase Hall, East Campus, University of Nebraska-Lincoln, Lincoln, NE-68583-0726, Ph. No: 402-472-4944, Fax No: 402-472-6338, Email: jeyam.subbiah@unl.edu.

Citation: Pitchai, K., Chen, J., Birla, S., Jones, D., Subbiah, J. 2015. Modeling microwave heating of frozen mashed potato in a domestic oven incorporating electromagnetic frequency spectrum. Journal of Food Engineering. Submitted.

5.1. Abstract

Domestic microwave oven magnetrons produce microwaves in a frequency range of 2.45±0.05 GHz. Most microwave heat transfer simulations simplify that the magnetron produces a monochromatic electromagnetic wave of frequency of 2.45 GHz to

reduce the computational complexity. This study assumes that the magnetron produces a frequency spectrum defined by a Gaussian distribution of frequencies with a central frequency of 2.45 GHz and investigates the effect of Gaussian distribution variance of $(0.05\ \text{GHz})^2$, $(0.025\ \text{GHz})^2$, $(0.017\ \text{GHz})^2$ on prediction accuracy when compared to using monochromatic frequency of 2.45 GHz. A three-dimensional finite element model coupling electromagnetic and heat transfer physics was developed to simulate heating of 550 g of frozen mashed potato for 6 minutes. The model was validated in a 1250 W rated microwave oven with the mashed potato tray placed at the center of the stationary turntable. The electromagnetic power densities were determined separately at five different frequencies equidistant between 2.4 and 2.5 GHz. They were then weighted averaged, based on the selected Gaussian distribution. Simulated temperature profiles of the models using the monochromatic frequency of 2.45 GHz and Gaussian frequency spectrum with different variances were compared with experimental temperature profiles obtained using a thermal imaging camera at the end of cooking and five fiber-optic thermocouples during cooking. The model results showed that predicted spatial surface temperature pattern by the model using frequency spectrum with the largest variance $(0.05\ \text{GHz})^2$ had better agreement with the experimental temperature pattern when compared to that using a monochromatic frequency of 2.45 GHz. In the transient temperature profile measurement, the average RMSE value of five locations was 7.5 and 13.1 °C for simulations using frequency spectrum and monochromatic frequency of 2.45 GHz, respectively. Implementing the frequency spectrum in the simulation improved the accuracy of temperature field pattern and transient temperature profile.

Keywords: Multiphysics modeling; electromagnetic power density; coupled electromagnetic and heat transfer modeling; Gaussian frequency spectrum; monochromatic microwave frequency; magnetron; microwave thawing.

5.2. Introduction

According to the Industrial, Scientific, and Medical (ISM) band allocated by Federal Communications Commission (FCC) for the food applications, microwave ovens are designed to be operated at 2450 MHz with a frequency tolerance limit of 50 MHz (Buffler, 1993). The modern day microwave ovens use "cooker" magnetron which is 70% efficient in its performance and whose performance is inconsistent due to lower price (Osepchuk, 2010). The cooker magnetron is complex in its operation due to various factors such as varying anode current and the cold-start process. Due to these factors, a magnetron does not operate at a fixed single frequency but at a range of frequencies (Risman, 2009).

A magnetron frequency spectrum depends on type of power supply, dielectric properties of food material, magnetron temperature, and magnetron physical construction. Gerling and Fournier (1991) reported that the frequency bandwidth is also affected by the stability of the power supply to the magnetron. As the magnetron frequency bandwidth changes, the number of electromagnetic (EM) modes generated inside the cavity is also affected. Also, Gerling and Fournier (1991) reported that magnetron frequency can change as much as 0.25 MHz for every degree change in the magnetron temperature.

Simulation of electromagnetic and heat transfer during microwave heating is becoming a promising tool to understand and visualize the EM field patterns of

microwave heated foods. Many microwave heat transfer models have been developed using a monochromatic frequency of 2.45 GHz (Curcio et al., 2008; Dincov, 2004; Liu et al., 2012). Pitchai et al. (2012) and Birla et al. (2010) demonstrated through microwave heat transfer simulations that EM field patterns are affected by the selected frequency. Soltysiak et al. (2010) demonstrated the effect of different monochromatic frequencies on temperature pattern with respect to different rotational position of the food on the turntable through modeling. The predicted temperature showed that temperature within the food varies over 10 °C as the food heated with different frequencies. Thus the magnetron frequency influences the electromagnetic field patterns within the food (Tang and Resurreccion Jr, 2009; Schubert and Riegel, 2005). The EM power density is the heat source and therefore directly influences the final temperature distribution or cooking performance of a food product. Therefore, for accurate prediction of temperature distribution in food, frequency spectrum has to be incorporated in the model.

Previously, researchers have not included the frequency spectrum in the electromagnetic and heat transfer simulation of domestic microwave heating of food. As a new paradigm in the microwave heat transfer simulations, this study evaluates a methodology to incorporate the electromagnetic frequency spectrum in simulation in the form of Gaussian shape distribution. While adding frequency spectrum to computational model invokes more complexity and computational burden, this study investigates the effect of adding frequency spectrum in the simulation on the accuracy of temperature predictions.

The objectives of this study were to:

i) develop a methodology to incorporate electromagnetic frequency spectrum in the coupled electromagnetic and heat transfer model.
ii) investigate the effect of variance of Gaussian shaped frequency distribution on prediction accuracy in comparison to the monochromatic frequency of 2.45 GHz.

5.3. Materials and Methods

5.3.1. Governing equations and boundary conditions

Solution of the combined wave form of Maxwell's equations gives the estimated electromagnetic field strength at any point in the computational domain which is the entire oven cavity. The governing equations, boundary conditions applied in the simulation are explained in detail in Pitchai et al. (2014).

5.3.2. Geometric model

Geometric model was developed for a 1250 W rated power (1200 W available power measured using IEC 60705 method) microwave oven (Model no: NN-SD9675; Panasonic Corporation, Shanghai, China). The detailed geometric model of the microwave oven, mashed potato tray, and a turntable is shown in Figure 5. 1. A near perfect geometric model of the microwave oven and a 550 g mashed potato tray was created in the commercial Finite Element Method (FEM) software, COMSOL Multiphysics 4.3b (COMSOL, Burlington, MA). In this study, we included the magnetron as a coaxial power source feeding microwave energy into the waveguide.

5.3.3. Model assumptions

The shape of magnetron operating frequency spectrum was approximated to be as Gaussian function. It is challenging to accurately measure the frequency spectrum during microwave heating. Birla et al. (2010) measured the microwave frequency spectrum of a 700 W rated power microwave oven by the analysis of microwave leakage signal using a spectrum analyzer connected to horn antennas placed inside an anechoic chamber. From the frequency spectrum, the resonance frequency was in the range of 2.43 to 2.49 GHz for that particular microwave oven. Similarly, Chan and Reader (2000) also measured a microwave leakage spectrum generated by a 2.45 GHz magnetron which ranged from 2.40 to 2.46 GHz. It is also not clear whether the leakage spectrum is the representative of the microwave spectrum absorbed by the food or complimentary (i.e. whatever frequencies the food, that had not absorbed, leaked). Frequency spectrum is dynamic and can change with the type of food product heated in microwave oven. The properties of food products dramatically changes with cooking time especially during phase change, which can then dynamically affect the magnetron frequency spectrum during cooking. Because the dynamic nature of magnetron performance is unknown and can vary significantly for various food products and during cooking, it is difficult to input the exact magnetron frequency into the model. Therefore, we assumed the frequency spectrum to be Gaussian shaped to cover the entire FCC allowable range of 0.05 GHz as a bell shape normal distribution curve with the central frequency of 2.45 GHz and variance of 0.05^2, 0.025^2, and 0.017^2 GHz frequency in this study (Figure 5. 2). All three frequency spectrums were normalized to the area under the curve between 2.4 and 2.5

GHz as a value of 1. At the mashed potato tray surface, we considered a convective natural heat flux boundary of 20 W/m^2 °C at the food-air interface and air temperature was assumed to be constant at 20 °C. A fan circulated the ambient air into the cavity and therefore the temperature of air inside the cavity can be assumed to be constant. The mass transfer of water and vapor were not considered in the model.

5.3.4. Simulation strategy

The coupled electromagnetic wave and heat transfer equations were solved using a Generalized Minimal Residual (GMRES) method based iterative solver. The simulation was performed on a Dell Precision T7500 workstation with an 72 GB DDR3 RAM running on two quad-core Intel Xeon X5570 2.93 GHz processor. At the beginning of the simulation, mashed potato was at the constant initial temperature of -10 °C. Liu et al. (2013) reported that the temperature-dependent dielectric properties of mashed potato did not change significantly during 10 s of heating time and therefore would not significantly change the electric field distribution. Therefore, the dielectric properties were assumed to be constant during one rotational cycle. The electromagnetic power density was calculated by solving Maxwell's equations for each frequency starting from 2.41 GHz until 2.49 GHz with 5 equal intervals (Figure 5. 2). The averaged electromagnetic heat source for 10 s of heating was calculated by weighted average of power densities calculated at each frequency, where the weight for each frequency is shown in Figure 5. 2. The averaged electromagnetic heat source as a function of frequency was calculated based on the flow-short outlined in Figure 5. 3.

This process was performed with a MATLAB livelink interface communicated with the COMSOL server. The MATLAB routine then passed the electromagnetic power

density to COMSOL Multiphysics® v4.3b for simulating the heat transfer model for 10 s of heating time. At the end of the 10 s microwave heating, the temperature field was used to update the dielectric properties and then Maxwell's equations were solved to determine electromagnetic power density separately for the discrete frequencies for next rotational cycle. This cyclic process continued until a complete heating time of 6 minutes reached.

5.3.5. Meshing scheme

The size and shape of mesh elements are important factors in influencing convergence and accuracy of the finite element analysis (Liu et al., 2013). Microwave cavity, glass turntable and mashed potato domains were assigned to create four-node unstructured tetrahedral elements with the quadratic shape functions. Three meshes with different refinement levels were enforced for tetrahedral elements (i.e., cavity domain, size: 2-30 mm; glass turntable, size 3-6 mm; mashed potato domain, size: 2-4 mm). Chen et al. (2014) studied the effect of mesh refinement on normalized power absorption. The mesh sizes applied in the domains were found to be sufficient to produce mesh independent results (Chen et al., 2014). Three dimensional meshes created 546,853 total tetrahedral elements, out of which 134,285 elements comprised the mashed potato domain. The meshed microwave oven cavity is shown in Figure 5. 4.

5.3.6. Sample preparation

The mashed potato sample was prepared based on the procedure outlined in Chen et al. (2013). A 550 g mashed potato was filled in a microwaveable tray and a plastic

film was used to cover the top to prevent moisture lose before experiment. The prepared mashed potato was stored at ~-10 °C temperature.

5.3.7. Material properties

The temperature-dependent dielectric properties (dielectric constant and dielectric loss factor) and thermal properties (thermal conductivity and specific heat capacity) of mashed potato measured in a previous work (Chen at al., 2013) were used in the model. The material properties of air and turntable domains were obtained from Pitchai et al. (2014).

5.3.8. Experimental validation

The mashed potato tray was stored at -10 °C at the freezer. The prepared mashed potato tray was removed from the freezer and subjected to 6 minutes of microwave heating. The transient temperature profile at five locations was recorded using fiber-optic sensors (8-channel signal conditioner, FISO Technologies Inc., Quebec, Canada). All the fiber-optic sensors were inserted 15 mm deep from the top surface of the mashed potato as shown in Fig. 5. Immediately after microwave heating, a thermal image of the top surface of the mashed potato was captured using an infrared camera (SC640, 640 × 480 pixels, accuracy ±2 °C, FLIR systems, Boston, MA). Experiments were repeated thrice and all temperature profiles are reported in this study.

5.4. Results and Discussion

5.4.1. Effect of frequency on total microwave power absorption

The electromagnetic power density calculated at each frequency was integrated for the entire mashed potato domain to estimate the volumetric microwave power

absorption. Figure 5. 6 shows the time-dependent volumetric microwave power absorption calculated for the monochromatic frequency (2.45 GHz) simulation was compared with the G (2.45, 0.05^2) GHz frequency spectrum simulation in After 10 s of microwave heating, the volumetric microwave power absorption calculated at 2.45 GHz frequency was 752 W which was lower than the volumetric microwave power absorption of frequency spectrum of 792 W. The volumetric microwave power absorption using both 2.45 GHz frequency and frequency spectrum drastically increased in the first 30 s of heating and then stabilized. The volumetric microwave power absorption values of mashed potato at 2.45 GHz and G(2.45, 0.05^2) GHz frequency spectrum increased to 903 W and 894 W at the end of heating of 6 minutes. The lower volumetric microwave power absorption at the start of microwave heating as compared to the end of heating is due to the fact that dielectric constant and dielectric loss factor of mashed potato at frozen temperature was 12 and 60 times lower than those of the thawing temperature. Even though the mashed potato did not completely thaw for 5 minutes of heating, small layer of thawing on the surface in the first 30 s made the power absorption close to the value at the end of heating. The penetration depth (the depth at which microwave energy decreases to 36.8% of its value at the material surface) dramatically decreased from 32.5 mm at -10 °C to 6.4 mm at 20 °C. Thus, thin thawed layer drastically alters the volumetric power distribution. However the total volumetric power absorption within the food product changes only by 10-15%.

5.4.2. Validation of spatial temperature patterns

Three experimental surface temperature patterns at the top surface recorded from IR imaging camera were compared with the simulation temperature patterns using

monochromatic frequency of 2.45 GHz and the three Gaussian frequency distribution after 6 minutes of microwave heating of mashed potato (Figure 5. 7). The 2.45 GHz frequency simulation showed the surface temperature pattern with location of cold middle spots consistent with all the three experimental surface temperature patterns. However, there was a location of cold spot of 40 °C in the 2.45 GHz frequency simulation at right-middle corner, which was not observed in the experimental temperature patterns. Whereas, all three Gaussian frequency distribution simulations showed the similar surface temperature pattern of 2.45 GHz frequency temperature pattern; and there was no cold spot predicted in the right-middle corner in all three Gaussian frequency distribution simulation. The simulation temperature scale had the maximum value of 120 °C, whereas the IR image temperature scale had the maximum value of 100 °C. This is because, the mass transfer physics was not considered in the model.

As shown in Figure 5. 7, as the variance of Gaussian distribution decreases from 0.05^2 to 0.017^2 GHz, the regions of cold spots at the middle shrink and did not matched with the temperature observed in the experimental IR images. It is noted that as the variance decreases, frequency spectrum operates close to the range of 2.45 GHz and the contribution from 2.45 GHz was higher. Using a broader 0.05 GHz bandwidth, the averaged electromagnetic power density from all 5 frequencies was shared by similar weights and the average value worked the best. Therefore, it was important to include contribution from the tail-end frequencies into the model. The computation time for 6 minutes of microwave heating took about 42 h for the 2.45 GHz frequency simulation. Whereas, frequency spectrum simulation took 66 h. Even though, the predicted surface

temperature pattern of frequency spectrum simulation looked better match with experimental temperature pattern than single frequency of 2.45 GHz, it must be important to evaluate the accuracy through transient point temperature measurements.

5.4.3. Validation of transient temperature profile

To corroborate the results of the spatial temperature pattern results, as shown in Figure 5. 8, as the variance decreases, average RMSE of five locations increased. As the variance decreased to 0.017 GHz, the predicted error was close to the monochromatic frequency of 2.45 GHz because close to one fourth of the weightage of $(0.017\ \text{GHz})^2$ variance was shared at 2.45 GHz frequency. The temperature prediction of G(2.45, 0.05^2) GHz frequency spectrum had smaller error value in the temperature prediction as compared to that of 2.45 GHz frequency temperature prediction. Therefore, it must be important to include the frequency spectrum in the model rather than assuming single frequency of 2.45 GHz. Therefore, heating rate of the microwave heating of food products prediction can be improved by including the electromagnetic frequency spectrum into the simulation.

Figure 5. 9 shows comparison of simulated and observed transient temperature at five points. The three experimental transient temperature profiles collected at five points shown in Figure 5. 9 during 6 minutes of heating of mashed potato were compared with the predicted temperatures at those points using the simulations of 2.45 GHz frequency and G(2.45, 0.05^2) GHz frequency spectrum. The transient temperature profile of G (2.45, 0.025^2) GHz and G(2.45, 0.017^2) GHz were not compared with the experimental temperature profile, because the surface temperature pattern of those two frequency spectrums were over-predicted. The RMSE was calculated using averaged experimental

transient temperature profiles in comparison with simulated transient temperature profiles for each location. Generally, G(2.45, 0.05^2) GHz frequency spectrum showed good agreement with the experiment, with RMSE values ranged from 4.9 to 9.3 °C as compared to the RMSE values ranged from 9.9 to 19.8 °C for the 2.45 GHz. The average RMSE values of five locations for the G(2.45, 0.05^2) GHz frequency spectrum and monochromatic frequency of 2.45 GHz were 7.5 and 13.1°C, respectively. The average RMSE was nearly two times higher in the monochromatic frequency of 2.45 GHz simulation as compared to the of G(2.45, 0.05^2) GHz frequency spectrum. In both the G(2.45, 0.05^2) GHz frequency spectrum and 2.45 GHz frequency, the simulated transient temperature profiles showed a phase-change effect in their trend (change in slope around the thawing region) similar to the experimental temperature profiles.

This study has developed a protocol to use the frequency spectrum in the model simulation and demonstrated a simplified assumption of Gaussian distribution that can be used to improve the accuracy of temperature predictions. In future, if we can determine the actual frequency spectrum, the same methodology of splitting spectrum into weighted function, determining EM field, averaging them, and then use them as a power density function can be implemented.

5.5. Conclusions

A microwave electromagnetic and heat transfer model was developed with the inclusion of frequency spectrum using an approximated Gaussian shape distribution to calculate the electromagnetic power density. The developed model included the frequency spectrum as a Gaussian distribution with 2.45 GHz as a central frequency with

different variance of $(0.05\ GHz)^2$, $(0.025\ GHz)^2$, $(0.017\ GHz)^2$. Gaussian distribution was discretized into 5 bins and electromagnetic power density was determined at 5 frequencies and then weighted average of power density was determined based on discretized Gaussian distribution weightage. The surface temperature profile and transient temperature profiles calculated using the monochromatic frequency of 2.45 GHz and frequency spectrum were evaluated against the experimental results. Effect of frequency spectrum variance on the prediction accuracy was investigated. The study also found that including the $(0.05\ GHz)^2$ variance frequency spectrum had better temperature prediction accuracy as compared to $(0.025\ GHz)^2$ and $(0.017\ GHz)^2$ variance frequency spectrum. The model results showed that predicted spatial surface temperature pattern implemented using the frequency spectrum had better pattern matching with the experimental temperature pattern as compared to that of 2.45 GHz frequency. In the transient temperature profile measurement, the average root mean square error value of 5 locations was 7.5 °C in frequency spectrum simulation; whereas, the average root mean square error value was 13.1 °C in 2.45 GHz frequency simulation. Implementing the microwave frequency spectrum in the simulation improved the accuracy of temperature field pattern and transient temperature profile.

Acknowledgements

The authors gratefully acknowledge the financial support provided by the USDA CSREES – NIFSI Grant (Project Number: 2008-51110-04340).

5.6. References

Birla, S., Pitchai, K., Subbiah, J., & Jones, D. (2010). Effect of magnetron frequency on heating pattern in domestic oven. In 44th Annual Symposium, International Microwave Power Institute, Denver, CO.

Buffler, C.R. (1993). Microwave cooking and processing. Van Nostrand Reinhold, New York.

Chan, T., Reader H.C. (2000). Understanding microwave heating cavities. Artech House publishers, Norwood, MA.

Chen, J., Pitchai, K., Birla, S., Gonzalez, R., Jones, D., & Subbiah, J. (2013). Temperature-dependent dielectric and thermal properties of whey protein gel and mashed potato. Transactions of the ASABE, 56(6), 1457-1467.

Chen, J., Pitchai, K., Birla, S., Negahban, M., Jones, D., & Subbiah, J. (2014). Heat and mass transport during microwave heating of mashe dpotato in domestic oven- model development, validation, and sensitivity analysis. J ournal of Food Sciecne, 79(10), 1991-2004.

Curcio, S., Aversa, M., Calabrņ, V., & Iorio, G. (2008). Simulation of food drying: FEM analysis and experimental validation. Journal of Food Engineering, 87(4), 541-553.

Dinčov, D.D., Parrott, K.A., & Pericleous, K.A. (2004). A new computational approach to microwave heating of two-phase porous materials. International Journal of Numerical Methods for Heat and Fluid Flow, 14(6), 783-802.

Geedipalli, S.S.R., Rakesh, V., & Datta A.K. (2007). Modeling the heating uniformity contributed by a rotating turntable in microwave ovens. Journal of Food Engineering, 82(3), 359-368.

Gerling, J.F., & Fournier, G. (1991). Techniques to improve the performance of microwave process systems which utilize high Q cavities. Microwaves: Theory and application in materials processing ceramic transactions, 21, 667-674.

Ghammaz, A., Lefeuvre, S., & Teissandier, N. (2003). Spectral behavior of domestic microwave ovens and its effects on the ISM band. In Annales des télécommunications, Springer.

Liu, S., Fukuoka, M., & Sakai N. (2013). A finite element model for simulating temperature distributions in rotating food during microwave heating. Journal of Food Engineering, 115(1), 49-62.

Osepchuk, J.M. (2010). The magnetron and the microwave oven: A unique and lasting relationship. International IEEE conference in Origins and Evolution of the Cavity Magnetron.

Osepchuk, J.M. (2002). Microwave power applications. Microwave theory and techniques, Transactions on IEEE, 50(3), 975-985.

Pitchai K., Birla S., Subbiah J., Jones D., $ Thippareddi, H. (2012). Coupled electromagnetic and heat transfer model for microwave heating in domestic ovens. Journal of Food Engineering, 112(1-2), 100-111.

Pitchai, K., Chen, J., Birla, S., Gonzalez, R., Jones, D., & Subbiah, J. (2014). A microwave heat transfer model for a rotating multi-component meal in a domestic oven: development and validation. Journal of Food Engineering, 128, 60-71.

Risman, P.O. (2009). Advanced topics in microwave uniformity. In Lorence, M.W., Pesheck P. S., (Eds.), Development of packaging and products for use in microwave ovens. First edition, CRC Press LLC, Boca Raton, FL, 66-104.

Schubert, H., & Regier, M. (2005). The microwave processing of foods. Woodhead Publishing Limited, Cambridge, UK.

Soltysiak, M., Erle, U., & Celuch, M. (2010). Influence of the magnetron operating frequency on the results of microwave heating. In IEEE Microwave Symposium Digest.

Tang, J., & Resurreccion, Jr. F.P. (2009). Electromagnetic basis of microwave heating. In Lorence, M. W., Pesheck, P. S., (Eds.), Development of packaging and products for use in microwave ovens, First edition, CRC Press LLC, Boca Raton, FL, 3-36.

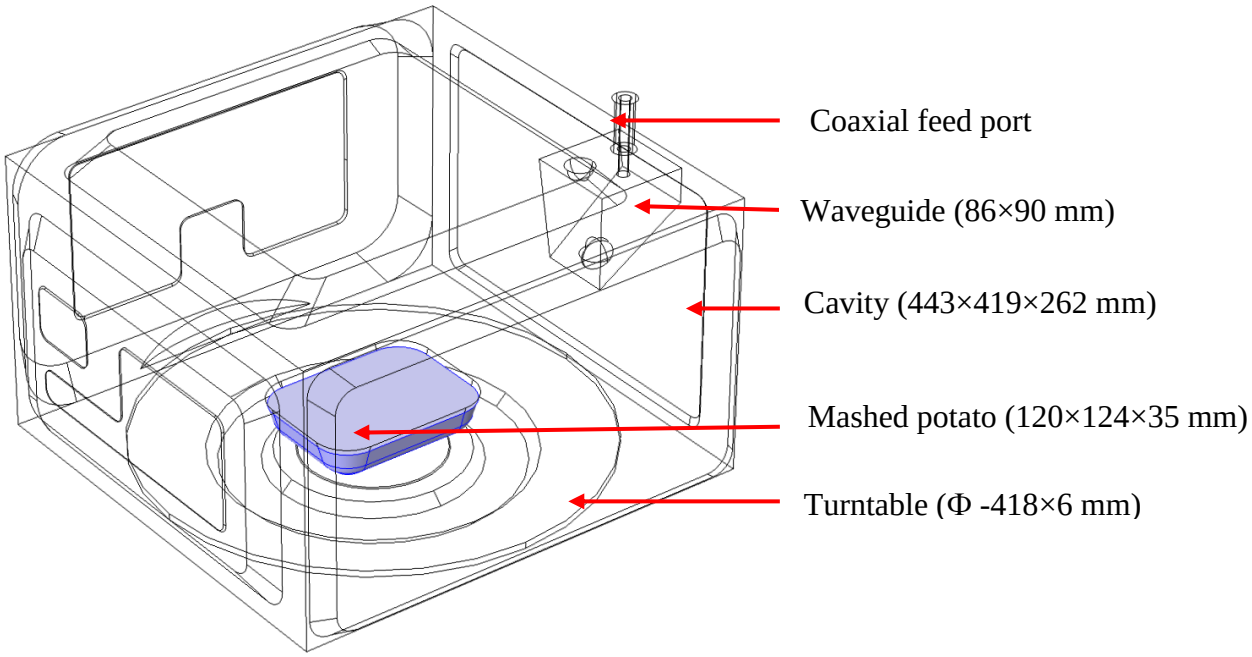

Figure 5. 1. Geometric model of a 1250 W rated power domestic microwave oven (Model No: NN-SD9675, Panasonic Corporation, Shanghai, China).

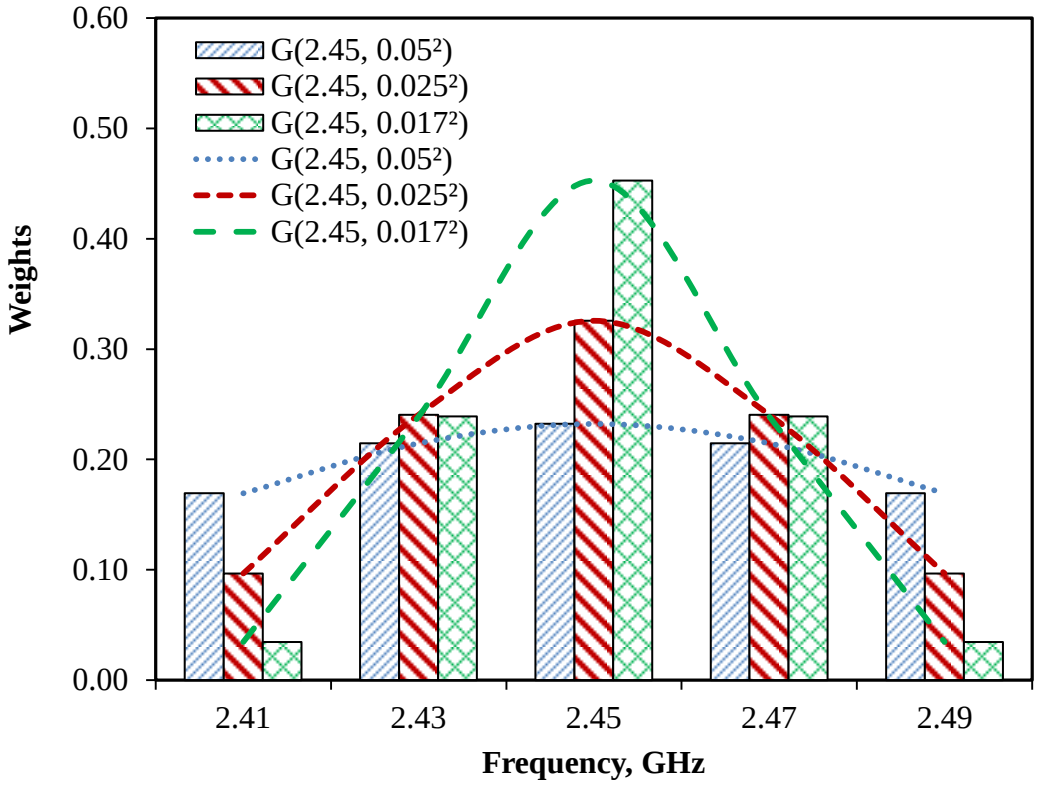

Figure 5. 2. Electromagnetic Gaussian shape frequency spectrum with a central frequency of 2.45 GHz and three variance.

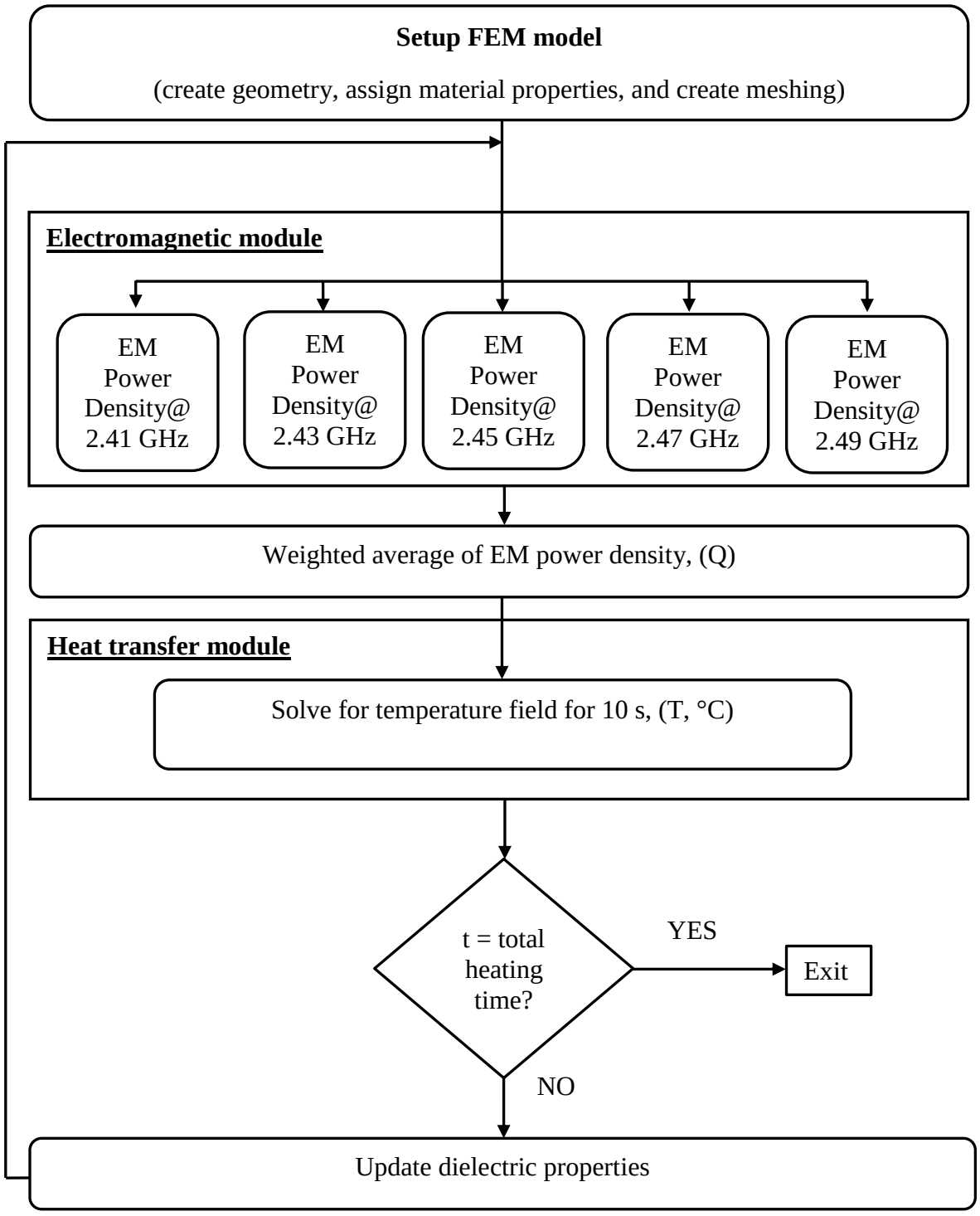

Figure 5. 3. Flow chart depicting inclusion of electromagnetic frequency spectrum to calculate heat source in the microwave heat transfer simulation.

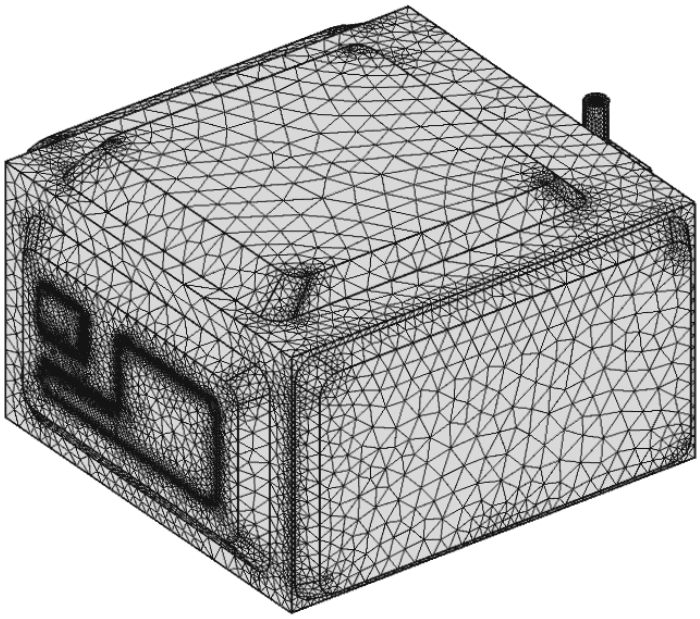

Figure 5. 4. Meshing of the 1250 W rated power domestic microwave oven cavity.

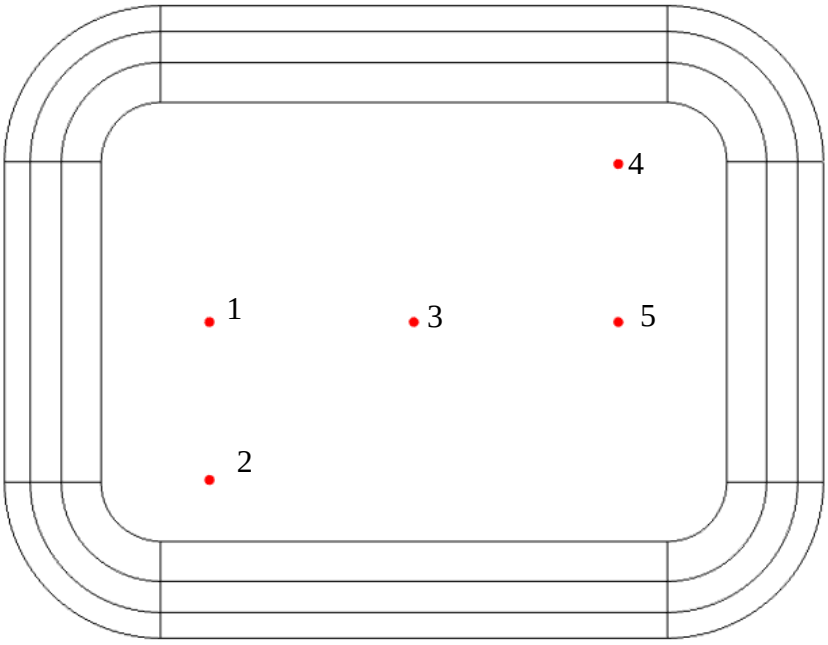

Figure 5. 5. Location of the fiber-optic sensors inserted in the mashed potato (all sensors are inserted 15 mm from the top surface).

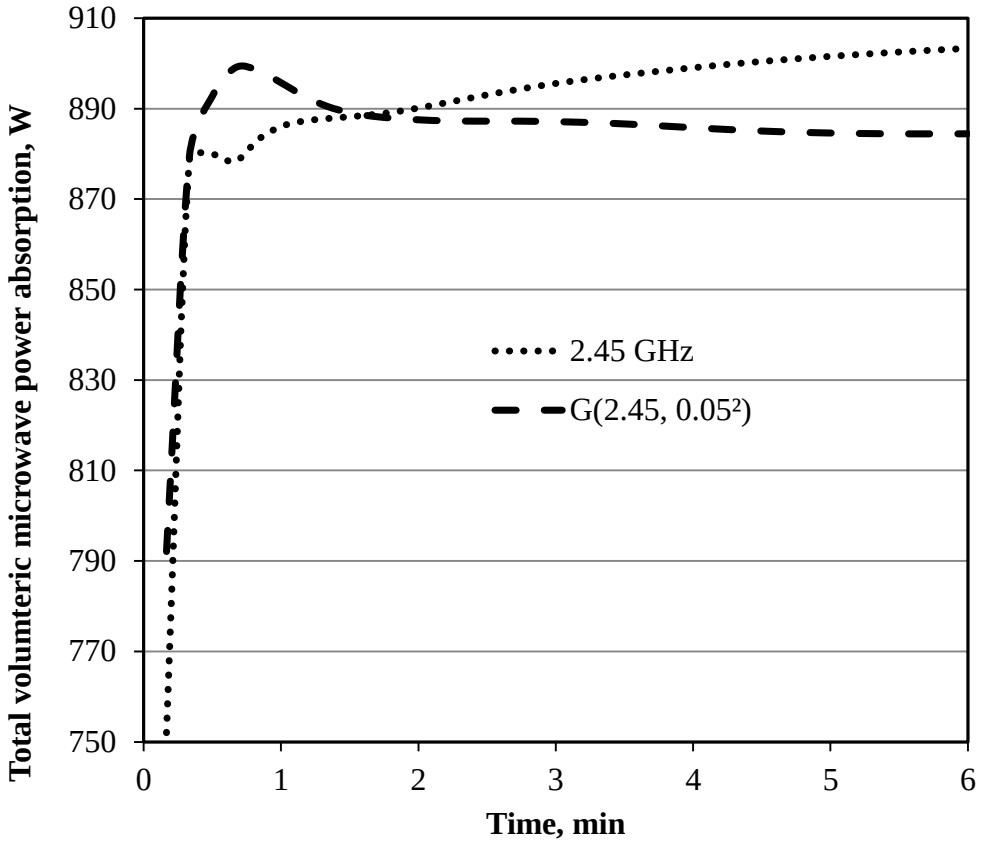

Figure 5. 6. Time-dependent volumetric microwave power absorption in mashed potato comparison between 2.45 GHz frequency and electromagnetic frequency spectrum of $G(2.45, 0.05^2)$.

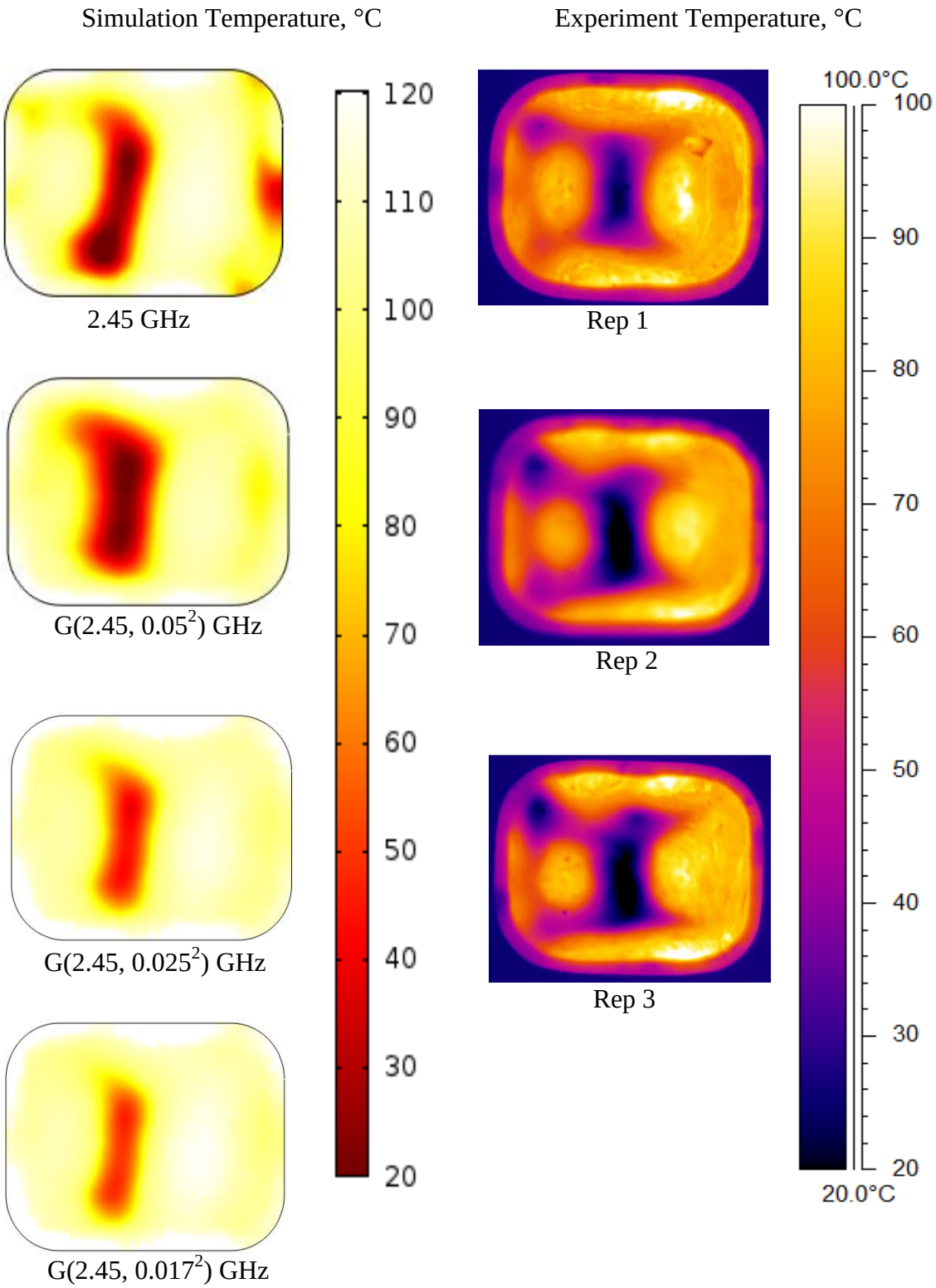

Figure 5. 7. Comparison of spatial surface temperature profiles between experiment (3 replications) and simulations of different frequencies after 6 min frozen mashed potato microwave heating.

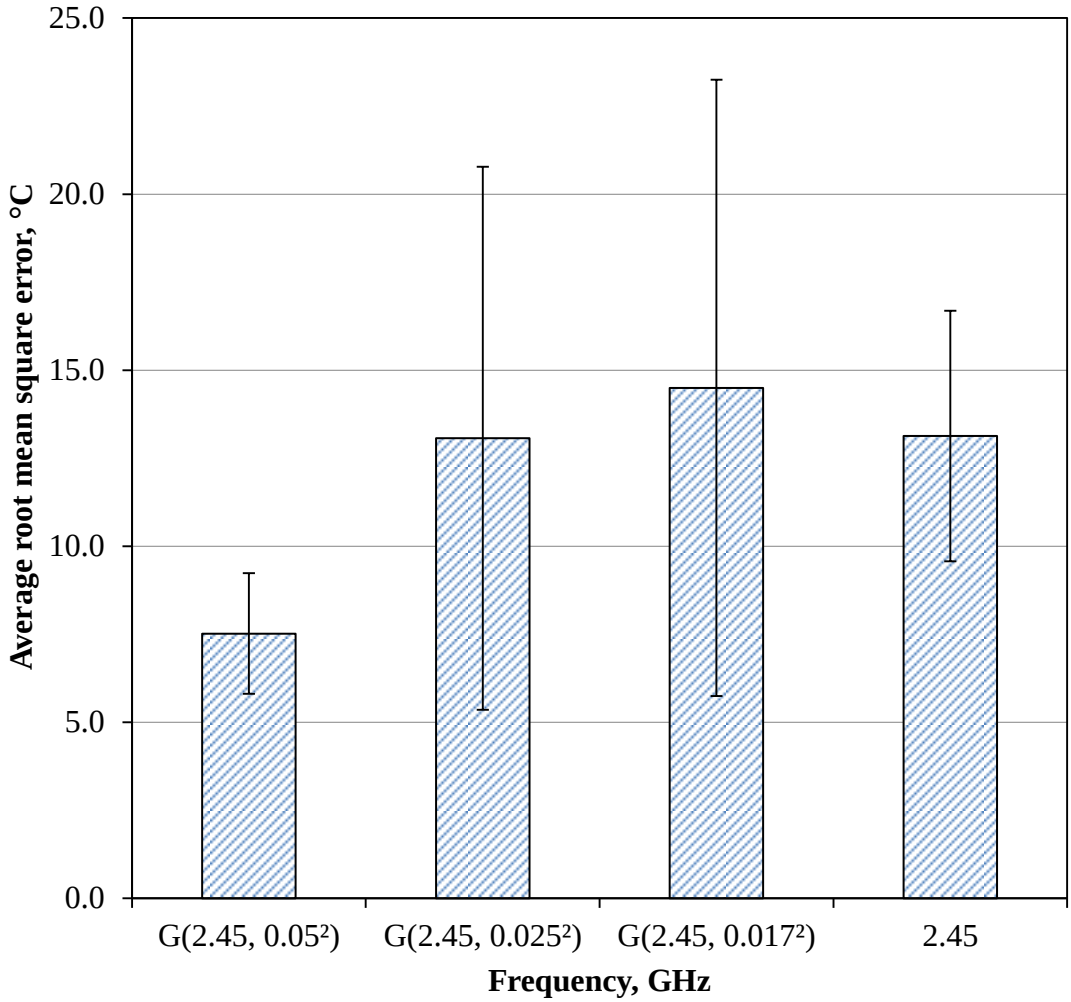

Figure 5. 8. Average root mean square error of five point transient temperature profiles comparison between monochromatic-frequency of 2.45 GHz and microwave frequency spectrum with selected variance (Error bar indicates one standard deviation of RMSE of temperature at 5 locations).

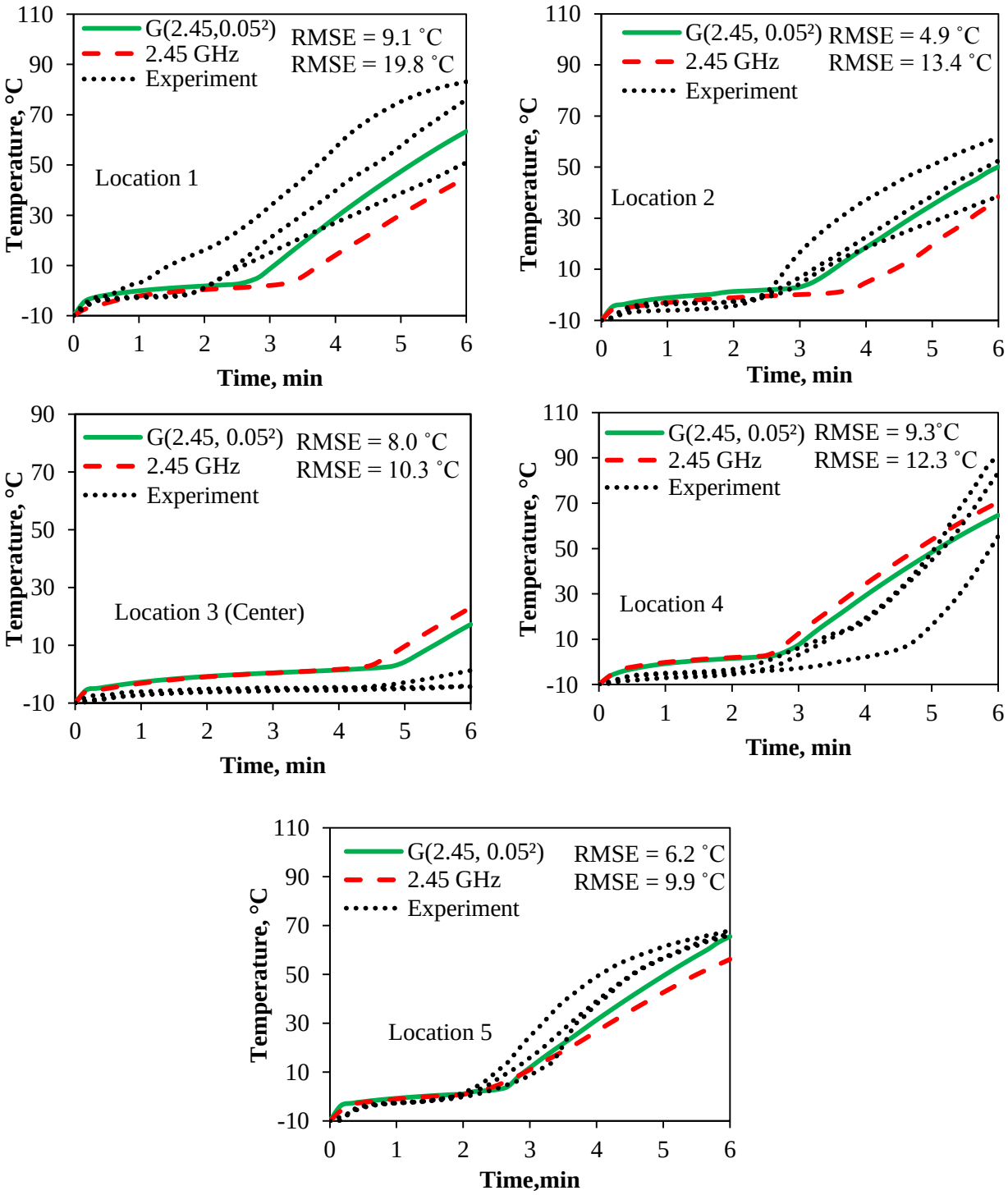

Figure 5. 9. Transient point temperature profiles comparison between experiment (3 replications) and simulations at five locations during 6 minutes of microwave heating of frozen mashed potato.

CHAPETR VI

MOISTURE DESORPTION ISOTHERM CHARACTERISTICS AND THERMODYNAMIC PROPERTIES OF COOKED PASTA

Krishnamoorthy Pitchai [a, b], Jiajia Chen [b], Curtis Weller [a, b], and Jeyamkondan Subbiah [a, b, *]

[a] *Department of Food Science and Technology, University of Nebraska-Lincoln, NE – 68583*

[b] *Department of Biological Systems Engineering, University of Nebraska-Lincoln, NE – 68583*

*Corresponding author: Jeyamkondan Subbiah, Kenneth E. Morrison Distinguished Professor of Food Engineering, 212 L.W.Chase Hall, East campus, Lincoln, NE-68583-0726, Ph. No: 402-472-4944, Fax No: 402-472-6338, Email: jeyam.subbiah@unl.edu.

Citation: Pitchai, K., Chen, J., Weller, C., Subbiah, J. 2015. Moisture desorption isotherm characteristics and thermodynamic properties of cooked pasta. International Journal of Food Properties. In review.

6.1. Abstract

The desorption isotherm profile of cooked pasta was determined using an automated vapor sorption analyzer at each of five temperatures (20, 30, 40, 50 and 60 °C), and over a water activity range of 0.1 to 0.9. The isotherms exhibited Type II behavior in that equilibrium moisture content decreased with increasing temperature at a constant water activity. The parameters and goodness-of-fit of four sorption models

(Oswin, Halsey, Smith, and Guggenheim-Anderson-de Boer) were evaluated with the experimental isotherm data. The Halsey model was found to be in good agreement with the experimental desorption data over the entire water activity range and at each temperature with the mean percentage deviation ranging only 1.2 – 2.7%. The net isosteric heat of desorption, determined using the Clasius-Clapeyron equation, decreased with an increase in the equilibrium moisture content. Effect of equilibrium moisture content on latent heat ratio, calculated based on the Othmer equation, decreased with increased equilibrium moisture content. Desorption bulk moisture diffusion coefficient, calculated as a function of water activity at different temperatures, increased at a constant water activity as temperature increased. Desorption bulk moisture diffusion coefficient of liquid water in cooked pasta increased linearly from 6.45×10^{-8} m^2/s at 20 °C to 13.24×10^{-8} m^2/s at 60 °C.

Keywords: Cooked pasta, isotherm models, isosteric heat sorption, latent heat ratio, bulk moisture diffusion coefficient.

6.2. Introduction

Moisture loss from one region of food product to another region during processing depends on the thermodynamic equilibrium with the surrounding food components and the environment. A moisture isotherm defines the relationship between equilibrium moisture content (EMC) and equilibrium relative humidity (ERH) or water activity (a_w) at a constant pressure and temperature for a food [1]. Understanding the kinetics of any isotherm profile and knowledge of thermodynamic properties are important for controlling quality and safety of food products during processing and

storage [2]. Measured sorption isotherms for various food and agricultural products were extensively summarized in Al-muhtaseb et al.[3]. Moisture sorption isotherms of most foods exhibit a non-linear relationship between EMC and a_w, generally sigmoidal in shape [3].

Several empirical and semi-empirical mathematical models exist to describe the moisture sorption isotherms of food materials. The reason for there being different sorption models evaluated for any particular food is that no one sorption model gives an accurate prediction throughout the entire water activity range [6]. No one sorption model predicts accurately EMC over the entire a_w range because water is associated with the food by different mechanisms in different a_w regions[7]. Boquet et al. [4] evaluated eight isotherm equations for 39 different foods to describe which sorption model best describes for a particular food in an entire water activity region. Similarly, Van den Berg and Bruin [5] evaluated 77 isotherm equations. Al-muhtaseb et al. [3] reviewed and discussed six most commonly applied sorption models for food products. Andrade et al. [8] reviewed and classified eight sorption models to discuss about the suitability of fitting data for different food products and the working a_w ranges of the models. Therefore, it is important to evaluate the different sorption models for a particular food to predict the accurate equilibrium moisture content over a range of water activity.

Net isosteric heat of desorption can be used to estimate energy required for removing water from a food material during its drying process [1]. The net isosteric heat of desorption is defined as the total isosteric heat of desorption taken in by the food during drying minus the latent heat of evaporation of water at the system temperature [9]. The total isosteric heat of desorption is defined as the total heat required for drying of a

food material which include both isosteric and latent heat of evaporation [10]. In general, the latent heat of evaporation of sorbed water in food may increase to values well above the vaporization of pure water as food undergoes dehydration at low moisture content [11]. The extent of moisture content at which total isosteric heat of desorption approaches the latent heat of vaporization of water is considered as an indication of the amount of "bound-water" in the food [12]. The net isosteric heat of desorption can be calculated based on the Clausius-Clapeyron equation at different temperatures given constant EMC [10- 11].

In the recent development of a heat and mass transfer model for microwave heating of mashed potato, since moisture diffusion coefficient values were not available for mashed potato, Chen et al. [13] used moisture diffusion coefficient values of raw potato from the literature. Root mean square error for the model temperature predictions ranged from 1.6 to 11.7 °C. Reason of that error was attributed to the use of assumed values of moisture diffusion coefficient for raw potato rather than mashed potato. Therefore, it is important to use the most representative moisture diffusion coefficient value to predict accurate moisture and temperature profiles.

The amount and rate of moisture transfer during drying are influenced by a_w and diffusion rate [14]. Thus, the moisture diffusion coefficient is an important physical parameter to use to determine the rate of moisture transfer. In a multi-domain and highly porous food, moisture migrates more quickly because of several moisture migration mechanisms such as liquid diffusion, surface diffusion, and capillary diffusion. In the case of a low porosity food, the moisture migration is dominated only by liquid diffusion.

For all of these situations, the moisture diffusion coefficient of water in a food material can be determined using a sorption isotherm [15].

A sorption isotherm can be determined by exposing a food sample into a saturated salt solution environment of known relative humidity and tracking the weight change in the sample over time until equilibrium reached [16-19]. Equilibrating moisture in the food sample to various relative humidity values using saturated salt solutions is a cumbersome and time-consuming procedure. With the advent of automated vapor sorption analyzer instruments, relative humidity and temperature can be controlled precisely, providing a faster and convenient method of determining moisture sorption isotherms. Numerous researchers in recent times have used automated vapor sorption analyzer instruments to develop moisture sorption isotherms of different food products and to calculate moisture diffusion coefficients using the Fick's second law [15, 20-22]. Most researchers have developed both adsorption and desorption isotherms.

To understand moisture diffusion kinetics during microwave heating of pre-cooked pasta in a domestic oven, desorption and its associated EMC and a_w values are relevant to study for pasta over a range of temperatures. Therefore, the objectives of this study are to:

i. measure the experimental desorption EMC and a_w values of cooked pasta at each of 20 °C, 30°C, 40°C, and 50°C and 60°C using an automatic vapor sorption analyzer to fit an experimental isotherm for different sorption models in evaluation of the parameters and goodness-of-fit for accurate prediction of isotherm behaviours of cooked pasta;

ii. determine the net isosteric heat of desorption and latent heat ratio as a function of EMC from the experimental isotherms; and

iii. determine the bulk moisture diffusion coefficient as a function of a_w and evaluate the bulk moisture diffusion coefficient as a function of temperature at a constant a_w.

6.3. Methods and Materials

6.3.1. Sample preparation

Dry durum wheat based pasta (Barilla Lasagna, Barilla America, Inc., Bannockburn, IL) was purchased from a local grocery store and poured into a steam kettle containing boiling water. The pasta was cooked in the boiling water for 8 min; and then the cooked pasta was retained in a colander so boiling water was removed and then the retained cooked pasta rinsed using the distilled water. Immediately after rinsing the cooked pasta, the cooked pasta was stored in a plastic container and stored in a refrigerator maintained at 5 °C temperature.

6.3.2. Moisture content determination

The moisture content of the cooked pasta was determined using a method based on the ASAE S352.2 standard method [23]. The temperature of the cooked pasta was controlled by a natural convection oven preset at 103 °C. Four cooked pasta samples were taken in four separate aluminum pans and initial pan weight was noted and then subtracted from initial sample and pan weight to calculate initial sample weight. Initial sample weight of four samples was 3.5±0.23 g. The cooked pasta weight loss was measured for every 30 min until there was no weight change in the cooked pasta. The

final weight of the cooked pasta and pan were measured and then the pan weight subtracted to calculate final sample weight which used for moisture content determination. The calculated initial moisture content of cooked pasta was 1.45 ± 0.14 kg water/kg dry solids (dry basis).

6.3.3. Vapor sorption analyzer system

Desorption equilibrium isotherms were developed based on the dynamic gravimetric vapor sorption (DVS) method described by the manufacturer of the vapor sorption analyzer (Decagon Devices, Pullman, WA). The equilibrium desorption isotherm was determined by tracking the weight change of cooked pasta approximately every 5 min as exposed to air with selected controlled humidity. The humidity of air and the vapor partial pressure around the pasta was controlled by mixing the dry air from a desiccant tube. Vapor sorption analyzer (Serial no: VSA1075; Aqualab, Decagon Devices, Pullman, WA) was used to measure uptake and loss of vapor gravimetrically using an ultra-balance with a capacity of measuring 500 to 5,000 mg and mass resolution of ±0.1 mg.

6.3.4. Moisture desorption isotherm

The cooked pasta was cored to the size of 32 mm diameter and 1.5 mm thickness. The initial mass of the cooked pasta sample was 1900 ± 50 mg. The cored cooked pasta was placed on the bottom of the stainless steel sample pan and sealed inside analyzer. The gas flow rate was set at 100 ml/min and was parallel to the top surface of the cooked pasta. Before each isotherm determination, the vapor sorption analyzer was calibrated using two standard salt solutions (0.250 a_w 13.41 molal LiCl; 0.760 a_w 6.0 molal NaCl) per manufacturer's instructions. Kinetic water desorption isotherm profile of the cooked

pasta was constructed by measuring EMC values against a_w levels of 0.9 to 0.1 in increments of 0.1. For each a_w interval, the cooked pasta was equilibrated to that particular a_w level using the equilibration criteria of a change in mass over time of not more than 0.02% for 2 consecutive time steps of 5 min. After the equilibration reached to the set a_w, the mass of cooked pasta was measured to determine the EMC of the pasta and then a_w was decreased to the next targeted a_w and equilibrated using the same criteria. During the equilibration process, the change in cooked pasta mass was recorded automatically at every ~5 min. A desorption isotherm profile was collected at each of five different temperatures ranging from 20 to 60 °C at 10 °C increments. A new cooked pasta sample was used for each isotherm temperature. The relative humidity and temperature of the sample chamber were controlled to the targeted relative humidity and temperatures with the precision of ±0.2% and ±0.1 °C, respectively.

6.3.5. Sorption isotherm models

To understand the storage stability of the food products during storage, sorption models are needed to describe the behaviour of moisture sorption isotherms [24]. There are many sorption models that exist to describe moisture sorption isotherm behaviours of food products; however, no one single sorption model provides accurate predicted results throughout the entire relative humidity range of 0 to 100%, and for all types of foods [3]. Prominent in literature are four sorption models (namely Oswin, Halsey, Smith, and Guggenheim-Anderson-de Boer (GAB) as shown below in Eq. 6.11-6.44) used to fit experimental moisture desorption isotherm data. Parameters of the models are estimated using non-linear least-square regression analysis which minimizes the residual sum of

squares [1]. For this study, non-linear least-square regression analysis was performed using the Levenberg-Marquardt algorithm method in Matlab R2013a.

Oswin equation [25]

$$M = k\left[\frac{a_w}{(1-a_w)}\right]^n \tag{6.1}$$

Halsey equation [26]

$$M = \left[\frac{-C}{\ln a_w}\right]^{1/k} \tag{6.2}$$

Smith equation [27]

$$M = a + b\ln(1-a_w) \tag{6.3}$$

Guggenheim-Anderson-de Boer (GAB) equation [28]

$$M = \frac{M_o C K a_w}{[(1-Ka_w)(1-Ka_w+CKa_w)]} \tag{6.4}$$

where C, K, k and n are the constant parameters in sorption models, a_w is the water activity, M is the EMC in g of water/g of dry solid (dry basis) and M_o is the monolayer moisture content in g of water/g of dry solid (dry basis).

The following criterion was used to evaluate the goodness-of-fit of each model with the experimental data or the mean percentage deviation (P) value [1]

$$P(\%) = \frac{100}{N}\sum_{i=1}^{N}\frac{|Me_i - Mc_i|}{Me_i} \tag{6.5}$$

where Me_i and Mc_i are experimental and predicted EMC in g of water/g of dry solid (dry basis), respectively, and N is the number of experimental data.

6.3.6. Determination of net isosteric heat of desorption

The net isosteric heat of desorption can be calculated from the moisture sorption isotherm data using the Clausius-Clapeyron equation [9]

$$q_{st} = -R\frac{\partial \ln(a_w)}{\partial(1/T)} \quad (6.6)$$

and

$$q_{st} = Q_{st} - \lambda \quad (6.7)$$

where a_w is the water activity, q_{st} is the net isosteric heat of sorption in kJ/mol, Q_{st} is the total isosteric heat of sorption in kJ/mol, λ is the latent heat of vaporization in kJ/mol, R is the universal gas constant (8.314 J/mol K) and T is the absolute temperature in K.

The net isosteric heat of desorption was determined by plotting the sorption isotherm in $\ln(a_w)$ versus 1/T for specific EMC with the slope of the plot equals to $-q_{st}/R$ [9, 29]. The net isosteric heat of desorption was calculated for different EMC from 0.12 to 0.3 g of water/g of dry solid (dry basis) at every 0.02 in order to understand the dependence of q_{st} on EMC. It was assumed that the net isosteric heat of desorption was not temperature dependent.

The net isosteric heat of desorption as a function of EMC can be predicted from the following equation [10] and can be compared with the observed net isosteric heat of desorption as a function of EMC.

$$q_{st\_p} = q_0 e^{\left[\frac{-M_E}{b}\right]} \quad (6.8)$$

where parameter q_0 is the isosteric heat of desorption for the strongest bound water molecule in kJ/mol, b is the parameter indicates the changes in binding energy with changes in the water content, M_E is the equilibrium moisture content in g of water/g of dry solid (dry basis), and q_{st_p} is the predicted net isosteric heat of desorption in kJ/mol. For this study, non-linear least-square regression analysis was performed using the Levenberg-Marquardt algorithm method in Matlab R2013a to predict the net isosteric heat of desorption and associated parameters.

6.3.7. Determination of latent heat ratio

The linear relationship between saturated vapor pressure (P_{vs}) of pure water and the vapor pressure in food products (P_v) at constant EMC was described by Othmer [30].

$$\ln(P_v) = \ln(P_{vs})\left[\frac{Q_{st}}{\lambda}\right] + Z \tag{6.9}$$

where P_v is the vapor pressure of water in food products in kPa, $P_{vs}$is the saturated vapor pressure of pure water in kPa, Q_{st} is the total isosteric heat of desorption in kJ/mol, and λ is the latent heat of vaporization of pure water in kJ/mol, and Z is the intercept.

The latent heat ratio, denoted by $\left[\frac{Q_{st}}{\lambda}\right]$, is calculated from the slope of the plot between $\ln P_{vs}$ and $\ln P_v$ at constant EMC. This process was repeated for different EMC from 0.12 to 0.3 at every 0.02 interval. The saturation vapor pressure of pure water (P_{vs}) was calculated using the Tetens equation [31]

$$P_{vs} = 0.61078e^{\left[\frac{17.269T}{237.3+T}\right]} \tag{6.10}$$

where P_{vs} is the saturation vapor pressure of pure water in kPa, and T is the temperature in °C.

The vapor pressure of water in food (P_v) was calculated as:

$$P_v = ERH \times P_{vs} \quad (6.11)$$

where ERH is the equilibrium relative humidity in %.

6.3.8. Determination of bulk moisture diffusion coefficient

The moisture diffusion coefficient (D) can be calculated from Fick's second law using the assumption that the water content gradient is the potential for mass transfer over a unit cross section of a sample [32].

$$\frac{\partial M}{\partial t} = \nabla[D(\nabla M)] \quad (6.12)$$

where M is the EMC of the sample in g of water/g of dry solid (dry basis), D is the bulk moisture diffusion coefficient in m^2/s.

Calculation of each desorption bulk moisture diffusion coefficient (D_d) analytically used the following assumptions: i) bulk moisture diffusion coefficient is constant for a given sorption experiment, ii) shrinkage during desorption is negligible, iii) sample thickness is homogeneous, iv) sample formed an infinite slab with moisture diffusion occurring only through the top surface, v) moisture transport is only by diffusion, vi) moisture content of the sample instantaneously reaches equilibrium with the condition of surrounding air, and vii) moisture is initially distributed uniformly throughout the sample.

The solution to the Fick's second law to calculate desorption bulk moisture diffusion coefficient for an infinite slab can be found through the following equation [15].

$$\frac{M_t - M_e}{M_o - M_e} = 1 - 2\left(\frac{D_d t}{\pi L^2}\right)^{1/2} \quad (6.13)$$

where M_o, M_t, M_e are the sample moisture content at time 0, time t, and equilibrium level, respectively, D_d is the desorption bulk moisture diffusion coefficient in m^2/s, t is the time in s, and L is the sample thickness in m (i.e., L = 0.0015 m for the pasta samples).

The experimental values of $\frac{M_t - M_e}{M_o - M_e}$ between 0.4 and 1 were plotted against square root of time in seconds for each a_w level. The relation between $\frac{M_t - M_e}{M_o - M_e}$ and square root of time in seconds yields a linear fit and slope of the equation is substituted in Eq. (6.13) to solve for D_d.

6.4. Results and Discussion

6.4.1. Desorption isotherms

The experimental desorption isotherms of cooked pasta at each of five temperatures between 20 °C to 60 °C over a_w range of 0.9 to 0.1 are shown in Figure 6. 1. The isotherm profiles demonstrate that EMC increased with an increase in a_w at a constant temperature. The desorption isotherms exhibited the characteristics of sigmoidal shape curves, which is typical shape of many starch food products such as cooked pasta [33]. On the basis of the Van der Waals adsorption of gases on various solid substrates, isotherms of different food products were classified and grouped into five shape curves [34]. The desorption isotherms of cooked pasta exhibited one of the five types of isotherm shape behaviours of food products, Type II shape [3]. As shown in Figure 6. 1, the EMC decreased with the increase in temperature at a constant water activity. This phenomenon

was related to the condition of food especially starch products becoming less hygroscopic [33, 35]. Palipane and Driscoll [36] suggested that at higher temperatures water molecules in food were activated to higher energy levels that allow the water molecules to break away from water binding sites, thereby decreasing EMC. The effect of temperature on equilibrium sorption isotherms was reported by Viollaz and Rovedo [2] for potato starch, which showed the similar isotherm trend to this study. Al-muhtaseb et al.[33] reported the desorption isotherms of potato starch powder at 30 °C, 45 °C , and 60 °C demonstrated that starch food products exhibit a stronger temperature dependence on EMC at a given a_w. It is noticeable that cooked pasta exhibited a stronger temperature effect on EMC at a given a_w. As shown in Figure 6. 1, raising temperature of cooked pasta at a given EMC effectively raises a_w in cooked pasta. The temperature shift on a_w at a given EMC affects chemical and biological reaction rates, which eventually can lead to quality deterioration of food [33].

6.4.2. Sorption models for fitting experimental desorption isotherms

Data points used to develop the experimental desorption isotherms were fitted into Eqs. (1-4) using non-linear least- square regression analysis so that the parameters of the sorption models could be analyzed. The goodness-of-fit for each of the models was evaluated based on mean percentage deviation (P, %) and regression coefficient (R^2). The resultant parameters of the models, mean percentage deviations, and regression coefficients are given in Figure 6. 1.

It can be seen from the Table 1 that the Halsey equation gives the best fit to the experimental isotherms with the mean percentage deviation ranging from 1.2% to 2.7%, with mean of mean percentage deviation of 1.8%, throughout the entire water activity

range (Figure 6. 1). A model is considered acceptable if the mean percentage deviation values are below 10% [29]. Even though, all other models (Oswin, Smith, and GAB) showed less than 10% of mean percentage deviation, the regression coefficient (R^2) was less than 0.99 for some isotherms. In case of the Halsey equation prediction, the regression coefficient was higher than 0.99 for all the isotherms. Furthermore, it has been reported that multilayer adsorption or desorption at a relatively large distance from a food surface for a food product is best described by the Halsey equation [1, 4]. Crapstine and Rotstein [37] reported that starch-containing foods were well described by their sorption behaviour by the Halsey equation.

Van den Berg [38] and Timmermann et al. [39] reported that the GAB model was adequately useful to represent the sorption isotherms of potato, wheat starch, and other starchy materials. The GAB model mean percentage deviation for all the isotherms was lower than acceptable criteria of less than 10% with the average of 4.1% and the regression coefficient ranged from 0.963 to 0.990. The GAB model physical parameter, monolayer moisture content value (M_0), which was a measure of sorption possibility of a food material at a single layer, showed a trend of decreased M_0 value with the increasing temperature. The similar results were observed in Kaymak-Ertekin and Sultanoglu [1] and McLaughlin and Magee [40].

6.4.3. Isosteric heat of desorption

The net isosteric heat of desorption (q_{st}) values were calculated as a function of EMC from the experimental isotherm data at different temperatures using the Clausius-Clapeyron equation (Eq. (6.6)). The net isosteric heat of desorption of cooked pasta as a function of EMC is shown in Figure 6. 2. As shown in Figure 6. 2, net isosteric heat of

desorption decreased exponentially as the equilibrium moisture content increased. The net isosteric heat of desorption decreased from 43.0 to 1.9 kJ/mol as the EMC increased from 0.12 to 0.3 g of water/g of dry matter (dry basis). The similar trend of net isosteric heat of desorption decreasing with the increasing EMC has been reported for many other foods such as potato [29], tomato [12], and peppers [1]. This trend indicates that amount of energy required for desorption of water at lower moisture content was higher as compared to at higher moisture content and increased net isosteric heat of sorption at lower moisture content was due to the presence of bound water in the solid matrix [41].

The net isosteric heat of desorption of food from the EMC can be analytically calculated from the Eq. (6.8). The predicted net isosteric heat of desorption as a function of EMC is shown in Figure 6. 2. The predicted net isosteric heat of desorption matched well with the experimental net isosteric heat of desorption with the correlation coefficient of 0.99 and the root mean square error of 1.9 kJ/mol. The estimated q_0 was 250. 4 kJ/mol, and b was 0.067 g of water/g of dry solid (dry basis). At lower moisture content, the strong interaction between water molecules and the hydrophilic groups of food solids leads to the higher energy required to remove the strong bound water [41].

6.4.4. Latent heat ratio

The latent heat of vaporization ratio as a function of EMC was calculated based on the Othmer equation outlined in Eq. (6.9). The latent heat ratio $\left[\frac{Q_{st}}{\lambda}\right]$ at low moisture contents is close to the value of two, which indicates the total heat of desorption, nearly twice the latent heat of vaporization of pure water (λ) (Figure 6. 3). A value of 1 of latent heat ratio corresponds to the state of free water in the food sample. At low EMC of 0.12,

the energy required to remove water is nearly twice as that of latent heat of free water indicating the difficulty in removing the bound water in the food matrix. The value of $\left[\frac{Q_{st}}{\lambda}\right]$ is higher at lower moisture content and then decreases with an increase in the EMC. The similar trend has been observed in plantain pulp by Ciro et al. [10].

6.4.5. Moisture diffusion coefficient

The bulk moisture diffusion coefficients were calculated from the experimental desorption isotherms of 20, 30, 40, 50 and 60 °C using the Eq. (6.13). The calculated bulk moisture diffusion coefficients as a function of a_w and temperature are shown in Figure 6. 4. As a_w increased from 0.1 to 0.8, bulk moisture diffusion coefficient generally increased. Effect of water activity on bulk moisture diffusion coefficient trend was not visibly observed until the water activity rose to 0.4. Above the water activity of 0.4, bulk moisture diffusion coefficients increased as the temperature increased and differentiated themselves based on temperature.

Generally, the maximum bulk moisture diffusion coefficient was found to be at intermediate a_w of 0.6. The bulk moisture diffusion coefficient values ranged from 6.45 $\times 10^{-8}$ to 13.24 $\times 10^{-8}$ m^2/s at the a_w of 0.6. The location of maximum bulk moisture diffusion coefficient at the intermediate a_w level of 0.5 was found for corn starch by Yu et al. [15]. They reported that the maximum bulk moisture diffusion coefficient at intermediate a_w level was due to a change in the mechanism of liquid diffusion at higher relative humidity (a_w) to vapor diffusion at lower relative humidity (a_w).

The effect of temperature on the bulk moisture diffusion coefficient of cooked pasta at 0.6 a_w (60% relative humidity) is shown in Figure 6. 5. As shown in Figure 6. 5,

the bulk moisture diffusion coefficient increased as the temperature increased. The moisture diffusion coefficient increased with the increasing temperature because the water mobility in a food increases due to more available energy [15].

6.5. Conclusions

The moisture desorption isotherms of cooked pasta at different temperatures were determined using an automated vapor sorption analyzer instrument. The EMC decreased with the increasing temperature at constant a_w. Experimental isotherms were fitted to four sorption models, namely the Oswin, Halsey, Smith, and GAB models to evaluate model parameters and goodness-of-fit of sorption models for accurate prediction of isotherm behaviour of cooked pasta. Among the four tested sorption models, the Halsey equation was found to be in best agreement with the experimental sorption data over the evaluated a_w and temperature ranges with mean percentage deviation ranging only 1.2 – 2.7%. The net isosteric heat of desorption, determined using the Clasius-Clapeyron equation, decreased with an increase in the EMC. Effect of EMC on latent heat ratio, calculated based on the Othmer equation, decreased with increased equilibrium moisture content. The desorption bulk moisture diffusion coefficient of cooked pasta as a function of a_w at different temperatures was caluclctaed. The maximum bulk moisture diffusion coefficient was found to be at intermediate a_w of 0.6. Desorption bulk moisture diffusion coefficient, calculated as a function of water activity at different temperatures, increased at a constant water activity as temperature increased. Desorption bulk moisture diffusion coefficient of liquid water in cooked pasta increased linearly from 6.45×10^{-8} m^2/s at 20 °C to 13.24×10^{-8} m^2/s at 60 °C.

Acknowledgements

The authors gratefully acknowledge the financial support provided by USDA CSREES – NIFSI Grant (Project Number: 2008-51110-04340).

6.6. References

1. Kaymak-Ertekin, F.; Sultanoğlu, M. Moisture sorption isotherm characteristics of peppers. Journal of Food Engineering **2001**, 47 (3), 225-231.

2. Viollaz, P.E.; Rovedo, C.O. Equilibrium sorption isotherms and thermodynamic properties of starch and gluten. Journal of Food Engineering 1999, 40 (4), 287-292.

3. Al-Muhtaseb, A.H.; McMinn, W.A.M.; Magee, T.R.A. Moisture sorption isotherm characteristics of food products: a review. Food and Bioproducts Processing 2002, 80 (2), 118-128.

4. Boquet, R.; Chirife, J.; Iglesias, H.A. Equations for fitting water sorption isotherms of foods. International Journal of Food Science and Technology **1978**, 13 (4), 319-327.

5. Van den Berg, C. and S. Bruin. Water Activity: Influences on Food quality **1981**, 1-61.

6. Iglesias, H.A.; Chirife, J. Prediction of the effect of temperature on water sorption isotherms of food material. International Journal of Food Science and Technology **1976**, 11 (2), 109-116.

7. Labuza, T.P. Interpretation of sorption data in relation to the state of constituent water. Water relations in food **1975**, ed. R. Duckworth, Academic Press, New York, USA, 155-172.

8. Andrade, P.; Ricardo, D.; Lemus, M.R.; Perez, C. Models of sorption isotherms for food: uses and limitations 2011, Vitae, 18 (3), 325-334.

9. Tsami, E. Net isosteric heat of sorption in dried fruits. Journal of Food Engineering 1991, 14 (4), 327-335.

10. Ciro, H.; Osorio, J.A.; Cortés, E.A. Determination of the isosteric heat to plantain pulp (*Musa paradisiaca*) by sorption isotherms **2008**, Dyna, 75 (156), 127-134.

11. Rizvi, S.S.H. Thermodynamic properties of foods in dehydration. Engineering properties of food **2005**, CRC Press, New York, USA, 239-326.

12. Kiranoudis, C.T.; Maroulis, Z.B.; Tsami, E.; Marinos-Kouris, D. Equilibrium moisture content and heat of desorption of some vegetables. Journal of Food Engineering **1993,** 20 (1), 55-74.

13. Chen, J.; Pitchai, K.; Birla, S.; Negahban, M.; Jones, D.; Subbiah, J. Heat and mass transport during microwave heating of mashe dpotato in domestic oven- model development, validation, and sensitivity analysis. Journal of Food Sciecne, **2014,** 79(10), 1991-2004.

14. Labuza, T.P.; Hyman, C.R. Moisture migration and control in multi-domain foods. Trends in Food Science and Technology **1998**, 9 (2), 47-55.

15. Yu, X.; Schmidt, A.R.; Bello-Perez, L.A.; Schmidt, S.J. Determination of the bulk moisture diffusion coefficient for corn starch using an automated water sorption instrument. Journal of Agricultural and Food Chemistry **2007**, 56 (1), 50-58.

16. Spiess, W.E.L.; Wolf, W.R. Results of the COST 90 project on water activity. Physical properties of foods **1983**, *Applied* Science Publishers, London, UK, 65-91.

17. Labuza, T.P. Moisture sorption: practical aspects of isotherm measurement and use. American Association of Cereal Chemists **1984**, St. Paul, Minnesota, USA.

18. Arogba, S.S. Effect of temperature on the moisture sorption isotherm of a biscuit containing processed mango (*Mangifera indica*) kernel flour. Journal of Food Engineering **2001**, 48 (2), 121-125.

19. Akanbi, C.T.; Adeyemi, R.S.; Ojo, A. Drying characteristics and sorption isotherm of tomato slices. Journal of Food Engineering 2006, 73 (2), 157-163.

20. Roman-Gutierrez, A.D.; Mabille, F.; Guilbert, S.; Cuq, B. Contribution of specific flour components to water vapor adsorption properties of wheat flours. Cereal Chemistry **2003**, 80 (5), 558-563.

21. Burnett, D.J.; Garcia, A.R.; Thiemann, F. Measuring moisture sorption and diffusion kinetics on proton exchange membranes using a gravimetric vapor sorption apparatus. Journal of Power Sources **2006**, 160 (1), 426-430.

22. Roca, E.; Guillard, V.; Broyart, B.; Guilbert, S.; Gontard, N. Effective moisture diffusivity modelling versus food structure and hygroscopicity. Food Chemistry **2008**, 106 (4), 1428-1437.

23. ASAE. Moisture measurement-unground grain and seeds. ASAE Standards (ASAE S352.2 APR1988 (R2012) **1988**, 1-3.

24. Kingsly, A.R.P.; Ileleji, K.E. Sorption isotherm of corn distillers dried grains with solubles (DDGS) and its prediction using chemical composition. Food Chemistry **2009**, 116 (4), 939-946.

25. Oswin, C.R. The kinetics of package life. III. The isotherm. Journal of the Society of Chemical Industry **1946**, 65 (12), 419-421.

26. Halsey, G. Physical adsorption on non-uniform surfaces. The Journal of chemical physics **1948**, 16 (10), 931-937.

27. Smith, S.E. The sorption of water vapor by high polymers. Journal of the American Chemical Society **1947**, 69 (3), 646-651.

28. Van den Berg, C. Development of BET-like models for sorption of water on foods, theory and relevance. Properties of water in foods **1985**, Springer, 119-131.

29. Wang, N.; Brennan, J.G. Moisture sorption isotherm characteristics of potatoes at four temperatures. Journal of Food Engineering **1991**, 14 (4), 269-287.

30. Othmer, D.F. Correlating Vapor Pressure and Latent Heat Data. Industrial and Engineering Chemistry **1942**, 34 (9), 1072-1078.

31. Weiss, A. Algorithms for calculation of moist air properties on a hand calculator. Transactions of the ASAE **1977**, 20 (6), 1133-1136.

32. Meisami-asl, E.; Rafiee, S.; Keyhani, A.; Tabatabaeefar, A. Drying of apple slices (var. Golab) and effect on moisture diffusivity and activation energy. Plant Omics Journal **2010**, 3 (3), 97-102.

33. Al-Muhtaseb, A.H.; McMinn W.A.M.; Magee, T.R.A. Water sorption isotherms of starch powders: part 1: mathematical description of experimental data. Journal of Food Engineering **2004**, 61 (3), 297-307.

34. Brunauer, S.; Deming, L.S.; Deming, W.E.; Teller, E. On a theory of the van der Waals adsorption of gases. Journal of the American Chemical Society **1940**, 62 (7), 1723-1732.

35. Iglesias, H.A.; Chirife, J. Handbook of isotherms **1982**, Academic Press, New York, USA.

36. Palipane, K.B.; Driscoll, R.H. Moisture sorption characteristics of in-shell macadamia nuts. Journal of Food Engineering **1993**, 18 (1), 63-76.

37. Crapiste, G.H.; Rotstein, E. Prediction of sorptional equilibrium data for starch-containing foodstuffs. Journal of Food Science **1982**, 47 (5), 1501-1507.

38. Van den Berg, C. Description of water activity of foods for engineering purposes by means of the GAB model of sorption. Engineering and food **1984**, Elsevier Applied Science, New York, USA, 311-321.

39. Timmermann, E.O.; Chirife, J.; Iglesias, H.A. Water sorption isotherms of foods and foodstuffs: BET or GAB parameters. Journal of Food Engineering **2001,** 48 (1), 19-31.

40. McLaughlin, C.P.; Magee, T.R.A. The determination of sorption isotherm and the isosteric heats of sorption for potatoes. Journal of Food Engineering **1998**, 35 (3), 267-280.

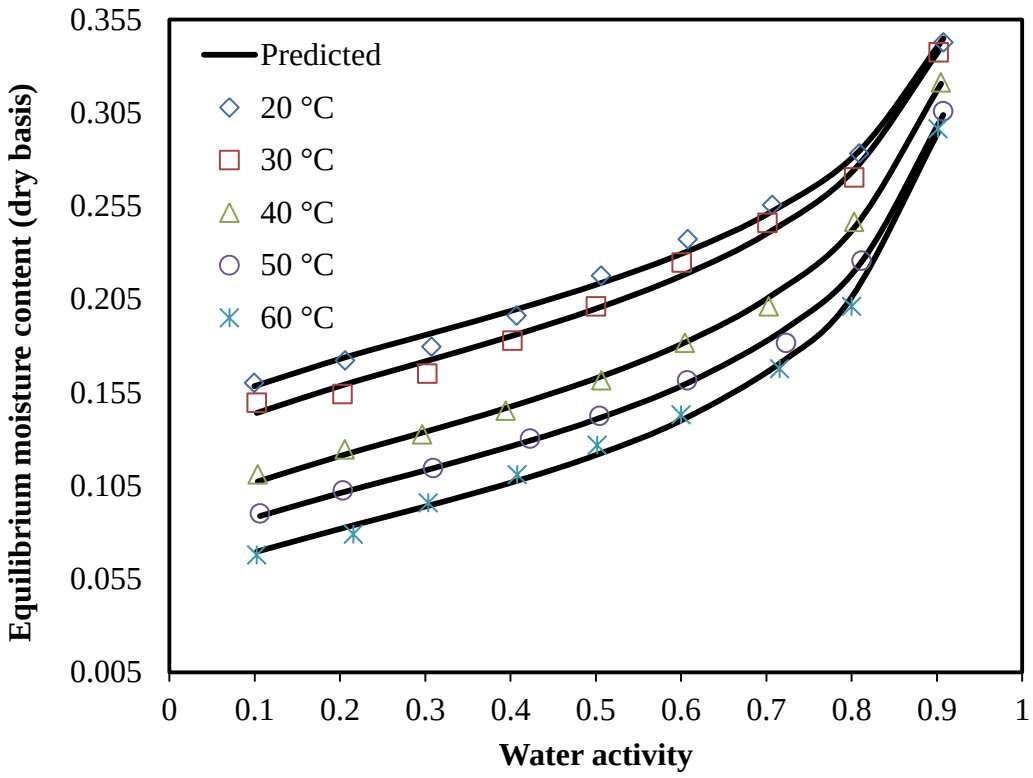

Figure 6. 1. Plot of experimental and predicted isotherm profile using Halsey equation of cooked pasta at different temperatures.

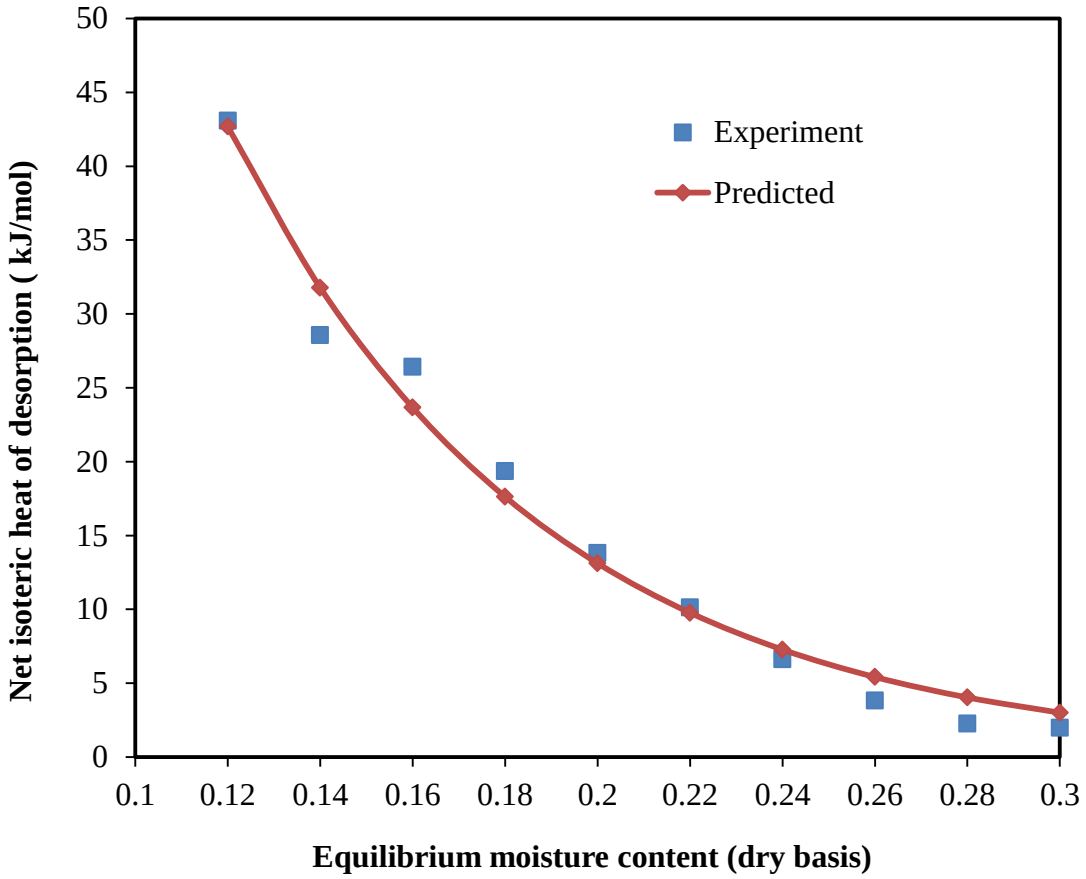

Figure 6. 2. Comparison plot of experimental and predicted net isosteric heat of desorption of cooked pasta as a function of equilibrium moisture content.

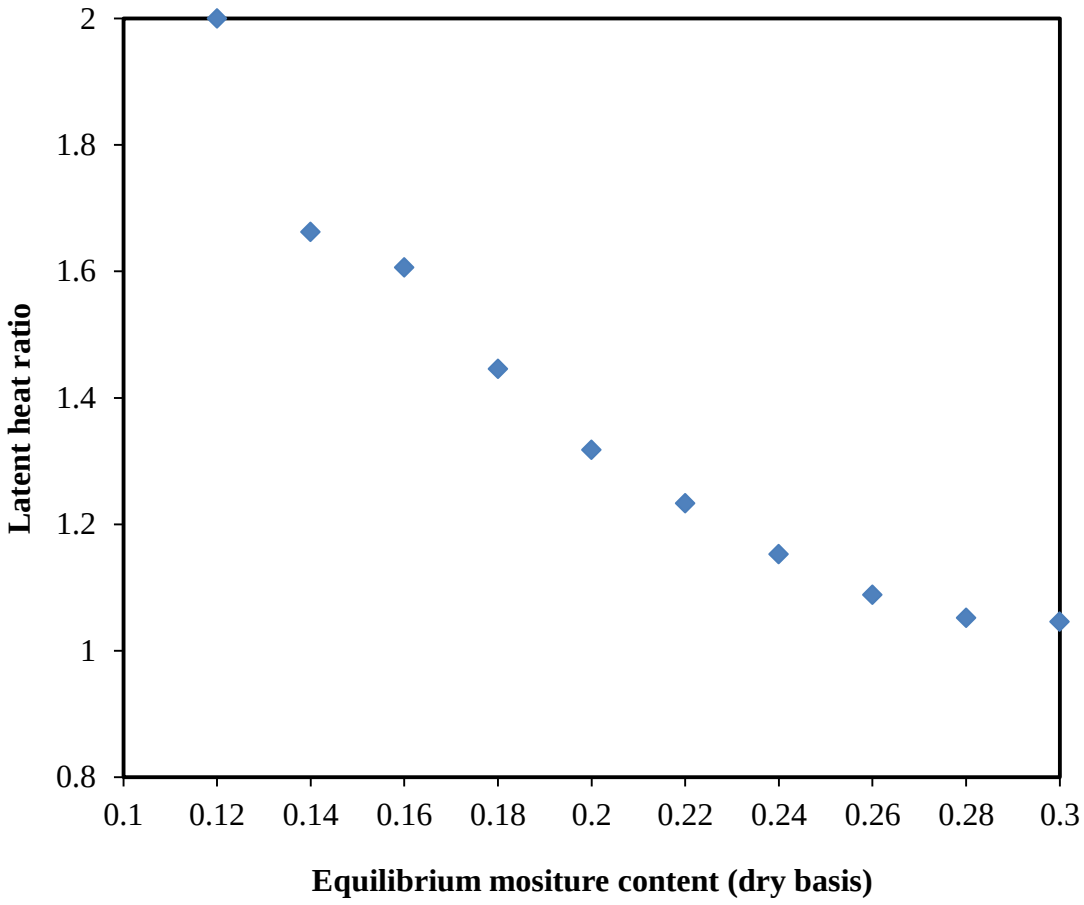

Figure 6. 3. Latent heat ratio of cooked pasta as a function of equilibrium moisture content.

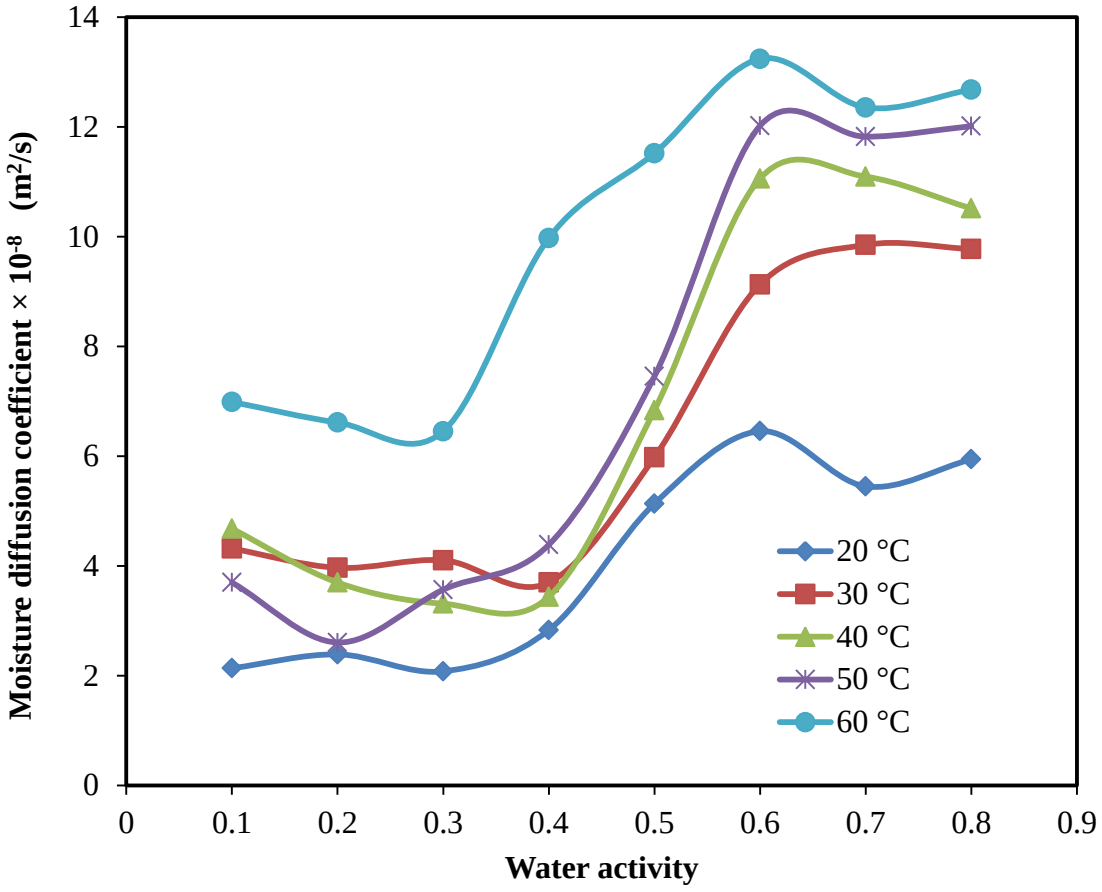

Figure 6. 4. Desorption bulk moisture diffusion coefficient of cooked pasta as a function of water activity at different temperatures.

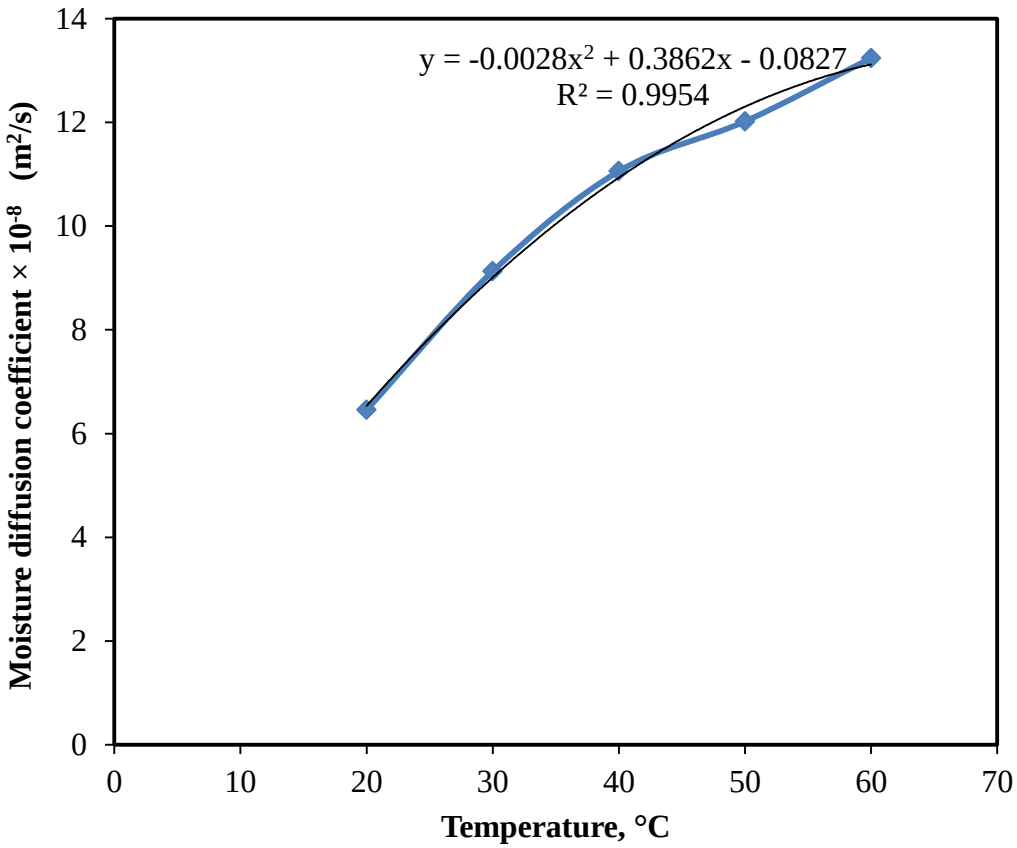

Figure 6. 5. Effect of temperature on the desorption bulk moisture diffusion coefficient at the water activity level of 0.6.

Table 6. 1. Estimated desorption model parameters and goodness of fit data for cooked pasta for four prominent isotherm models.

Models	Parameters	Temperature (°C)				
		20	30	40	50	60
Oswin	k	0.216	0.206	0.168	0.145	0.126
	n	0.187	0.211	0.273	0.309	0.372
	P (%)	2.744	3.205	4.838	4.936	4.486
	R^2	0.984	0.980	0.979	0.983	0.989
Halsey	C	0.0012	0.0020	0.0039	0.0047	0.0076
	k	4.076	3.629	2.852	2.550	2.142
	P (%)	1.651	2.253	1.411	1.157	2.691
	R^2	0.995	0.993	0.998	0.998	0.997
Smith	a	0.1551	0.1389	0.0987	0.0780	0.0554
	b	-0.0797	-0.0853	-0.0918	-0.0914	-0.0983
	P (%)	1.663	1.736	1.861	2.676	3.721
	R^2	0.994	0.994	0.996	0.990	0.987
GAB	M_0	0.161	0.144	0.105	0.087	0.070
	C	75	75	74.99	75	74.97
	K	0.572	0.621	0.734	0.781	0.841
	P (%)	4.139	3.486	4.456	4.451	3.831
	R^2	0.963	0.973	0.983	0.985	0.990

CHAPTER VII

SUMMARY AND RECOMMENDATIONS

7.1. Summary

To understand the non-uniform heating in microwave cooking of prepared, but not-ready-to-eat, microwavable foods, a computer simulation based microwave heat transfer model is needed to gain insights on how microwave heats different food components. Food product developers can use the microwave heat transfer model to design and optimize the food layout in a package based on the cooking performance of food components in domestic oven. Food product development of frozen microwaveable foods is more complex, because different components in the food interact with microwave energy at different rate based on their dielectric and thermophysical properties, variability in domestic oven performance, and consumer practices. Most of the frozen microwaveable food manufacturers rely on minimum scientific approach in their product development process and rather they focus more on cook and look approach by cooking a food product in different power levels of domestic ovens in a test kitchen. It is nearly impossible to develop a food product that can be cooked in varieties of domestic ovens for the same level of heating performance through the cook and look approach. Microwave heat transfer models provides an opportunity to virtually cook the food in different domestic ovens and come up with a cooking instructions that can work for different domestic ovens to achieve safe and of high quality cooking.

To rely on microwave heat transfer models to use for food product development, the model should be enabled to be robust and accurate in temperature prediction. The

microwave heat transfer models are highly useful when the model included with accurate dielectric and thermophysical properties, nearly perfect cavity design, and including all the microwave heat transfer physics into the model. In this study, microwave heat transfer models were developed to simulate microwave heating of frozen multi-component foods in domestic ovens. Maxwell‘s electromagnetic equations and Fourier‘s heat transfer equations were solved using the FEM based numerical solver, COMSOL Multiphysics® software. The protocol for developing coupled model included creating the geometry of oven and food, implementing rotation, mesh optimization, simulation, and validation of the model.

A microwave heat transfer model for a rotating frozen multi-component meal consisting of mashed potatoes and nine chicken nuggets was developed for a 1200 W rated power domestic oven. The model included detailed cavity geometry, phase change, and rotation of the food. Effect of rotation angle on temperature predictions was studied and 45° rotation angle was found to be sufficient. Predicted spatial surface temperature profile was in good agreement with the corresponding experimental profiles in terms of hot and cold spot patterns. The root mean square error values ranged from 5.8 °C to 26.2 °C in chicken nuggets as compared 4.3 °C to 4.7 °C in mashed potatoes. The predicted and experimental temperature profiles were provided as inputs to a microbial inactivation kinetics model for Salmonella Heidelberg to assess food safety risks in chicken nuggets. For 90 s of cooking in a 1200 W microwave oven, at least 7-log reductions of Salmonella Heidelberg was not achieved completely at all locations in the chicken nuggets due to non-uniform heating. A multiphase porous media model combining the electromagnetic heat source with heat and mass transfer, and including phase change of melting and

evaporation was developed for microwave heating of frozen lasagna in a 1200 W domestic microwave oven. The model simulated for six minutes of microwave cooking of a rotating 450 g frozen lasagna tray kept at the center of the turntable. Simulated temperature profiles were compared with experimental temperature profiles obtained using a thermal imaging camera and fiber-optic sensors. The total moisture loss in lasagna was predicted and compared with the experimental moisture loss during cooking. The simulated spatial temperature patterns predicted at the top layer was in good agreement with the corresponding patterns observed in thermal images. Modelled point temperature profiles at six different locations within the meal were compared with experimental temperature profiles and RMSE values ranged from 6.6 to 20.0 °C. The predicted total moisture loss matched well with the experimental result and RMSE value of 0.54 g.

Modeling of susceptor assisted microwave heating of a frozen pizza in a 1250 W domestic oven was performed using radio frequency and heat transfer modules of COMSOL Multiphysics v4.4. Temperature-dependent dielectric and thermophysical properties of frozen pizza components were measured as a function of temperature from -10 °C to 110 °C. Transient boundary condition was applied in radio frequency module to discretize a thin susceptor film in the computational domain. The boundary heat source was applied in the heat transfer module to calculate the temperature in the susceptor film. The root mean square error values of transient temperature profiles of five locations ranged from 5.0 °C to 12.6 °C. The validated model can be used to optimize the layout and food system/package modification to achieve more uniform heating.

In most of the microwave heat transfer simulations, researchers have considered monochromatic frequency of 2.45 GHz. Domestic microwave oven magnetrons produce microwaves in a frequency range of 2.45±0.05 GHz. In this study, a methodology was developed to include electromagnetic frequency spectrum in the coupled electromagnetic and heat transfer model. This study assumed that the magnetron produces a frequency spectrum defined by a Gaussian distribution of frequencies with a central frequency of 2.45 GHz and investigates the effect of Gaussian distribution variance of $(0.05\ \text{GHz})^2$, $(0.025\ \text{GHz})^2$, $(0.017\ \text{GHz})^2$ GHz on prediction accuracy when compared to using monochromatic frequency of 2.45 GHz. A three-dimensional finite element model coupling electromagnetic and heat transfer physics was developed to simulate heating of 550 g of frozen mashed potato for 6 minutes. The model was validated in a 1250 W rated microwave oven with the mashed potato tray placed at the center of the stationary turntable. The electromagnetic power densities were determined separately at five different frequencies equidistant between 2.4 and 2.5 GHz. They were then weighted averaged, based on the selected Gaussian distribution. Simulated temperature profiles of the models using the monochromatic frequency of 2.45 GHz and Gaussian frequency spectrum with different variances were compared with experimental temperature profiles obtained using a thermal imaging camera at the end of cooking and five fiber-optic thermocouples during cooking. The model results showed that predicted spatial surface temperature pattern by the model using frequency spectrum with the largest variance (0.05^2 GHz) had better agreement with the experimental temperature pattern when compared to that using a monochromatic frequency of 2.45 GHz. In the transient temperature profile measurement, the average RMSE value of five locations was 7.5 and

13.1 °C for simulations using frequency spectrum and monochromatic frequency of 2.45 GHz, respectively. Implementing the frequency spectrum in the simulation improved the accuracy of temperature field pattern and transient temperature profile.

In most of the multiphase porous media model, mass transport properties were considered from the literature. To predict the accurate temperature and moisture profiles during microwave cooking, temperature-dependent mass transport properties were needed to the model. One of the mass transport properties that needed for the model was moisture diffusion coefficient. Moisture diffusion coefficient was calculated as a function of temperature from the desorption isotherms collected using an automatic vapor sorption analyzer. The desorption isotherm profile of cooked pasta was measured using an automated vapor sorption analyzer at five temperatures from 20 to 60 °C, and over a water activity range of 0.1 to 0.9. The parameters and goodness of fit of four sorption models (Oswin, Halsey, Smith, and Guggenheim-Anderson-de Boer) were evaluated with the experimental isotherm data. Halsey model was found to be in good agreement with the experimental sorption data over the entire water activity range and temperature with the mean percentage deviation ranging only 1.2-2.7%. Desorption bulk moisture diffusion coefficient was calculated as a function of water activity at different temperatures. As the temperature increased, the bulk moisture diffusion coefficient increased at a constant water activity. Desorption bulk moisture diffusion coefficient ranged from 6.45×10^{-8} m^2/s at 20 °C to 13.24×10^{-8} m^2/s at the water activity of 0.6.

7.2. Recommendations for Future Research

In this study, the microwave heat transfer model was developed for frozen multilayered heterogeneous meals such as lasagna and frozen pizza. Also, the microwave heat transfer model was developed for a two-component meal consisted of chicken nuggets and mashed potato. A comprehensive microwave heat transfer model needs to be developed and validated for other frozen heterogeneous meals by including relevant physics involved during microwave cooking. The current food database needs to be expanded to other modern day microwave meals such as breakfast sandwiches (active package sleeve wrapped around sandwiches), Café steamers (steam movement inside the package), and Pot pies (mixed heterogeneous model).

The microwave heat transfer model needs material properties as one of the important input parameters. After identifying the food products, temperature-dependent dielectric, thermal, mass transport properties of each ingredient needs to be measured and the database has to be expanded to be readily available for further model development for those products. In case of heterogeneous products such as pot pie, there are ingredients (peas, carrot, sauce, and chicken) within the product mixed together and are not easy to be separated out from the product. When developing the microwave heat transfer model for pot pie, the whole ingredients may be combined together considered as single domain and provide the material properties for that single domain. To consider the material properties for a single domain entity of multiple ingredients, the mixed theory model approach can be used.

In the model setup process, 3-D geometry of cavity and food system need to be accurately created using the design and drawing tools available in the COMSOL

Multiphysics or can be created in other computer aided design software's and then imported to the COMSOL Multiphysics. Each microwave oven cavity studied in this dissertation was created manually by measuring the dimensions and then drawing in the COMSOL Multiphysics. It is a high time consuming and cumbersome process and also account for manual and measurement errors. The accuracy of electromagnetic field prediction inside the cavity will be compromised when the cavity and food system are not created close to the reality. To overcome this issue, researchers need to explore an option to construct the cavity and food system by using a mechanical scanning device and then construct the 3-D structure.

7.3. Improvement to the current microwave heat transfer model

In this study, the multiphase porous media model combining electromagnetic with heat and mass transfer was developed including mass transport properties collected from the literature. To improve the accuracy of the model, some of the mass transport properties such as intrinsic permeability, porosity, and moisture diffusion coefficient need to be measured experimentally and/or calculated analytically and included in the model. Temperature-dependent moisture diffusion coefficient was calculated through analytical methods using the desorption isotherms. The model accuracy should be evaluated with the inclusion of the measured moisture diffusion coefficient against using the constant values and/or literature values.

The current electromagnetic, heat and mass transfer model needs to be expanded to include other physics involves during microwave heating. For example, when a frozen pot pie is cooked in a microwave oven, the dough expands due to the internal steam

pressure developed during cooking. To account for the expansion of dough, solid mechanics physics needs to be included in the model. The electromagnetic, heat and mass transfer model was developed assuming no air flow inside the cavity. To include the air flow inside the cavity, the current model needs to be expanded to include momentum transfer in numerical computation. It is recommended that the present model include the Navier-Stoke‘s equations with the convective boundary condition at the air and food interface.

A protocol was developed to include the electromagnetic frequency spectrum in the simulation and demonstrated a simplified assumption of Gaussian distribution that can be used to improve the accuracy of temperature predictions. The actual electromagnetic frequency spectrum of a domestic oven can be determined by measuring the leakage signal using an antenna connected to a spectrum analyzer. The antenna and domestic oven need to be kept inside a large anechoic chamber to avoid interference of signal measurement. In future, the methodology should be adopted to include the actual frequency spectrum, the same methodology of splitting spectrum into weighted function, determining electromagnetic field, averaging them, and then use them as a power density function should be implemented.

7.4. Utility of the microwave heat transfer model

The temperature profiles collected in the frozen multi-component food products need to be incorporated into a ***risk assessment model*** to perform sensitivity analysis for identifying key factors leading to food safety risks. Risk assessment model determines the microbial population dynamics at each and every step of processing. In case of risk

assessment of microwaveable food products, the steps include storage in freezers, cooking in a microwave oven including standing time, consumption, and dose-response.

The current microwave heat transfer model typically takes about a week to simulate microwave heating of 6 minutes, depending on mesh resolution, solver methods, and physics coupling schemes. It is improbable that food industries do not want to wait for long days to see the outcome of the microwave heat transfer model. The current model needs to be ***simplified and optimized*** to reduce the computational time from days to hours. The model will have to be simplified by optimizing meshing, number of rotational steps, and physics coupling schemes. For example, when a new microwave oven and food selected for microwave heat transfer analysis, the current comprehensive microwave heat transfer model should be enabled to dynamically conduct "adaptive mesh refinement" study to come up with a reasonable mesh size for accurate temperature prediction and minimal computational time. To develop the optimized microwave heat transfer model, the microwave heat transfer model should be deployed in ***parallel processing system*** to run the same model for different scenarios such as different mesh size in microwave oven and food.

The microwave heat transfer models developed in this study are robust included all the relevant mechanisms involved in the microwave heating. However, the developed microwave heat transfer models are very complex and computationally intensive that food industries are reluctant to use these modes for their food product development. The current models need to be optimized and simplified to deploy them on an easy-to-use web based simulation interface. In future, ***web enabled simulation tool*** should be developed where the food processors can select a microwave oven, package layout, and product

layout from the database, and then run the simulation to understand the microwave heating performance of that particular combination of oven, food, and package. The food industry professionals can also simulate different combination scenarios of oven, food, and package.